MINISTRY OF EDUCATION AND TRAINING
HO CHI MINH CITY
UNIVERSITY OF TECHNOLOGY AND EDUCATION

NGUYEN THANH TU

IMPROVEMENT METHODS TO REINFORCE RIVERBED SILTY SOIL USING GEOTEXTILE - CEMENT - SAND CUSHION

PH. D THESIS
MAJOR: CIVIL ENGINEERING

Ho Chi Minh City, 11/2023

MINISTRY OF EDUCATION AND TRAINING

HO CHI MINH CITY

UNIVERSITY OF TECHNOLOGY AND EDUCATION

NGUYEN THANH TU

IMPROVEMENT METHODS TO REINFORCE RIVERBED SILTY SOIL USING GEOTEXTILE - CEMENT - SAND CUSHION

MAJOR: CIVIL ENGINEERING - 9580201

Supervisor 1: Dr NGUYEN MINH DUC

Supervisor 2: Dr TRAN VAN TIENG

Examiner 1:

Examiner 2:

Examiner 3:

Ho Chi Minh City, 11/2023

ORIGINALITY STATEMENT

I hereby declare that this is my research work.

The data and results presented in the thesis are accurate and have never been previously published.

Ho Chi Minh City, November 26, 2023

ACKNOWLEDGEMENTS

This dissertation was completed at the Faculty of Civil Engineering at the HCM City University of Technology and Education in Vietnam. There were many obstacles as well as excitement during the process of completing this thesis. Without the encouragement, support, and assistance of my advisors, colleagues, and family, I could not conduct my research.

First, I would like to thank my knowledgeable professors, Dr. NGUYEN MINH DUC and Dr. TRAN VAN TIENG, for admitting me as a Ph.D. student. They imparted knowledge and taught me a great deal about not only academics but also life. Before anything else, I would like to thank Dr. Nguyen Minh Duc for inspiring, motivating, and encouraging me to complete the thesis.

Second, I would like to thank HCM City University of Technology and Education, Falcuty of Civil Engineering, for the resources and equipment that allowed me to complete my research project. In addition, I would like to thank my coworkers for their consistent support during the implementation process.

Lastly, this dissertation is dedicated to my parents, who have always provided me with support and encouragement.

Finally, this thesis is a memorial to my parents, who have always supported and encouraged me.

Nguyen Thanh Tu

ABSTRACT

Using silty soil that was dredged from riverbeds to replace sand for road basements is considered an alternative with many advantages. However, the riverbed soil is soft, with low shear resistance, a high void ratio, weak permeability, and high swelling and bearing capacity loss when saturated. Geotextile, sand cushion, and cement methods are introduced to strengthen soil due to their popularity and effectiveness. The laboratory experiments, including the California Bearing Ratio (*CBR*), a triaxial compression test, a one-dimensional consolidation test with a modified oedometer apparatus, and a modified direct shear test, were conducted to investigate the swelling, *CBR* value, shear strength, and consolidation of reinforced soil. Then, evaluating the applicability of these methods to reinforce the dredged soil from the Cai Lon River would be carried out.

With the high permeability, geotextiles accelerated the soil expansion process, and the swell decreased by 1.3 times. In addition, the *CBR* values increased from 1.1 to 1.5 times for the unsaturated samples and up to 3 times for the saturated samples. Especially, samples reinforced by 2 layers got the highest *CBR* value. In the triaxial compression test, the shear resistance of the unsaturated sample reinforced with three geo-layers rose to approximately 1.6 times that of the unreinforced soil and about 2.1 times that of the saturated case due to the interaction between soil and geotextiles. In the saturated samples, the pore water pressure increased when the displacement was small before rapidly decreasing when slippage between the geotextile and the soil occurred. In addition, consolidation results indicated that the reinforced sample consolidated 1–2 times faster than the unreinforced sample of the same height.

In the one-dimensional consolidation test of reinforced soil, the height of the specimen must be significant. Side friction between the soil and the ring must be considered. A modified odometer apparatus was introduced to measure the friction force between the soil and the ring. The results indicated that friction pressure increased as the ratio of diameter to height (*D/H*) decreased. When the *D/H* ratio was less than 2.5, the effect of friction was significant and reduced the compression

pressure by up to 20% at the end of consolidation (*EOP*). Based on the Taylor method, an analytical method for predicting the stress loss and coefficient of variation of the void ratio, *COV*, along soil sample depth at *EOP* was proposed. The results indicated that the void ratio increased with depth, and if the *D/H* ratio exceeded 2.5, the *COV* would be less than 1.2%.

When reinforced with sand cushions, the swelling, and the dried unit weight reduction decreased with increasing sand cushion thickness. In addition, the *CBR* value was effectively increased for saturated clay rather than unsaturated samples. In the *UU* triaxial compression test, the shear resistance of the reinforced soil in the unsaturated condition increased as the horizontal pressure increased. The shear strength of unsaturated samples with a 20 mm-thick sand cushion increased approximately 1.9 times compared to that of unreinforced samples and about 3.3 times for the saturated case. Specifically, the pore water pressure in the saturated samples increased when the strain was small, and then the water pressure decreased. In addition, the consolidation results indicated that the reinforced sample consolidates between 3.5 and 5 times faster than the unreinforced sample.

As a binder, cement reduced the swelling of riverbed clay by 1.77 to 2.5 times when the cement ratio increased from 3 to 10%. In the case of a 28-day saturation curing, the *CBR* value of the soil-cement mixture increased from 1.7 to 3.8 times that of the soil. In the *UU* triaxial compression test, the shear strength of soil cement increased in both unsaturated and saturated samples. The increase in strength of the soil cement was due to the hydration and pozzolanic processes, which resulted in a change in particle composition. In the case of 10% cement, the percentage of sand granules doubled after 28 days. Brittle failure and an increase in shear resistance and interface shear were also observed by the direct shear test of soil cement and the modified shear test of soil cement and steel. The peak shear strength and residual shear resistance of cement soil increased to 2.4 and 1.8 times those of clay, respectively. In the case of the interface shear strength of cement and steel, the maximal and residual shear resistance of cement-metal soils were 1.55 and 1.40 times

greater than soil-steel, respectively. Then, a formula was proposed for estimating shear resistance over 28 days and predicting the shear strength of the soil-cement mixture at 28 days based on the water content and cement weight.

In summary, the results indicated that the methods of reinforcing riverbed soil with geotextile, sand cushion, and cement are effective. Based on the results, the cement method was the most effective compared to these methods. Soil cement mixtures can be used as backfill material for roads with car traffic, whereas geotextile and sand cushions can be used for roads with car-free traffic. The results of laboratory experiments formed the theoretical basis for practical applications.

TÓM TẮT

Sử dụng đất sét nạo vét từ lòng sông thay thế cho cát san lấp nền đường giao thông được xem là giải pháp thay thế với nhiều lợi ích. Tuy nhiên, đất từ lòng sông là đất yếu, sức kháng cắt thấp, hệ số rỗng cao, tính thấm kém, đặc biệt là có độ trương nở cao và mất khả năng chịu lực khi bão hoà. Vải địa kỹ thuật, đệm cát và xi măng được sử dụng để gia tăng cường độ đất do tính phổ biến và hiệu quả. Các thí nghiệm trong phòng, bao gồm California Bearing Ratio (*CBR*), cắt 3 trục trong điều kiện *UU*, cố kết 1 trục với thiết bị cải tiến và cắt đất trực tiếp được hiệu chỉnh, được thực hiện để khảo sát sự trương nở, cường độ và quá trình cố kết của đất và đất gia cường. Từ đó, đánh giá khả năng áp dụng của các phương pháp gia cường này cho đất nạo vét từ sông Cái Lớn.

Vải địa kỹ thuật với tính thấm cao thúc đẩy nhanh quá trình trương nở của đất và độ trương nở giảm đến 1.3 lần. Bên cạnh đó, giá trị *CBR* tăng lên từ 1.1 đế 1.5 lần cho trường hợp không bão hoà và đến 3 lần khi mẫu bão hoà. Đặc biệt, mẫu gia cường bằng 2 lớp vải cho giá trị *CBR* lớn nhất. Trong thí nghiệm 3 trục với các mẫu không bão hoà, sức kháng cắt trong điều kiện *UU* của đất sét được gia cường bằng 3 lớp vải tăng đến 1.6 lần so với mẫu không gia cường và khoảng 2.1 lần khi mẫu bão hoà do tương tác giữa đất và vải. Trong các mẫu bão hoà, áp lực nước lỗ rỗng gia tăng khi chuyển vị nhỏ, sau khi có sự trượt giữa vải và đất, áp lực nước giảm nhanh. Bên cạnh đó, kết quả cố kết cho thấy, thời gian cố kết của mẫu gia cường giảm từ 1- 2 lần so với mẫu không gia cường có cùng chiều cao.

Trong thí nghiệm cố kết một trục đất gia cường, chiều cao mẫu phải lớn. Ma sát thành giữa đất và dao vòng cần phải được sét đến. Thiết bị cố kết cải tiến được giới thiệu để đo được lực ma sát giữa đất và dao vòng. Kết quả cho thấy áp lực ma sát tăng khi tỉ lệ đường kính và chiều cao *D/H* giảm. Ảnh hưởng của ma sát là đáng kể khi tỉ lệ *D/H* nhỏ hơn 2.5 và áp lực nén giảm đến 20% tại thời điểm kết thúc quá trình cố kết (*EOP*). Dựa trên phương pháp Taylor, phương pháp giải tích được đề xuất để dự đoán sự mất mát ứng suất và hệ số sai khác hệ số rỗng, *COV*, dọc theo chiều sâu

mẫu tại tời điểm kết thúc quá trình cố kết, *EOP*. Kết quả cho thấy, hệ số rỗng tăng dần theo chiều sâu và với tỉ lệ *D/H* lớn hơn 2.5, giá trị *COV* sẽ nhỏ hơn 1.2%.

Với phương pháp đất gia cường bằng đệm cát, độ trương nở và độ giảm trọng lượng đơn vị khô cũng giảm khi tăng bề dày đệm cát. Bên cạnh đó, giá trị *CBR* được cải thiện một cách hiệu quả cho trường hợp đất bão hoà hơn là trường hợp đất không bão hoà. Trong thí nghiệm 3 trục UU, sức kháng cắt trong điều kiện không bão hoà của đất sét gia cường đệm cát tăng khi áp lực ngang tăng. Sức kháng cắt mẫu không bão hoà với đệm cát dày 20mm tăng đến 1.9 lần so với mẫu không gia cường và khoảng 3.3 lần đối với mẫu bão hoà. Đặc biệt, áp lực nước lỗ rỗng trong mẫu thí nghiệm gia tăng khi chuyển vị nhỏ, sau đó, áp lực nước giảm mạnh. Bên cạnh đó, kết quả cố kết cho thấy, thời gian cố kết của mẫu gia cường giảm từ 3.5- 5 lần.

Xi măng đóng vai trò như chất dính làm giảm độ trương nở đất lòng sông từ 1.77 đến 2.5 lần khi hàm lượng xi măng gia cường tăng từ 3% đến 10%, so với trường hợp không gia cường. Trong trường hợp ngâm bão hoà, sau 28 ngày, giá trị *CBR* của xi măng đất được gia tăng từ 1.7 đến 3.8 lần so với trường hợp đất không gia cường. Cường độ kháng cắt của xi măng đất cũng gia tăng trong điều kiện nén 3 trục *UU* khi mẫu không bão hoà và bão hoà. Sự gia tăng cường độ của hỗn hợp xi măng đất là kết quả của quá trình hydart và pozzolanic của xi măng và đất, dẫn đến sự thay đổi thành phần hạt. Kết quả sau 28 ngày cho thấy, phầm trăm hạt cát tăng lên 2 lần cho trường hợp 10% xi măng. Sự phá huỷ giòn và sự gia tăng trong sức kháng cắt và sức kháng ma sát bề mặt được tìm thấy trong thí nghiệm cắt trực tiếp đất xi măng và thí nghiệm cắt trực tiếp bề mặt đất xi măng và kim loại. Sức kháng cắt đỉnh và sức kháng cắt bền của xi măng đất tăng đến 2.4 và 1.8 lần so với đất không gia cường. Các giá trị sức kháng cắt ma sát đỉnh và bền của đất xi măng – kim loại tăng đến 1.55 lần và 1.4 lần so với đất- kim loại. Từ đó, các công thức được đề xuất để dự toán sức kháng cắt theo thời gian đến 28 ngày và dự đoán sức kháng cắt của xi măng đất tại 28 ngày theo độ ẩm và khối lượng xi măng.

Như vậy, các kết quả cho thấy các phương pháp gia cường bằng vải địa kỹ thuật, đệm cát và xi măng có hiệu quả trong việc cải thiện đất lòng sông. Dựa trên các kết

quả thu được, so sánh các phương pháp, phương pháp gia cường bằng xi măng cho hiệu quả nhất. Hỗn hợp xi măng đất có thể dùng làm nền cho đường ô tô, trong khi phương pháp vải địa kỹ thuật và đệm cát có thể sử dụng cho đường nông thôn không có ô tô. Các kết quả được trình bày từ các thí nghiệm ở trong phòng, là cơ sở cho việc áp dụng thực tế.

TABLE OF CONTENTS

ABBREVIATION AND NOTATION

ABBREVIATION:

UU	:	Unconditioned- Undrained Condition
CU	:	Consolidated- Undrained Condition
CD	:	Consolidated- Drained Condition
CBR	:	California Bearing Ratio
EOP	:	The end of consolidation
COV	:	Coefficient of variation of void ratio
USCS	:	Unified Soil Classification System
DMM	:	Deep Mixing Method
LVDT	:	A linear variable differential transformer
CL	:	Low plasticity clay
CH	:	High plasticity clay (Fat clay)
MH	:	High plasticity silt

NOTATION

Basic SI units are given in parentheses.

D	:	Diameter of a sample (m)
H_0	:	The initial height of a sample (m)
H	:	The height of a sample at the end of primary consolidation (m)
e	:	Void ratio of soil (dimensionless)
P	:	The compression pressure due to external forces (Pa)
$P_{average}$	:	The average consolidation pressure (Pa)
R	:	The reaction pressure measured at the bottom of the specimens (Pa)
z	:	The depth from the top of soil sample (m)
t_z	:	Interface shear stress at the depth z of soil (Pa)
P_z	:	average consolidation pressure at the depth z of soil (Pa)
e_P	:	Void ratio at the top soil layer (dimensionless)
e_R	:	Void ratio at the bottom soil layer (dimensionless)

e_{EOP}	:	Void ratio at the end of consolidation (dimensionless)
PL	:	Plastic limit (%)
PI	:	Plastic index (%)
LL	:	Liquid limit (%)
G_s	:	Specific gravity (dimensionless)
γ	:	Moisture unit weight (N/m^3)
D_{50}	:	median particle size (m)
$D_{10}; D_{30}; D_{60}$	:	the diameter of a particle whose diameter is smaller than that, accounts for 10%, 30%, 60% of the total weight, respectively (m)
γ_d	:	Dry unit weight (N/m^3)
S	:	the swelling of soil (%)
S_{96h}	:	The percent swell after 96 hours of soaking (%)
s	:	Vertical swell (m)
CBR_1, CBR_2	:	*CBR* at 2.54 mm and 5.09 mm of penetration, respectively
R_{CBR}	:	The strength ratio was the ratio of the *CBR* of the reinforced specimen to that of the unreinforced specimen (dimensionless).
$P_1; P_2$	:	Value of pressure in piston (MPa) at 2.54 mm and 5.09 mm in CBR test, in turn (Pa)
σ	:	Compression pressure in soil (Pa)
σ_1	:	The vertical (longitudinal) compression pression (Pa)
σ_2, σ_3	:	The horizontal compression pression (Pa)
U	:	Pore water pressure (Pa)
$\Delta\sigma$	:	Increasement of compression pressure in soil (Pa)
Δu	:	Increasement of pore water pressure in soil (Pa)
C_c	:	Compression index (dimensionless)
C_v	:	Coefficient of consolidation (m^2/s)
$H_{drainage}$	:	The length of the drainage route (m)
$T_{100}; T_{90}; T_{50}$	:	Time related to the specific degree of consolidation (100%, 90% and 50% of consolidation) (second)
E	:	Elastic modulus (Pa)

ε	:	Axial strain (%)
ΔH	:	Soil settlement (m)
A	:	Cross-sectional area (m^2)
A_1	:	The average cross-sectional area due to lateral expansion (m^2)
c	:	The cohesion of soil (Pa)
φ	:	Internal friction angle of soil (degree)
ϕ'_{int}	:	Interface friction angle between the clay and the steel (degree)
K_p	:	Passive earth pressure coefficient (dimensionless).
S_u	:	Shear strength in the UU triaxial test of saturated samples (Pa)
h_{geo}	:	The geotextile spacing (m)
D_{piston}	:	the diameter of the load piston in *CBR* test (m)
R_{uf}	:	The shear strength increasement in the unsaturated condition due to reinforcement (dimensionless).
R_f	:	The shear strength increasement in the saturated condition due to reinforcement (dimensionless).
T_{shear}	:	Shear strength reduction due to saturation (%)
K_0	:	The horizontal expansion coefficient of soil (dimensionless).
P_0	:	The pre-consolidation pressure (Pa)
σ_{sd_Po}	:	the standard deviation of the pre-consolidation pressure (Pa)
h_{sand}	:	The height of sand cushion at EOP (m)
P_{b_sand}	:	the bottom pressure of the sand cushion (Pa)
P_{t_sand}	:	the top pressure of the sand cushion (Pa)
C_{c_sand}	:	compression index of the sand (dimensionless)
P_{o_sand}		pre-consolidation pressure of sand at the void ratio e_{0_sand} (Pa)
e_{0_sand}	:	the void ratio of sand at the pre-consolidation pressure (dimensionless).
H_{o_sand}	:	The initial height of the sand cushion (m)
K_{0_sand}	:	the coefficient of the sand cushion at rest (dimensionless).
ϕ'_{Int_sand}	:	interface friction angle between sand and ring (degree)

P_{ave_soil}	:	The average pressures at the center of all the soil (Pa)
$\lambda_{loss\ pressure}$	:	The loss pressure due to side friction (degree)
σ_{SD_H}/H	:	factional error of estimated height (%)
$\sigma_{SD\_P}/P_{o\_average}$	:	factional error of pre-consolidation pressure (%)
σ_{SD_e}	:	The standard deviation of the void ratio (dimensionless)
r	:	The reduction due to side friction (dimensionless)
H'	:	The height of specimens at EOP without side friction effects (m)
α	:	The height factor accounts for the effects of side friction. (dimensionless)
c_m	:	Cement content (%)
R_s	:	shear strength ratio of soil-cement mixture (dimensionless).
IEF	:	interface efficiency ratio (dimensionless)
q_u	:	the unconfined compressive strength of cement-treated soil (Pa)

LIST OF FIGURES

LIST OF TABLES

CHAPTER 1: INTRODUCTION

1.1. AN OVERVIEW OF THE RESEARCH DIRECTION:

Sand plays a vital role in construction and is the primary component of cement, asphalt, backfill, and other building materials. Nowadays, the demand for building sand in Vietnam is extremely high. In 2015, the demand for sand was approximately 92 million m3, but by 2020, it will increase by more than 1.7 times to 160 million m3. The nation's total amount of sand is around 2,300,000,000 m^3, with a yearly licensed capacity of 62,000,000 m^3. Hence, the supply only fulfills about 50% of the demand. For backfill sand, the yearly need is about 575 million m^3, and there are now 71 permitted organizations with a total capacity of 4.58 million m^3/year, which only meets 1% of the annual demand. According to Mr. Luong Duc Long, Director of the Institute of Building Materials (Ministry of Construction), using natural sand as a fill material is one of the primary causes of the shortage of sand. Especially for rural road construction in the Mekong Delta, sand for embankments is in high demand. Additionally, many primary and small projects, including the North-South Expressway, Long Thanh International Airport, and other residential neighborhoods and highways, will be under construction as Vietnam enters a time of robust economic expansion. Hence, sand is in high demand.

Sand is a naturally occurring granular substance composed of small stones and mineral particles. Natural sand includes mineral sand and river sand. The production of sand is much slower than required; the sand source is progressively depleted; river sand has a chance to form, and all mined sand will be exhausted. Additionally, building projects upstream or on the river, such as hydroelectric dams and irrigation, have obstructed the flow, halted the sand production process, and prevented the upstream sand from reaching its destination. Extracting sand from the riverbed will increase the danger of irrigation and transportation insecurities, negatively impacting the levees and the natural environment. In the past, when sand was mined, it was quickly formed, but in the last 7-8 years, when sand was extracted, it took a long time

to form, leading to the change of the riverbed and consequently the water flow. Excavating sand can affect an area of 5 to 10 kilometers (or even more).

Many road construction projects are facing the situation of needing more sand for backfill material. So, it is necessary to have solutions to supply more sand or use another material to replace sand. According to Resolution No. 46/NQ-CP issued by the Government on September 6, 2017; the Government Office's Notification No. 269/TB-VPCP dated June 15, 2017; and the Ministry of Construction's Official Letter No. 1421/BXD-VLXD dated June 22, 2017, the situation of using construction sand is rising. It is vital to have solutions to expand production, using materials to replace natural sand.

At that time, the annual cost of removing the soil from the riverbed was enormous, specifically in the Mekong Delta, where a dense network of rivers existed. So, the construction costs of rural roads will be drastically lowered if riverbed soil is substituted for sand. This method prevents the loss of local arable land, increases the riverbed depth, and mitigates the consequences of rising water levels caused by global climate change.

However, the muddy soil from the riverbed has a high void ratio and poor shear strength, creating instability and excess settlement for the works. When using riverbed soil to replace sand as a backfill, reinforced methods should be used to strengthen the soil's capacity.

1.2. REINFORCED METHODS

There are presently a variety of techniques for reinforcing poor soil. There are three noteworthy methods to improve its strength, including geotextile, sand cushion, and cement reinforcement, since they are cheap and popular.

1.2.1. Geotextile reinforcement

Geotextiles are frequently placed between layers of roadbed structure in roadbed construction. Geotextiles help promote soil durability and drainage. The load operating on the surface is predominantly vertical, whereas the geotextile's tensile direction is horizontal. Thus, the fabric's tensile strength and flexural stiffness have

little impact on the increase in the bearing load capacity of the platform under vertical wheel pressure. In reality, the geotextile pavement's load-bearing capability is primarily attributable to the separation function (to retain the design thickness and original mechanical properties of the pavement aggregate layers) rather than the structure's tensile strength. A sufficiently significant settlement in the road foundation structure is required to generate lateral tensile tension in the geotextile, but this settlement must be limited.

In the case of the construction of a bridge access road with a considerable embankment height, which may lead to the possibility of roof slippage or horizontal displacement of the embankment, geotextiles can be used as reinforcement to provide anti-slip force in the horizontal direction to increase slope stability. In addition, geotextiles provide a drainage function. Geotextiles can perform a drainage role to preserve and even improve the shear strength of the subsoil, enhancing long-term structural stability. Nonwoven, needle-piercing geotextiles with high water permeability are materials with good drainage vertical and horizontal drainage (perpendicular and parallel to the surface). Thus, this geotextile may rapidly exhaust excess pore water pressure, increasing the soft ground's shear resistance. Soil holding capacity and permeability coefficient are two evaluation criteria for the features of geotextiles. Besides, geotextiles must have a small pore size to prevent the passage of soil particles while having a pore size large enough to ensure adequate water permeability and dissipate the pore water pressure quickly.

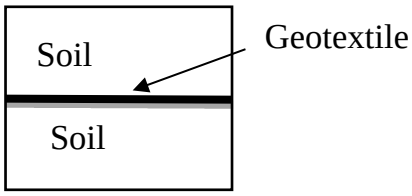

a) Geotextile b) Soil reinforced by a layer of geotextile

Figure 1.1: Geotextile and soil reinforced by a layer of geotextile

1.2.2. Sand cushion reinforcement

The sand cushion is formed by adding sand between two layers of geotextile. The sand cushion, like the geotextile, functions as a drainage border, forcing the rapid

pore water pressure to release rapidly. The sand cushion can be utilized efficiently for saturated soft soil layers (slurry clay, silt clay, mixed sand, silt, etc.).

In addition, it can work as a load-bearing layer, absorbing the building load and transferring it to the soft soil layers below. The sand mat can minimize the building's settlement and settlement differences due to the redistribution of stress induced by external loads in the soil beneath the sand buffer layer.

In addition, the sand layer has the following effects: reducing the depth of foundation burial, thereby reducing the volume of foundation materials; reducing the pressure of the construction work down to the value that the soft ground can resist; increasing the stability of the structure, even when a lateral load is applied, because the compacted sand increases the frictional force and the slip resistance; and speeding up the consolidation of the ground, thereby reducing the time required to complete the consolidation.

Besides, the sand cushion does not necessitate complex equipment during construction and is, therefore, frequently utilized.

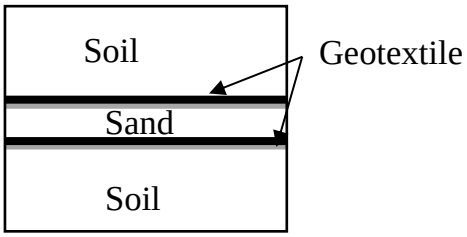

Figure 1.2: Soil reinforced by a sand cushion

1.2.3. Cement reinforcement.

This technique combines cement and soil in a particular proportion to form a soil-cement mixture with a greater load capacity. The mixed soil-cement can be used as a backfill or as a deep soil-mixed wall. For the former, its application can be widely used to increase the strength of embankments with or without pile sheets. For the latter, to make a deep soil-mixed wall for excavation support, H-piles are penetrated into the cement-soil mixture, enhancing the stability of excavations, decreasing the horizontal displacement of walls, and minimizing the excavation's impact on adjacent structures.

The cement and aggregate mixture considerably increase the strength and bearing capability of the clay. Strength is developed through the curing process of the soil-cement mixture. The cement reacts with water to produce calcium hydroxide $Ca(OH)_2$, which then combines with soil to form a CSH sealant called hydration. This quick and decisive reaction generates a great deal of heat and decreases the soil's moisture content. This hydration generates a combination that binds the improved soil's particle components to form stable, hard matrix minerals. The strength and permeability depend on the soil's chemistry and features (fine particle content, organic content, clay type, particle composition, etc.), the mortar's quantity and type, and the mixing procedure.

Due to its increased strength, this technique is commonly used to reduce settlement, increase ground stability, increase the stability of sloping roofs, strengthen shallow foundation pits, strengthen the foundations of buildings, reduce active soil pressure, and increase passive soil pressure on the walls of deep pits and ditches, etc.

Figure 1.3: The appearance of soil-cement as a base [1]

1.3. THE URGENCY OF THE RESEARCH

Using riverbed soil instead of sand for backfill material has brought numerous benefits to construction projects and environmental protection, particularly in the south of Vietnam. They include cost savings, the use of local materials, an increase in riverbed depth, the preservation of natural resources, and so on. Significantly, this solution can help solve the problem of lacking sand in many road projects. However, riverbed mud exhibits low characteristics such as a high void coefficient, low shear resistance, and a decrease in bearing capacity as moisture content rises. Hence, when utilizing riverbed silt instead of sand as a fulfilling material, the maintenance capacity

of the soil is a vital key. Reinforcement techniques, including geotextiles, sand cushions, and cement, have been explored and developed to improve soil capacity.

Consequently, research on utilizing geotextile, sand cushion, and cement to improve riverbed clay is necessary to maintain its strength as a backfill material in road construction. It would bring many benefits, such as conserving natural resources, reducing the cost of construction projects, and so on.

1.4. SPECIFICATION OF ROAD EMBANKMENTS

1.4.1. Road classification

Rural roads are defined by TCVN 10380:2014 [2] as linking roads from provincial roads and national highways to villages, hamlets, farms, etc., for the purpose of production and economic growth and categorized as district roads (grade A), commune roads (grades A, B), village roads (grade B, C), roads in production zones (with more than 10% of axle weights above 6000 kg), and residential roads (grade D). Grades A, B, and C are designed for 100–200 $x_{qd/day}$, 50–100 $x_{qd/day}$, and lower 50 $x_{qd/day}$, respectively, and grade D is car-free.

According to TCVN 4054:2005 [3], district roads are categorized as grades IV, V, and VI when the designed traffic volume is greater than 200 $x_{qd/day}$ and as grade VI when the designed traffic quantity is between 100 and 200 $x_{qd/day}$. Roads in production zones are likewise classified as grades IV, V, and VI.

1.4.2. Road embankment specifications

Regarding the subbase, TCVN 10380:2014 [2] specifies that the soil compaction coefficient must exceed 90%, and while installing the pavement, the soil compaction coefficient of the soil on the top 30 centimeters exceeds 93 percent.

TCVN 4054:2005 [3] specifies the following regulations for the pavement layer:

- The basement is not excessively moist and is unaffected by external moisture sources (rainwater, groundwater, and so on).
- The top 30 centimeters of soil must have a minimum *CBR* load capacity of 8 for roads graded I and II. It is 6 for roads of other grades.

- The following 50 centimeters of soil must have a minimum *CBR* load capacity of 5 for roads rated I and II and 4 for roads of other grades.

This standard specifies that the compaction coefficient for roads graded V and VI must be at least 0.95.

Regarding rural roads with car traffic, TCVN 9436-2012 [4] requires the swelling of the backfill material to be lower than 3%.

In summary, the swelling and capacity of the subbase are essential. The minimum *CBR* load capacity for rural roads is 6 for the top 30 cm and 4 for the following 50 cm, and the minimum compaction coefficient is 0.95.

1.5. LITERATURE REVIEW

1.5.1. International research:

a) Using riverbed soil as a backfill material for road construction

It is common practice to use riverbank soil for road construction and land reclamation [5]. These silty soils are very settled [6]. By analyzing settlement and permeability coefficients for weak mud, Zhang et al. [7] discovered that void ratio and clay content had a significant effect on the permeability of silt soil. The results indicate that the void ratio steadily decreases with time, and stabilization of the mud layer may take many years. Methods of reinforcement are utilized to strengthen the strength and speed the consolidation of this backfill soil [8, 9]. As a material that has low permeability, the use of soft clay as backfill needed an appropriate drainage system and construction techniques to guarantee its durability [10–12]. There have been numerous studies using geosynthetics and sand cushions as reinforcement to increase strength and handle the above challenges due to their high permeability. Besides, cement is added to soil to improve its mechanical properties, such as deformation behavior, shear strength, and permeability.

To evaluate the soil's improvement ability, the reinforcement method's swelling, strength, and consolidation need to be assessed. The California Bearing Ratio (*CBR*) test is usually used to determine the swelling and strength of soil, whereas the triaxial compression test was used to investigate the soil's strength under different conditions.

Besides, a one-dimensional consolidation test is usually utilized to evaluate soil consolidation.

b) Side friction in a one-dimensional consolidation test

The standard of the one-dimensional consolidation test specifies a minimum specimen diameter-to-height ratio, D/H_0, of 2.5 in order to reduce the effects of side friction between the specimen's periphery and the inside of the ring [13]. However, the reinforced samples are usually high due to the number of layers of geotextile and the sand cushion's thickness. For non-standard specimens, the side friction would significantly reduce the applied consolidation pressure during the one-dimensional consolidation test, resulting in an overestimation of the compression curve (i.e., *e-logP*) for settlement evaluation [14–17].

The factors controlling the side friction during the one-dimensional consolidation test have been investigated in earlier studies. Those factors included the diameter-to-height ratio of specimens, stress level, shear strength of soil, and interface shear strength between soil and the inner surface of the consolidation ring. The side friction increased significantly with the decrease in the diameter-to-height ratio of the remolded clay [16–18]. It was also suggested that a large D/H_0 can be used to minimize the impact of soil-wall friction [19]. For the stress level, several studies reported that the consolidation pressure loss was smaller when applying higher consolidation pressure [16, 17]. In addition, the specimens exhibited higher side friction in the over-consolidation pressure range than in the normally consolidated pressure range. When performing the test on the sample with the initial height H_0 = 60 mm and diameter D = 75 mm, Sivrikaya et al. [16] found that the friction was the most significant at low stresses where the clay was overconsolidating. Similarly, significant frictional pressure was observed for the Osawa Bay Clay in the over-consolidation range [17]. Last, the shear strength of the soil and the interface friction angle between the inner side of the ring and the soil also controlled the magnitude of side friction [14, 15, 20]. The side friction would be higher for soil specimens with a lower shear strength and a higher interface friction angle. Table 1.1

summarizes the variations in dimension parameters and compression pressures of the one-dimensional consolidation test in previous studies. Although a number of studies have determined the consolidation behavior of soils under the effects of side friction, most of the previous studies with side friction measurements examined specimens with a ratio of D/H_0 higher than 1.25. For other studies without the side friction measurement, the consolidation behavior of soil under the effects of friction pressure loss would not be able to be fully determined.

Table 1.1: Conditions of the one-dimensional consolidation test in different studies

D (mm)	H_0 (mm)	D/H_0	Compression pressure, P (kPa)	Side friction measurement	References
75	60	1.25	25-1600	Available	Sivrikaya and Togrol [16]
60	20	3.00	628-10045	Available	Watabe et al. [17]
65	10-40	1.63- 6.50	75-1200	Available	Nakase [18]
60, 120	20	3.00, 6.00	24.5-1200	Not avalaible	Kolay & Bhattacharya [21]
77	100-165	0.47-0.77	10-600	Not avalaible	Lovisa and Sivakugan [22]
61.8	20-100	0.62-3.09	50-1600	Not avalaible	Yao et al. [23]
50, 75	10-50	1.00-7.50	24.8-398.3	Available	This study

The side friction would induce various effects on the consolidation behavior of clay, which were also investigated previously. The reduction in the consolidation pressure caused by the side friction was the most significant effect, which had been evaluated using the friction pressure loss ratio [17]. It was defined as the ratio of the total friction pressure along the specimen height, T, and the compression pressure on the top of the samples, P. The side friction pressure would affect the compression curve of the soil at the end of the primary consolidation (*EOP*). For the case of Osawa Bay clay, although the friction pressure loss ratio exceeds 0.2, the influence of the friction pressure for the 20 mm-thick specimens on the compression curve (e-log$P$) was not significant [17]. On the other hand, Kolay et al. [21] conducted consolidation tests on kaolinite with a large diameter (120 mm) consolidation ring. The study

asserted that the effects of side friction on the coefficient of consolidation, coefficient of volume change, and compression index were more significant at low stress levels and diminished at higher stress levels. Furthermore, the side friction also causes the non-uniform void ratio condition in the soil specimens at *EOP*. The interface shear stress along the periphery of the soil specimens would reduce the average consolidation pressure, acting on the soil layer at depth *z*. The higher the depth, the lower the average consolidation pressure [14, 16]. As a result, the void ratio of the soil would not be uniform in the specimens. While the void ratio of the top soil layer, e_P, would be the smallest, that of the bottom soil layer, e_R, would be the highest, causing an uneven density in the soil specimens in one-dimensional consolidation tests.

In fact, when conducting laboratory experiments, the non-uniformities in soil properties that were previously examined were frequently observed. During triaxial experiments, Atkinson et al. [24] discovered that radial drains influenced the water content of specimens subjected to undrained loading followed by consolidation or rapid drained loading. Due to side drainage, significant nonuniformities can occur during the consolidation of soil specimens in routine triaxial experiments. Kolekar and Dasaka [25] were the first to present the variation of water content and undrained shear strength of reconstituted clay bed specimens under consolidation compression. Using a unit cell and detachable collar of 350 mm internal diameter and 520 mm and 250 mm heights, respectively, the soil samples were consolidated from a slurry state. According to the test results, the coefficients of variation (*COV)* of measured water content and shear strength were less than 10%. Mir et al. [26] observed a similar nonuniformity of these two parameters along the horizontal distance and the depth of clay specimens in a container measuring 350 mm in diameter and 500 mm in overall height. In addition, the study revealed that pre-consolidation pressures decrease significantly with depth (*COV* = 32%) and tend to become uniform after a certain depth, indicating highly non-uniform conditions. In previous investigations, the variation in the void ratio in consolidated specimens was not adequately quantified.

Previously, numerous analytical methods for predicting the side friction pressure have been proposed. Taylor [14] presented an early analytical method for estimating the side friction and friction pressure loss ratio in soil specimens at *EOP* under normal consolidation conditions. Using the measured results of the side friction between the specimen and consolidation ring with a newly designed oedometer cell [20], this method was validated. Lovisa and Sivakugan [22] also devised a similar analytical solution for determining the vertical effective stress within the soil by combining two components: the soil self-weight and the externally applied pressure. Last but not least, Monden [15] presented an additional analytical method for determining the side friction pressure in unloading and reloading cases, which was equivalent to the soil under an over-consolidation pressure range. However, the applicability of these prediction methods is limited because they are calculated based on the height of specimens at *EOP*, *H*, which is challenging to estimate prior to tests.

c) Geotextile reinforcement method:

Geotextile reinforcement has been widely used due to its essential qualities, which include filtration, drainage, separation, and reinforcing of soil layers [27].

According to Wu et al. [28], geotextiles are an environmentally acceptable way to strengthen soft soils, protect slopes, and serve as efficient drainage systems. There are various forms of geosynthetics: geotextile, geogrid, geonet, geomembrane, erosion control mat, geosynthetic clay liner, and geocomposite [29]. The main advantages of the fabric include lowering swelling, increasing the material's strength, and decreasing the soil consolidation time. The safety factor of soft ground increased by 1.2 times when geotextiles were utilized to reinforce it [30]. Sitharam and Hegde [31] presented a method for evaluating the load-carrying capability of a weak mud layer strengthened using geocell and geotextile mesh. According to research findings, this combination was more effective than geocell alone.

Malizia et al. [32] indicated that the water content significantly affected the strength and swelling of the soil. Wu et al. [33] showed that under identical local loading, the geosynthetic sheet reduced settlements more effectively than the free-

end condition due to the tensile strains of the geosynthetic sheet. The displacement resistance of geotextiles was confirmed by Guo et al. [34].

Many studies have analyzed the capacity of reinforced ground by *CBR* (California Bearing Ratio) laboratory experiments. With polyethylene, the *CBR* of sand was enhanced by three times [35]. Choudhary et al. [36] conducted *CBR* experiments to examine the strength and expansion of clay reinforced with a single layer of fabric or geogrid. At a particular depth, the reinforcement will have the greatest influence on the soil's strength and swelling. In lab and field checks, geogrid increased the *CBR* of wet clay by 1.9 to 2.6 times [37]. The *CBR* of geogrid clay was approximately 1.9 to 4.5 times that of clay for dry specimens. Under a wetting condition, Carlo et al. [38] conducted *CBR* experiments for fine soil on nonwovens reinforced with high-tenacity polyester yarns. The answers indicated that the trials with reinforcement had a higher maximal capacity than the samples without reinforcement. Additionally, the *CBR* of soil improved with 1 or 2 geogrid layers [39]. The tensile strength of reinforced specimens increases with the number of reinforced layers.

Regarding the soil capacity in *UU* triaxial compression tests, by using *CL* soil in Taiwan, Yang et al. [11] showed that as the number of geotextile layers increased, the shear strength of reinforced clay increased. The failure shapes were different from Classical Rankine-type to bulging between adjacent geotextile layers. Ingold and Miller [40] found that because the excess pore water pressure produced by undrained loadings can be eliminated through radial migration from the soil into the reinforcements, permeable reinforcements can increase the shear strength of reinforced clay. Al-Omari et al. [41] reported that experimental results of triaxial consolidation for drainage and non-drainage with geotextile-reinforced clay demonstrated improvement in both cases. When soil is draining, the effect is caused by an increase in the internal friction angle, whereas when soil is undrained, the effect is caused by an increase in the cohesive force component. By using the *CU* test, Yang et al. [42] showed that the geotextile can improve the shear strength of soil.

d) Sand cushion reinforcement method:

A sand cushion is a combination of sand and geotextile, in which sand is located between two layers of geotextile. Sand cushions are usually used to improve the soil's strength as well as handle weaknesses. Geotextiles with remarkable permeability enhance the reinforced soil's capacity to carry loads and maintain stability. Numerous studies confirmed the drainage function of geotextiles and sand cushions in enhancing the structure's load capacity and stability. Using geogrid-reinforced sand cushions increased the capacity of soft soil, and the subgrade reaction coefficient was improved by 30 times as well as the deformation, which was reduced by 44% [43]. Sitharam et al. [31] introduced the construction of a 3 m high embankment on the geocell foundation over the softly settled red mud, a waste product from the Bayer process of the aluminum industry. In this case, the combination of geocell and geogrid was recommended to stabilize the embankment base. Zhang et al. [44] applied sand cushion combined with geotextile under a breakwater on soft ground to limit the lateral movement of both the embankment and the soil, and the reinforcement suppressed high-stress levels in the system. The geotextile and sand cushion could improve the bearing capacity of the reinforced soil by up to 7 times [45]. Encapsulating geogrids in thin layers of sand to enhance the strength of clay was investigated in the direct shear test [46], pullout tests [31, 47], and triaxial compression test [48]. These results showed that a thin sand cushion improves the interface friction between clay and geotextile, leading to an increase in strength. This sand cushion was also a drainage boundary, decreasing the pore pressure with increasing loads. Regarding the drainage boundary, geotextile prevented the interlocking effect of fine particles of clay penetrating into the sand cushion layer [49]. Hufenus et al. [50] investigated the load-carrying capacity and behavior of geotextile-reinforced soft soils at full scale. According to research, only a thin layer of coarse aggregate sandwiched between geotextiles can reinforce porous soil. When settlement occurs on the roadbed, it induces long-term deformation and tensile force in the geotextile and creates a ground-reinforcing effect.

Many researchers performed laboratory tests to investigate the California Bearing Ratio (*CBR*) of reinforced soil. The *CBR* values of sand, when reinforced with high-density polyethylene, increased 3 times [35]. Similarly, the *CBR* of geogrid clay in the water condition could be enhanced by 1.9-2.6 times [37]. For unsoaked samples, the *CBR* value was about 1.9-4.5 times that of clay. With one or two layers of geogrid, the *CBR* value of lateritic soil was also increased. When increasing the number of layers, the load-bearing ability of the samples with reinforcement also increased. [39].

In the triaxial test, the optimum height of sand was 8-10 mm to effectively improve the strength and deformation behavior of reinforced clay soils under both static and cyclic loadings in the unconsolidated - undrainage test (*UU*) [48]. By using CL soil in Taiwan, Yang et al. [11] showed that increasing the thickness of the sand cushion from 5 mm to 10, 15, and 20 mm also led to an increase in shear strength in the *UU* test. The overall shear strength of the reinforced clay could be improved because of the increase in the interaction between the clay and reinforcement. Additionally, during the test, the sand served as a lateral drainage layer to release excess pore water pressure.

Nogami and Li [51] conducted consolidation experiments with horizontal (sand cushion and geotextile) and vertical (standing pipe) drainage systems. Based on the transformation matrix method, the traditional consolidation calculation method was devised to assess the level of consolidation, the pore water pressure under horizontal and vertical drainage, and the degree of consolidation.

Although there were many *CBR* tests to investigate the behavior of reinforced clay, the reduction of shear strength and the swelling of clay reinforced by sand cushions because of the soaking condition still needed to be entirely determined.

e) Soil-cement mixture

Cement is commonly used to increase soft soils' strength, stiffness, and stability [52]. The factors affecting the strength of soil cement included fine grain content, minerals, compaction, flow limit, moisture, pH, amount of cement added, and curing

time [53]. Horpibulsuk et al. [54] analyzed the strength development in clay and cement mixtures based on microstructure observation. Cement would fill the voids in the soil and combine with the compaction process to increase the density due to the soil particles sliding on each other. When adding cement at 3%, 5%, and 10%, the *CBR* value increased to 22%-69% after 4 hours of sample preparation [55]. Okonkwo and Nwokike [56] showed that the *CBR* value of soil from Anambra State ranged from 27% to 122% for the cement percentages of 5%, 5.5%, 6%, 6.5%, 7%, and 7.5%. These studies just concentrated on the strength and did not investigate the changes due to water content. Zoubi [57] investigated the swelling and *UU* shear strength of soil cement in Jordan at water contents of 15% and 17%. With 7 kPa of seating pressure, the swell of the soil treatment decreased for a cement content of up to 4%, then dramatically went up for a cement content of 4 to 6%. After that, the swell changed depending on the initial water content. Undrained shear strength was typically shown to rise as cement content increased from 0 to 20%; however, the maximum rate of this increase was found to be in the region of cement concentration between 6 and 10%. The characteristics of soil-cement included compressive strength, tensile strength, stress-strain relationships, and elastic properties [58]. According to Venkatarama and Gupta [58], doubling the cement content from 6 percent results in a 2.5-time improvement in strength. The modulus of the soil-cement block ranged from 2000 to 6000 MPa. When cement content was increased from 6 to 8 percent, elastic modulus multiplied by 2.5, whereas when cement content was increased from 8 to 12%, the increase in modulus was negligible.

On the other hand, there are 2 methods to create a cement-soil mixture: mixing and injecting cement into the soil, depending on the purpose. The former is commonly used for embankment, while the latter is frequently used for soil cement piles, called the deep mixing method (DMM). In the DMM procedure, cement is the most popular binder that is injected and mixed with soil utilizing a rotating shaft, paddles, or jet. In addition, temporary H-piles were installed in the excavation to support the shoring system vertically [59]. In these instances, the shear strength and interface shear

strength parameters would be utilized to quantify either the lateral earth pressure of the treated soil acting on sheet pile walls or the skin friction of the H-piles.

The improvement in characteristics of cement-treated soil has been attributed to the cement reaction. The primary cementitious materials are formed by the hydration reaction [60, 61]. The secondary pozzolanic reaction between the hydrated lime and the silica and alumina from the clay minerals results in the formation of calcium silicate hydrates and calcium aluminate hydrates. Hydration and pozzolanic reactions improved the strength of cement-treated soil, with hydration occurring in the early stages of hardening and pozzolanic reactions occurring considerably later [62]. As a result, the cementitious materials gradually fill the void spaces and enhance soil particle connections. Since the rate of strength development with time is mostly determined by the hydration process [63], numerous studies have used the strength of cement-stabilized soil at 28 days as a reference value [54, 64]. In the majority of prior investigations, a correlation between unconfined compressive strength and curing time was established to assess the rate of strength growth in cement-treated soil [54, 64]. Neither the development of the shear strength nor the interface shear strength of the treated soil have been determined in previous studies.

To determine the shear strength of soil, standard triaxial compression and unconfined compressive strength tests are the most typical laboratory techniques. According to the outcomes of laboratory experiments, the unconfined compressive strength of the cemented soil rose when adding cement [65–70]. The conclusions were based on the tests of different soil types, including Bangkok soft clay [65], [66], marine clays [67, 69], some Washington State soils [68], and silica sand [70].

Some research has demonstrated that the metrics of after-curing void ratio and water-cement ratio are enough to characterize the strength and compressibility of cement-treated clay [66, 67]. Several investigations using the triaxial compression test to examine the undrained shear strength of cement-treated soils have indicated that the undrained shear strength rises with increasing confining pressure and curing time [71, 72]. Under unconfined and triaxial compression, cement-treated soils

demonstrated much more brittle behavior than untreated soils [68]. For the plane strain test, laboratory tests revealed that the behavior of the soil-cement mixture's shear strength and excess pore pressure was comparable to that of overconsolidated clays [69]. A few studies have conducted direct shear testing of various types to investigate the shear behavior of the changed soil. The findings of the tests indicated that the cohesiveness and friction angle of cement-treated soil increased with increasing binder amount and cure time [73, 74]. Using direct shear and unconfined compression, the experimental investigations illustrated that the utilization of cemented specimens increased strength parameters, reduced displacement at failure, and changed soil behavior to a noticeable brittle behavior [73]. Sukpunya et al. [75] designed a large, simple shear test rig for determining the shear strength of stabilized soil columns in the composite ground. The study recommended that a correction factor be given to stabilized soil for slip circle analysis of stabilized soil columns.

The shear strength of the soil-steel interface was evaluated by utilizing the modified direct shear test apparatus. The most commonly used shear test apparatus was a conventional direct shear box, with the lower portions of the box replaced with an interface plate [73, 74, 76–78]. Tsubakihara et al. [76] estimate the effective interface shear behavior of clay and mild steel under consolidated-drained shear conditions using a direct, simple shear type of test apparatus. In addition, the ring shear box and conventional direct shear box were utilized to determine the shear properties of the clay-steel interface [77]. However, prior research rarely assessed the shear strength of the cement-treated soil-steel interface. Using a large-scale direct shear apparatus, Hamid et al. [78] investigated the interface shear performance of a bio-cemented soil-steel interface. The test results revealed that bio-cementation significantly increased the shear strength parameters of the soil-steel interface.

1.5.2. National research:

Geotextiles, sand cushions, and cement have been widely researched for basement applications. Vinh [79] suggested the solution of foundation treatment and stability calculation for a road graded III on a thin, soft soil layer. The research treated

soft soils with sand cushions, geotextiles, and melaleuca poles. The study proposed a method to calculate the coefficient of slippage safety for the natural foundation by considering the effect of the reinforced geotextile to increase the stability of the soft ground. Roanh [80] proposed methods for foundation treatment of the dikes and dams on soft ground. Research and analysis of some technologies to treat soft clay foundations included (1) using sand cushions that act as the bearing layer and drainage layer for the dam foundation; (2) using absorbent wicks to increase the permeability of soil through the vertical drainage system; (3) using a sand well that both acts as a vertical permeation boundary and plays the role of load-bearing, enhancing the foundation's bearing capacity; (4) using geotextile to reinforce the foundation, separating the foundation and the dam, distributing the embankment pressure, and increasing the soil strength; (5) using raft trees; (6) using sand piles; and (7) using soil-cement piles. The study showed that using materials such as sand or piles of bulk materials helps shorten the drainage distance by arranging drainage paths in the vertical and horizontal directions and on the ground surface, covering a drainage sand layer, and putting loads to accelerate consolidation. Additionally, Kham [81] proposed a graph of the relationship between c, φ, and the number of reinforced layers corresponding to each slope height value for Ha Giang soil.

Furthermore, Nguyen Minh Duc et al. [82] proposed that the cement and sand ratios were 150 kg/m^3 and 200 lit/m^3, respectively, to ultilized the material, and the *CBR* value increased 3.5 times (for only cement reinforcement) and 5 times for using both sand and cement. Binh [83] studied soil components' influence on cement-reinforced soil's strength by uniaxial compression. The results showed that, with organic content greater than 20%, the initial strength increased and decreased with curing time. A cement containing a lot of CaO would be suitable for saline soil.

Nguyen et al. [84] used the sheet pile wall integrated with soil cement to enhance the stability of excavations, decrease the horizontal displacement of walls, and minimize the excavation's impact on adjacent structures in the Mekong Delta. Additionally, sheet pile walls and cement-treated soil were also utilized to maintain

cofferdam structures and prevent water leakage between sheet pile wall segments during riverbed excavation in the Hau River [85].

There were many studies about soil in the Mekong Delta, but research about the soil reinforced by geotextile, sand cushion, and cement was not thoroughly investigated, especially the swelling, *UU* strength, and consolidation due to soaking.

1.5.3. Comments:

Improving the soft soil excavated from riverbed clay is necessary for road basements. Although there were some studies about the soil reinforced by geotextile, sand cushion, and cement, these methods were not entirely investigated, including:

- Previous studies showed results with many types of soils, but there were several separate studies about the soil in the Mekong River.

- The effects of the soaking process on the *CBR* strength reduction, the swelling, and the behavior of soil and reinforced soil under Unconsolidated-Undrained conditions in the triaxial consolidation test were not determined.

- Although there are many studies about the effect of side friction on the one-dimensional consolidation as well as the prediction of the compression pressure in soil layers, the applicability of these methods is limited because they are determined by the height of the samples at the end of primary consolidation, *H*, which is challenging to estimate prior to tests.

- The effects and behaviors of curing time and cement ratio on the peak and residual shear strength of soil cement and the peak and internal interface shear strength between the mixture and the steel were not entirely investigated. Besides, research on the change and the effect of grain size on its strength and interface shear strength was not extensive. The cement ratio was usually about 3% to 10% to reinforce the soft soil for backfilling.

- The previous study investigated the reinforced soil separately. Each study was about one property of reinforced soil. It needs a whole study about the application of reinforced soil.

Therefore, it is necessary to do more research on soil reinforced by geotextile, sand cushion, and cement for basements on transportation roads.

1.6. RESEARCH OBJECTIVES

1.6.1. Goals of the dissertation

Based on the literature review and the specifications of the road embankment, the soil's swelling, capacities, and soil consolidation are the most critical keys to evaluating if a material can be a backfill. When soft soil becomes wet, it needs to be reinforced to ensure its capacity. Geotextiles, sand cushions, and cement are the most popular and easiest ways to enhance soil strength. Thus, the research objectives are:

- Consolidation behavior of clay under the effects of side friction: analysis of friction pressure and non-uniform void ratio.
- Effect of *geotextile reinforcement* on swelling, *CBR* value, UU shear strength in saturated and unsaturated conditions, and saturated soil consolidation.
- Effect of *sand cushion reinforcement* on swelling, *CBR* value, UU shear strength in saturated and unsaturated conditions, and saturated soil consolidation.
- Effect of *cement reinforcement* on swelling, *CBR* value, UU shear strength in saturated and unsaturated conditions, and saturated soil consolidation. Additionally, direct shear tests were performed to investigate the behavior of the shear strength of soil cement and the interface shear strength between soil cement and steel under consolidated, drained conditions.

The laboratory experiments to achieve the above objectives are shown in Figure 1.4. In this study, the *CBR* test was chosen to evaluate the swell and strength of the soil and soil reinforcement. Besides, UU shear strength was used to investigate the soil and soil reinforcement when the road was built and loaded in a short time. Besides, during the construction process, the soil is subjected to its self-weight. And, the soil is sometimes subjected to an additional load to speed up the consolidation process and shorten the time to reach stability. Thus, an assessment of the settlement of reinforced soil is necessary. A one-dimensional consolidation test was performed to

explore the settlement of soil and reinforced soil under load. However, when the soil was reinforced by sand cushions and geotextiles, the height of the samples was usually high. Therefore, the effect of side friction between soil and ring must be explored by a one-dimensional consolidation test with many samples' diameters and heights. Finally, for the cement methods, a modified direct shear test was examined to explore the interface shear strength of cemented soil and steel. It would be beneficial if soil-cement mixtures were used as backfill after steel sheet piles. In this case, the interface shear between the soil or cement-treated soil and the steel is needed to calculate the active earth pressure coefficient, K_a, and passive earth pressure coefficient, K_p, by the Coulomb equations, as follows:

$$K_a = \frac{cos^2(\phi' - \eta)}{cos^2\eta\, cos(\eta+\delta)\left[1+\left(\frac{sin(\phi'+\delta)\, sin(\phi'-\beta)}{cos(\eta+\delta)\, cos(\eta-\beta)}\right)^{\frac{1}{2}}\right]^2} \quad (1.1)$$

$$K_p = \frac{cos^2(\phi' + \eta)}{cos^2\eta\, cos(\eta- \delta)\left[1-\left(\frac{sin(\phi'+\delta)\, sin(\phi'+\beta)}{cos(\eta-\delta)\, cos(\eta-\beta)}\right)^{\frac{1}{2}}\right]^2} \quad (1.2)$$

In which: ϕ' (degree): internal friction angle between the wall and soil.

η: an angle that the wall face is inclined to the vertical

β: an angle that the backfill is sloping to the horizontal.

The outstanding results of this research will be:

- The effect of the soaking process on the swelling and *CBR* of soil reinforced by geotextile, sand cushion, and cement.
- The reduction of UU shear strength due to the soaking process.
- A modified oedometer was introduced to measure side friction pressure in the one-consolidation test with many different diameter-to-height ratios. Then, a modified method was developed to predict the friction pressure loss ratio and analyze the void ratio distribution along the depth of the clay specimens, and the *COV* at the end of primary consolidation.
- The effect of cement and curing time on the shear strength, the interface shear strength of soil cement, the grain size, and the brittle behavior under

high deformation. And an equation with a high correlation coefficient was proposed for predicting the ratio in strength development of cement-treated soil with the curing period.

The outcome of the study would be the basic concept of using the riverbed soil reinforced by geotextile, sand cushion, and cement for backfill.

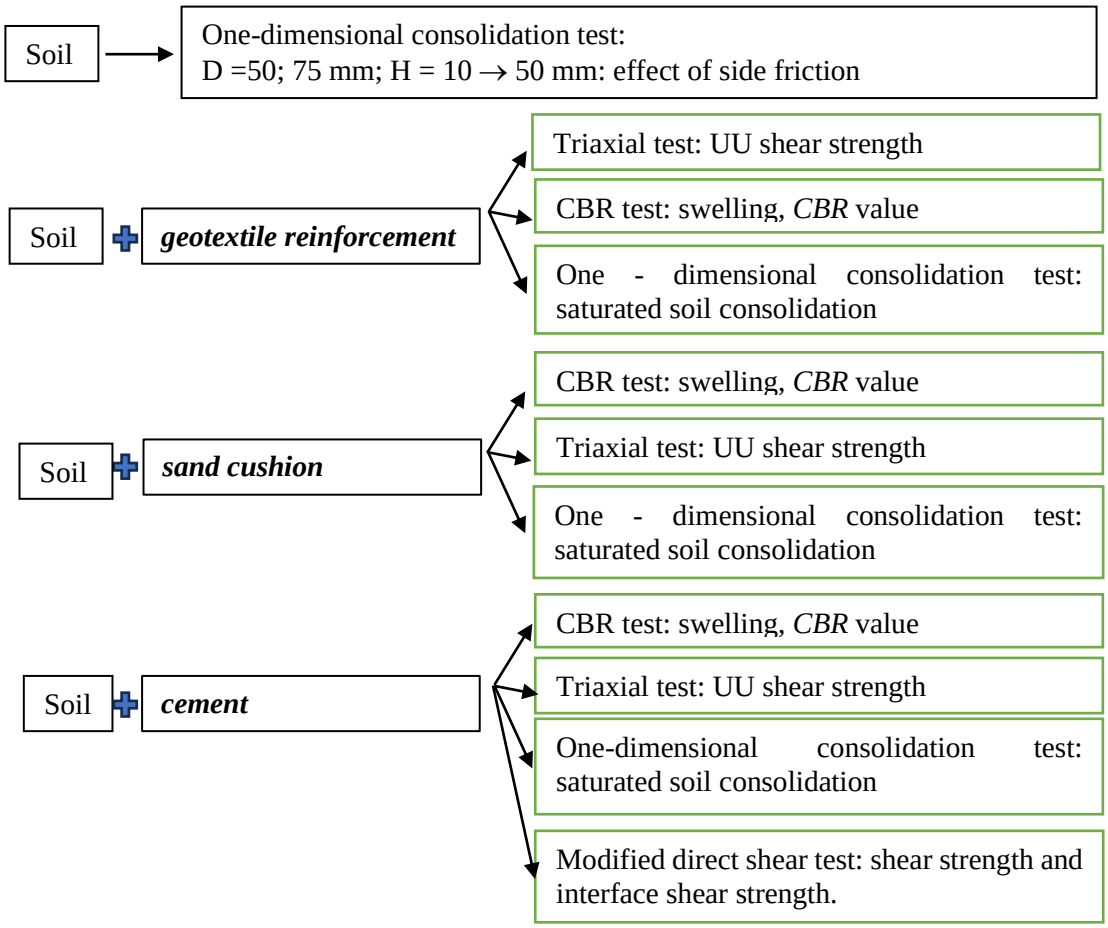

Figure 1.4: The laboratory experiments in this study.

1.6.2. Research scope

The research scope of this study includes the following:

- The soil was excavated from the Cai Lon River in Kien Giang Province.

- Experiments were performed on the remolded samples. Using the remolded sample will eliminate unwanted effects and evaluate the applicability of reinforced riverbed soil as a backfill for roads.

- The outcome of the research would be the basic idea of enhancing the soft soil from riverbeds for backfill instead of costly sand for the basements of countryside roads. The application needs further study with many field tests.

- The results would illustrate the improvement of the soil. Because the water content increases, the silty soil loses its strength. Particularly, the case where the soil was saturated was considered the weakest and most critical condition. Thus, this study just demonstrates the effect of saturation on the strength behavior of reinforced soil. Therefore, this study did not focus on the mechanical behavior of the unsaturated samples when the strength changed. Particularly, the effect of matrix suction on the UU strength of unsaturated samples was not examined.

- In this research, the consolidation settlement under permanent loads will be investigated. The loads that cause consolidation settlement can be self-weight, the cover layers of the road, or pre-loads under the construction process. The elastic settlement due to the live loads or cycling loads will not be investigated in this study.

The contents of this research are as follows:

Chapter 1: Introduction

Chapter 2: Materials – Theories – Modified Devices.

Chapter 3: Behavior of silty soil reinforced by geotextile under CBR, UU, and consolidation tests.

Chapter 4: Behavior of silty soil reinforced by sand cushion under CBR, UU, and consolidation tests.

Chapter 5: Behavior of silty soil reinforced by cement under CBR, UU, consolidation, and shear tests.

Chapter 6: Conclusions and Recommendations.

CHAPTER 2: MATERIALS – THEORIES- MODIFIED DEVICES

2.1. MATERIAL

2.1.1. Riverbed soil:

a) Soil properties

This study utilized soil collected from the Cai Lon River in southern Vietnam. Its properties are shown in Table 2.1:

Table 2.1: Soil properties

Property	Value
Unified Soil Classification System	MH
Plastic limit, *PL* (%)	44.9
Plastic index, *PI* (%)	46.6
Specific gravity, G_s	2.75
Moisture unit weight, γ (kN/m^3)	16.13
Void ratio, *e*	1.57
Water content (%)	57.4
Saturated degree (%)	96.6
Liquid limit (%)	91.5

According to the Unified Soil Classification System (USCS), the soil is classified as riverbed silty soil with high swelling potential. When $PI > 35$ and $LL > 70$, the soil has a high swelling ability [86–88]. Additionally, the free swelling index (based on IS:2720-40 [89]) was 45.9%, confirming the great expansive soil characteristics during inundation. Figure 2.1 depicts the grain size, where the sand content, fines content, and median particle size, D_{50}, are 12.3%, 87.7%, and 0.006 mm, respectively. The ignition loss of the soil was 3.96% at about 900 ^{0}C at which the decarbonization would be completed [90]. Although the ignitability loss cannot definitively indicate the amount of organic matter in the samples, it does indicate minimal organic content.

The water content of natural soil was 57.4%, which was difficult to compact. The soil needs to be dried to decrease the water content. Duc et al. [91] showed the

time to decrease the water content of riverbed silty soil from An Giang province, which was similar to silty soil in this study. In this research, a silty soil layer with a thickness of 0.5 m took 3 weeks to decrease its water content from about 50% to 46%. However, with 5 cm of sand cushion under this soil layer, after 3 weeks, its water content decreased to 34%, which can be used for compacting. The construction diagram for drying silty soil using two methods is shown in Figure 2.2.

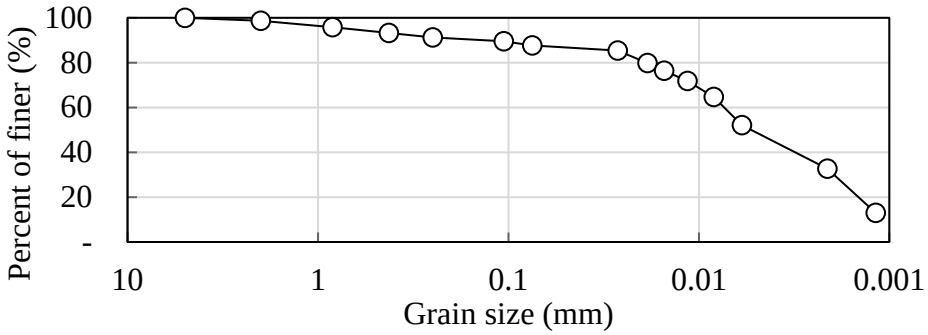

Figure 2.1: Grain size distribution of the soil

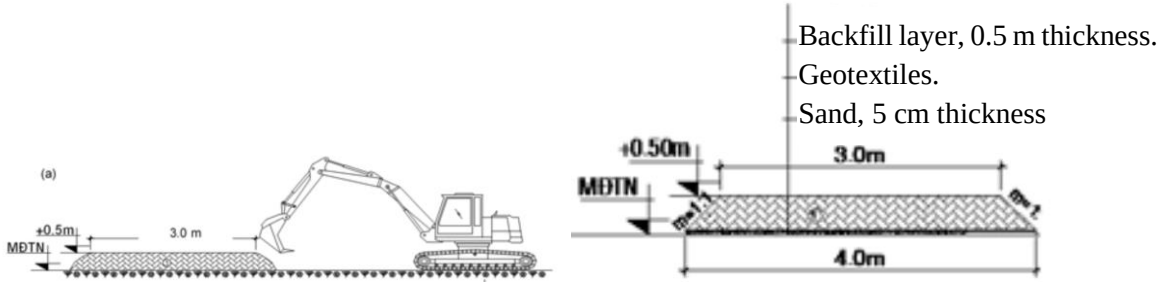

a) Conventional drying method b) A layer of sand cushion

Figure 2.2: Construction diagram for drying mud according to methods (a) conventional drying method; (b) a layer of sand cushion

b) <u>Process of remolding silty soil</u>

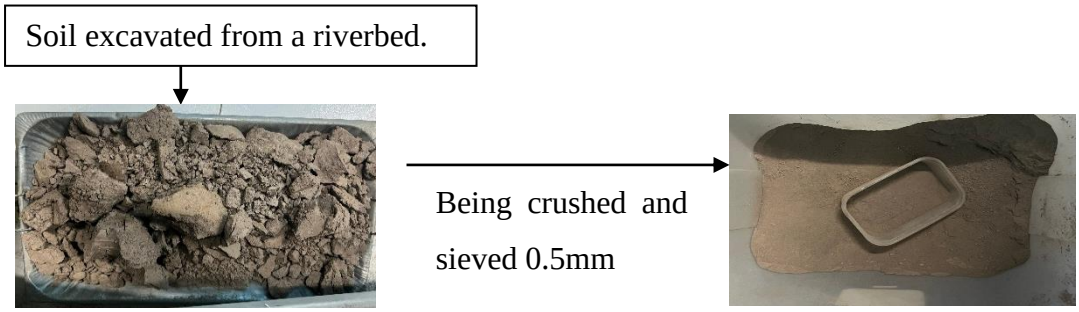

Silty soil after being filtered and dried

Remoulded soil

Figure 2.3: Process of recycling soil

The excavated soil was filtered and dried in an oven at 105 ^{o}C to remove garbage and organic impurities such as leaves, roots, etc. The material was then broken and polished into a powder. This powder was then filtered through a sieve of 0.5 mm and placed in an oven for 24 hours to release the water. This flour was ready to be used with the desired amount of water and/or cement. The process is shown in Figure 2.3.

2.1.2. Geotextile

A geotextile made of polyethylene terephthalate, which was nonwoven and needle-punched, was used. The geotextile's properties are briefly described in Table 2.2. This geotextile is suitable for reinforcement because its permittivity and cross-plane permeability are 1.96 s^{-1} and 3.5x10^{-3} m/s, respectively.

Table 2.2: The nonwoven geotextile properties

Property		Value	
Fabrication process		Needle-punched PET nonwoven geotextile	
Mass (g/m2)		200	
Thickness (mm)		2.78	
Apparent opening size (mm)		0.11	
Permittivity (s-1)		1.96	
Cross-plane permeability (m/s)		3.5x10-3	
Wide-width tensile test			
Direction	Ultimate strength (kN/m)	Failure strain (%)	Secant stiffness @ peak value (kN/m)
Longitudinal	9.28	84.1	11.03
Transverse	7.08	117.8	6.01

The following figure displays the settlement of a geotextile layer under many pressures over time. This figure was used to calculate the settlement of soil reinforced by geotextile layers based on the total measure of the specimen's settlement.

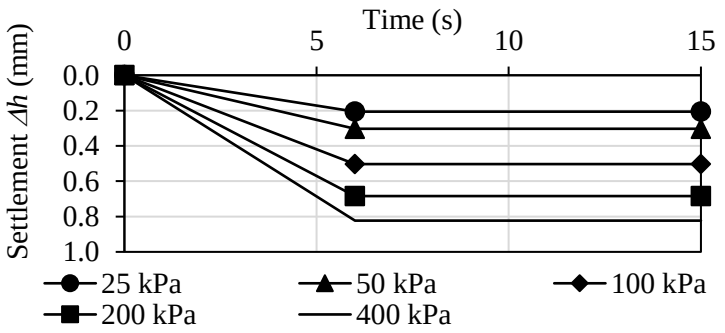

Figure 2.4: The settlement of a geotextile layer under pressure

Under pressure, the geotextile settles after a brief period, approximately six seconds, and becomes stable.

2.1.3. Uniform quart sand

Sand with the following properties is classified as clean sand: few fine particles and poor gradation, which is suitable for reinforcement. Its type is *SP*, according to the Unified Soil Classification System.

Table 2.3: Sand properties.

Property	Value
Unified Soil Classification System	*SP*
Specific gravity, G_S	2.66
D_{10} (mm)	0.121
D_{30} (mm)	0.169
D_{60} (mm)	0.242
Coefficient of curvature,	0.98
Coefficient of uniformity,	2.00
Minimum dry unit weight, $\gamma_{d\text{-}min}$ (kN/m^3)	12.56
Minimum void ratio e_{min}	0.692
Maximum dry unit weight, γ_{d_max}(kN/m^3)	15.43
Maximum void ratio e_{max}	1.078
At relative density, $D_r = 0.9$	
Dry unit weight, γ_d (kN/m^3)	15.09
Void ratio at D_{90}, e_{D90}	0.730
Friction angle from direct shear test (deg)	35.1

The grain-size distribution of sand was shown in Figure 2.5:

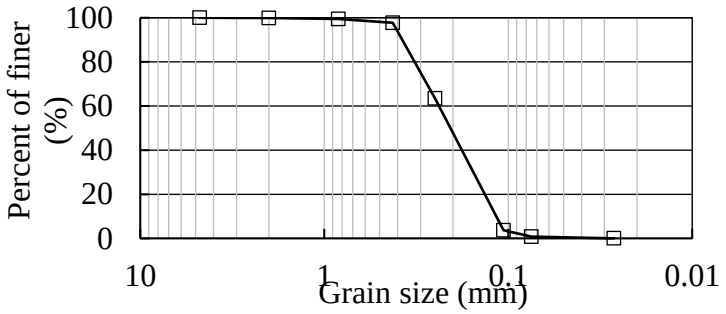

Figure 2.5: Sand's grain-size distribution

In this investigation, the sand experienced a relative density of 0.90. This density is average, easy for construction, and suitable for road backfill in rural areas.

The displacement of the sand cushion (including 2-layer geotextiles) under pressure happens in a brief period, approximately six seconds, and becomes stable, as shown in Figure 2.6.

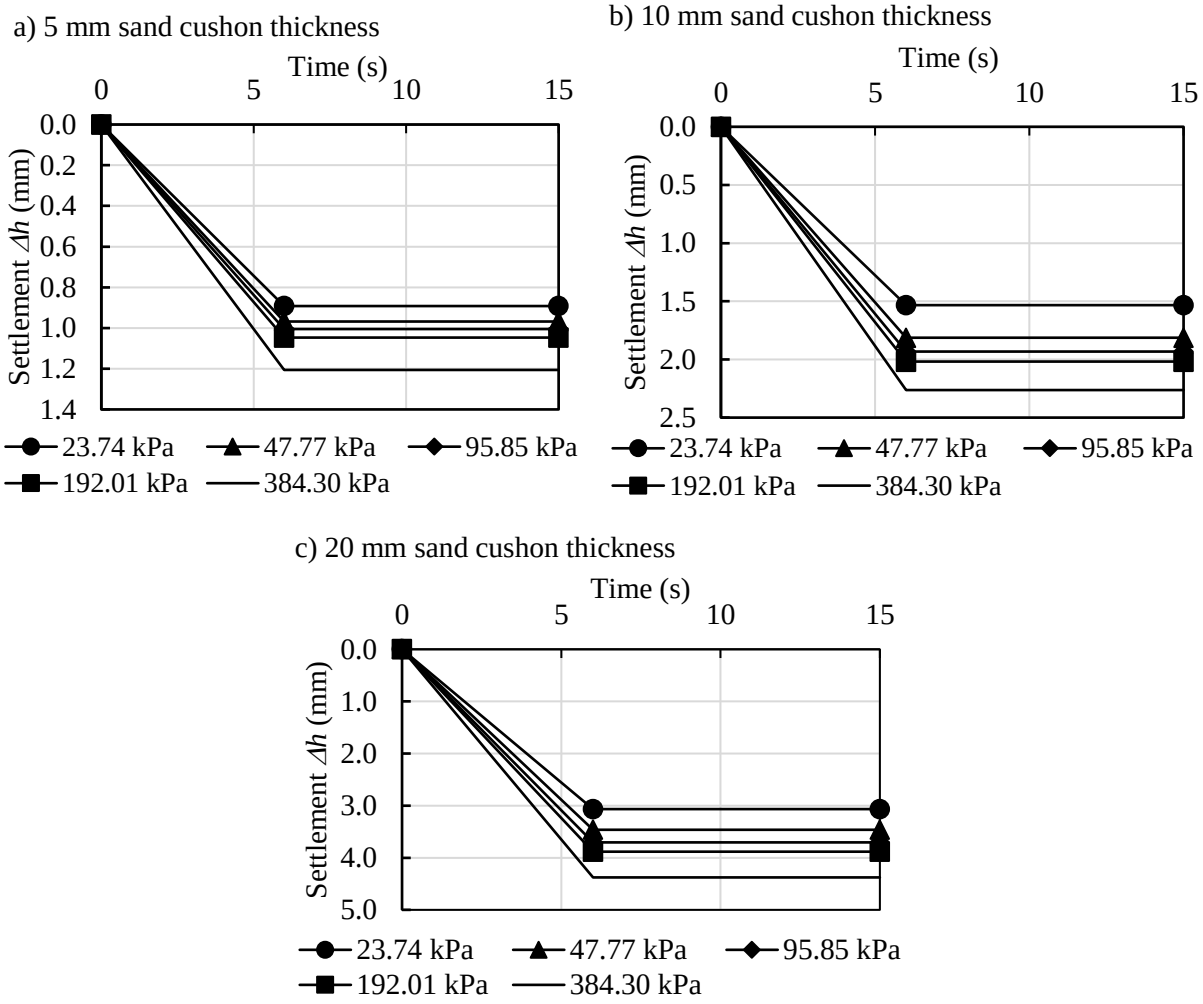

Figure 2.6: The settlement of a 5-, 10-, and 20-mm sand cushion under pressure

2.1.4. Ordinary Portland cement

Normal Portland cement PC40 with a specified density of 3 g/cm^3 was used in this study (ASTM C188 [92]) to improve the soil capacity. In accordance with ASTM C595 [93], the specific surface area (Blaine method) was 2800 cm2/g, and 10% of the sieve size was preserved. Using ASTM C191 [94], the initial and final setup times were roughly 185 minutes and 480 minutes, respectively. In addition, the minimum required compressive strength at 3 days and 28 days was 21 and 40 MPa, respectively. The result of the Le-Chatelier apparatus test was 10 mm. Table 2.4 presents the oxides

of ordinary Portland cement, PC40. Note that the ratio of CaO to SiO_2 was greater than 2.0, and the MgO content was less than 2.0%, which conformed to the European Cement Standard's specifications (EN 197-1) [95].

Table 2.4: Oxide composition of ordinary Portland cement PC40

Types of oxides	SiO_2	Al_2O_3	CaO	Fe_2O_3	MgO	SO_3	K_2O	Na_2O
Content (%)	22.0	5.5	64.5	3.0	1.5	2.0	0.6	0.2

2.2. EXPERIMENTAL THEORIES

2.2.1. California Bearing Ratio Test

The California Bearing Ratio (*CBR*) of pavement subsoil, subbase, and base course aggregates can be evaluated using this test method from experimentally compacted samples [96, 97].

The specimens were compacted using a 152.4 mm in diameter by 116 mm in height. Five layers of compaction were used to form a specimen. The compression energy level was 482 kJ/m3. (10 strikes per layer).

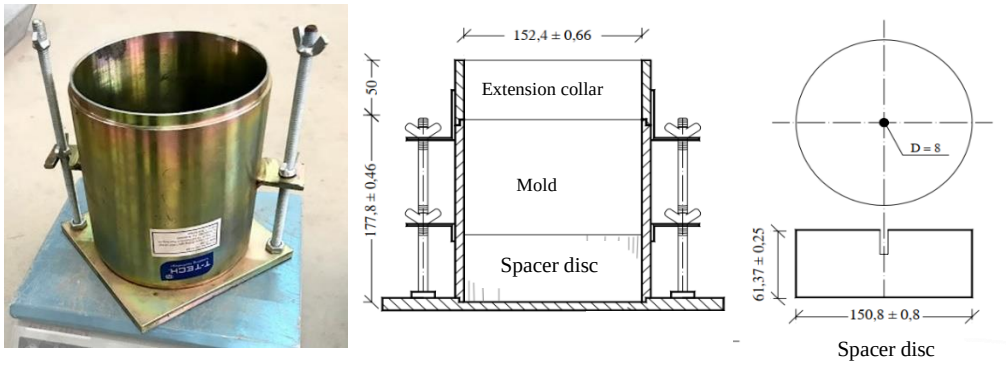

Figure 2.7: Mold with extension collar and spacer disc

The soil's quantity for every layer was determined by a series of compaction studies in many trials. The soil's quantity should be adequate for the final layer to extend slightly into the collar but a maximum of six millimeters above the upper edge of the mold. Prior to removing the collar for trimming the compaction specimen, the adjacent soil was trimmed to separate it from the collar and to avoid disrupting the soil beneath the top of the mold. Using a cutting instrument, the compacted sample was leveled with the top of the mold. The surface on top of the mold was then smoothed with a straight edge after any holes were packed with unused soil and

compressed using the fingertips. After that, the moisture weight, together with water content, was determined. The samples are ready for the *CBR* test or are soaked for 96 hours to measure swelling before *CBR* tests.

The swelling of the soil can be measured as follows:

$$S = \frac{s}{H_0} \quad (2.1)$$

in which: *S* (%): the swelling of soil

s (mm): vertical swell.

H_0 (mm): soil's height before soaking.

The *CBR* was calculated using ASTM D1883 [97], which states that the penetration rate is roughly 1.27 millimeters per minute. The examinations were terminated when the penetration achieved 20 millimeters, and the piston's pressure was measured over time. As advised by ASTM D1883, it was also adjusted due to surface imperfections or other causes. The *CBR* value was calculated as follows:

$$CBR_1\ (\%) = \frac{P_1}{6.9} x\ 100 \quad (2.2)$$

$$CBR_2\ (\%) = \frac{P_2}{103} x\ 100 \quad (2.3)$$

CBR_1 and CBR_2: *CBR* at 2.54 mm and 5.09 mm of penetration, in the same order.

P_1; P_2: value of the pressure of the piston (MPa) at 0.254 cm and 0.509 cm, in turn.

When CBR_1 is larger than CBR_2, the *CBR* value is CBR_1. On the contrary, repeat the test, and whether the result displays the same outcome, use CBR_2.

2.2.2. One-dimensional consolidation theory

a) Consolidation process

When a load, such as a building load, is applied to the soil, it experiences compressive pressure. The rearrangement of soil particles or the release of water and/or gas is called compression. Consolidation, according to Tezaghi, is the process of lowering the volume of water in saturated soil due to the lack of grain rearrangement. When compressive stress is applied to saturated soil, the water pressure instantly rises. The consolidation process refers to the progressive settlement of soil caused by sluggish water drainage due to inadequate soil permeability. It can

be assumed that soil and water particles are not compressed during consolidation. As a result, the rapid rise in stress induces an increase in pore water pressure. Pore water pressure progressively dissipates as it drains out of the soil. When all the pore water pressure has gone, the soil is consolidated. The mineral particles of the soil are considered uncompressed during consolidation.

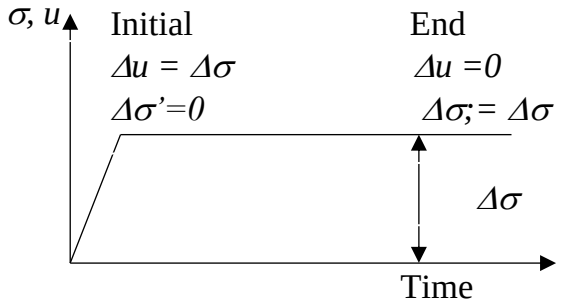

Figure 2.8: Change of pore water pressure during the consolidation process

If the soil becomes saturated, the drop in soil volume equals the amount of water released and is stated as a change in the void ratio, Δe.

b) <u>One-dimensional consolidation test</u>

The one-dimensional consolidation test aims to determine the soil's settling under vertical pressure because of the drainage process. Due to the rigidity of the ring, which contains soil, there is no lateral movement of soil during the test. With ASTM D2435 [13], the minimum specimen diameter shall be 50 mm, and the minimum beginning specimen height shall be 12 mm [0.5 in], but it shall not be less than 10 times the maximum particle diameter. The minimum specimen diameter-to-height ratio shall be 2.5 to reduce the impact of friction between the specimen's periphery and the inside of the ring. The optimal proportion is 4.

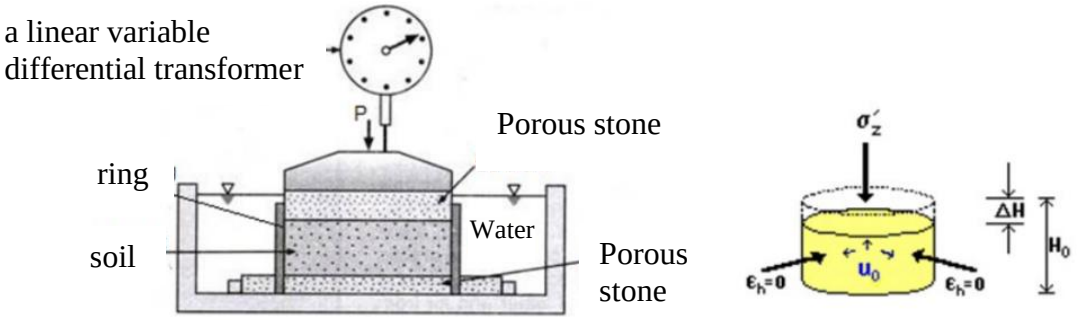

Figure 2.9: One-dimensional schematic

Based on the settlements of soil under different pressures, other soil parameters can be calculated, including compression index C_c, coefficient of consolidation C_v, void ratio- pressure curve, permeability coefficient, etc.

c) Determine the coefficient of consolidation C_v

The value of the consolidation coefficient C_v for each applicable load increase can be calculated by the D. Taylor method or the Cassagade method, using the following equation and interpretation-appropriate values:

$$c_v = \frac{0.848\ x(H_{drainage})^2}{T_{90}}\ or\ c_v = \frac{0.197\ x(H_{drainage})^2}{T_{50}} \qquad (2.4)$$

In which: $H_{drainage}$ (cm): the length of the drainage route at 90% or 50% consolidation, for double-sided drainage, is half the sample height at the appropriate increment, but for one-sided drainage, $H_{drainage}$ is the full specimen height.

T_{90}; T_{50} (second) time related to the specific degree of consolidation (90% and 50% of consolidation)

C_v (cm^2/s): the coefficient of consolidation

2.2.3. Triaxial Compression Test – Modified Triaxial Apparatus:

a) Triaxial compression test:

The value of soil strength depends on the building rate, the water drainage rate, and the calculation's objective. For a more accurate reflection of a soil sample in the field, a triaxial compression test is performed. In addition to determining the shear strength parameters, the triaxial compression test also determines the ground's deformation characteristics (pore water pressure u, elastic modulus E, Poisson coefficient ν, etc.). The benefits of the triaxial compression test include the following:

- Explain the load conditions of the soil during the actual building by applying strains in all three directions simultaneously.
- Via the adjustment of drainage valves, describe the actual behavior of the ground: drained - undrained, consolidated - unconsolidated.
- Control and measure pore water pressure and sample volume change.

- Furthermore, the triaxial compression test reveals the natural sliding angle of the soil as it is destroyed, allowing the sample cross-section to expand during the test, and so on.

Depending on the soil's properties and drainage conditions, there are three types of triaxial tests:

- The Unconsolidated – Undrained Test (*UU*): The principle of this test method is to measure the undrained shear resistance of a cohesive clay sample. The specimen is subjected to constant lateral pressure and axial force, with no volume change permitted. This test method is solely applicable to clays and is used to determine undrained strength.
- The Consolidated- Undrained Test (*CU*): Under this test procedure, the specimen is initially immobilized under constant isotropic stress (consolidation phase). Water can escape from the soil. When the axial load increases after the consolidation phase, and no drainage is permitted (compression phase), the initial consolidation phase transitions to a condition of definite volume and pore water pressure.
- The Consolidated-Drained Test (*CD*): In this test method, the material is first immobilized under constant isotropic tension (consolidation phase). After the consolidation stage, raise the axial load at a rate small enough to prevent an increase in pore water pressure (compression phase) and assess the sample's volume change by measuring the changes in water volume. The objective of this test method is to evaluate the effective shear parameters when the specimen is damaged, as well as the features of the specimen's volume change when it escapes during the shearing process.

b) Modified triaxial apparatus:

A modified triaxial schematic is shown in Figure 2.10, in which there is a small pipe from the middle of the sample to the pressure device to record the pore water pressure. As depicted, a rubber membrane is wrapped around the cylindrical soil sample to control drainage conditions. The specimen's upper cap and pedestal are

linked to tubes “ab” and “cd” in order to measure the specimen's volume change during the drained test. During the undrained test, they can also be used to monitor the pressure of the subsurface water.

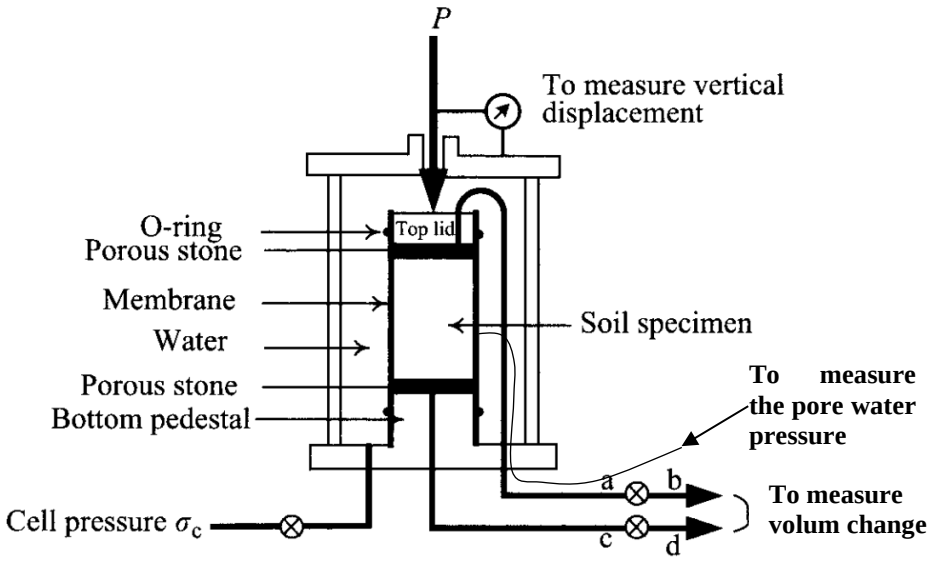

Figure 2.10: A modified triaxial compression aparatus

The triaxial test consists of two phases. In the initial phase, cell pressure is applied to the specimen. In the second stage, apply axial pressure until the specimen fails, at which point shear stress will begin to act on the specimen. By controlling the cell pressure and axial pressure, the stress conditions can be controlled $\sigma_2 = \sigma_3 = \sigma_c$, allowing for the performance of numerous sorts of stress path studies.

c) Unconsolidated- Undrained test (UU) for unsaturated samples

Test specimens:

- Based on ASTM D2850-03 [98], the samples must be cylindrical and a minimum of 33 mm in diameter. The ratio of height to diameter must be between 2 and 2.5. In this research, the diameter and height of the specimens are 50 and 100 mm, respectively.

- The strain rate in *UU* tests is typically 1% per minute.

- The stress state at which a specimen fails. Failure is commonly equated to the greatest principal stress difference (deviator stress) achieved or the principal stress difference (deviator stress) at 15% axial strain, whichever occurs first during the implementation of an experiment.

Unconsolidated- Undrained test (*UU*) was performed as follows:

- The specimen is placed on the base. Put the rubber membrane around the specimen and seal it with O-rings or other positive seals at the cap and bottom. A thin layer of silicone grease on the vertical surfaces of the cap or base improves the membrane's closing.

- Assemble the triaxial chamber with the specimen encased in the rubber membrane, which is attached to the specimen cap and base and positioned in the chamber. Several attempts should be made to bring the axial load piston into contact with the specimen cap to ensure appropriate seating and position. Throughout this operation, take care not to exceed 0.5% of the specimen's anticipated compressive strength when applying axial stress. If the weight of the piston is sufficient to provide an axial stress that exceeds about 0.5% of the projected compressive strength, lock the piston after confirming proper fitting and position and keep it locked until the chamber pressure is applied.

- Install the chamber into the axial loading device. Carefully match the axial loading device, the axial load-measuring device, and the triaxial chamber to avoid lateral forces from being applied to the piston during testing. Fill the chamber with the confining liquid and attach the pressure-maintaining and pressure-measuring apparatus. Set the pressure-maintaining and pressure-measuring apparatus to the required chamber pressure, and then apply pressure to the chamber water. Before applying the axial load, allow the specimen to stabilize under the chamber pressure for about 10 minutes.

- Apply the axial load to induce axial strain at a rate of roughly 1%/min for plastic materials, achieving maximal deviator stress at a strain of approximately 3 to 6%. At these rates, maximum deviator stress will be reached in around 15 to 20 minutes. Continue loading to 15% axial strain unless the deviator stress has peaked and fallen 20% or the axial strain has surpassed the strain at which the deviator stress peaked by 5%.

- Record load and deformation data to three significant digits at about 0.1, 0.2, 0.3, 0.4, and 0.5% strain; then at increments of approximately 0.5% strain to 3%; and finally, every 1%.

Test results include:

- Axial strain ε:

$$\varepsilon = \frac{\Delta H}{H_o} \tag{2.5}$$

Where: H_0 (mm)– the initial height of the specimen (mm);

ΔH (mm)- soil settlement under axial load, (mm).

- The average cross-sectional area A_1 (mm^2):

$$A_1 = \frac{A}{1-\varepsilon} \tag{2.6}$$

Where: A (mm^2): initial average cross-sectional area of the specimen.

ε (%): axial strain.

- Compute the principal stress difference (deviator stress) $\Delta\sigma$:

$$\Delta\sigma = (\sigma_1 - \sigma_3)_{max} = \frac{P}{A_1} \times 1000 \tag{2.7}$$

Where P: the observed axial load (corrected if required)

Thus, plot a graph showing the relationship between principal stress difference (deviator stress) and axial strain.

- Correction for Rubber Membrane in case the error in primary stress difference owing to the membrane's stiffness exceeds 5%:

$$\Delta\sigma = (\sigma_1 - \sigma_3) = 4E_m t_m \varepsilon / D \tag{2.8}$$

Where D: the soil diameter

t_m, E_m: the thickness and young's modulus membrane. It is usually 1400 kN/m^2 for latex membrane.

ε: axial strain.

- The internal friction angle (φ) and the cohesion (c) of unsaturated samples were determined:

$$\sigma_1 = \sigma_3 \times K_p + 2 \times c \times \sqrt{K_P} \quad (2.9)$$

in which K_p: passive earth pressure.

$$K_p = tan^2(45^o + \frac{\varphi}{2}) \quad (2.10)$$

Since excess pore water pressure cannot be measured, this value represents the sample's total shear resistance.

The 50, 100, 150, and 200 kPa lateral pressures were chosen because the thickness of clay in the river was about 20 m, which is approximately 200 kPa.

d) Unconsolidated- Undrained Test (UU) for saturated samples

Like the unsaturated samples, the samples would be saturated before testing by the following method:

- After installing the samples in the chamber, increase the chamber pressure to under 5 kPa to ensure that the sample is not damaged during saturation.
- Saturating samples by increasing the back pressure to 500 kPa and allowing water to run to the samples. During the increase and saturation processes, the chamber pressure is always about 5 kPa greater than the back pressure.
- After 24 hours, check the sample saturation by locking the water valve to the soil. Pore water pressure coefficient *B* is determined by the equation:

$$B = \frac{\Delta u}{\Delta \sigma_3} \quad (2.11)$$

where *B*: pore water pressure coefficient. If $B \geq 0.98$, the samples are saturated.

Δu: the changes in pore water pressure corresponding to the change of lateral pressure $\Delta\sigma_3$ in the undrained condition.

- Because samples are saturated in the unconsolidated condition, and pore water pressure can be measured during the test, shear strength S_u (kPa) can be determined by the equation:

$$S_u = \frac{\sigma_1 - \sigma_3}{2} = \frac{\Delta\sigma}{2} \quad (2.12)$$

where $\Delta\sigma$: deviator stress, which was not dependent on lateral stress σ_3.

Thus, chamber pressure does not affect the shear strength of saturated samples. In this test, the chamber pressure was 300 kPa.

2.2.4. Direct shear test

This test method determines the consolidated, drained shear strength of a single soil sample under direct shear boundary settings.

In the direct shear test, the applied normal (vertical) force is divided by the shear box's cross-sectional area. Besides, the applied shear force is divided by the shear box's cross-sectional area. During shear, the specimen's contact area with the imposed shear plane reduces, so the actual shear stress is uncertain.

Based on ASTM D3080 [99], failure is typically defined as the greatest shear stress attained, or in the absence of a peak condition, the shear stress at 10% relative lateral displacement. The minimum sample diameter for round samples or sample width for square specimens shall be 50 mm or not less than 10 times the maximum size of the particle diameter, whichever is greater. The minimum starting specimen thickness shall not be less than 6 times the maximum particle dimension, or 13 mm. The minimal sample diameter-to-thickness ratio, or width-to-thickness ratio, is 2:1.

Based on the shear rate and the soil drainage, direct shear tests are performed:

- Unconsolidated- Undrained shear test (*UU*)
- Consolidated- Undrained shear test (*CU*)
- Consolidated- Drained shear test (*CD*)

In this research, samples were soaked in water at least 24 hours before the test to ensure saturation (*CD* test).

Procedure for *CD*-*CU* tests:

- Assemble the soil, the shear box, and the shear box bowl in the load frame.
- Apply a small setting normal pressure to the soil.
- Consolidate the soil to the specified pressure. Just before shearing and following the consolidation of the final increment, record the pre-shear vertical displacement and remove the alignment screws or pins from the shear box. Use the gap screws to separate the two sides of the shear box to

about the diameter of the largest particle in the test specimen, or 0.64 mm as a minimum default setting for fine-grained materials. Remove the gap screws once the gap has been created.

- Calculate shearing rate: shear velocity must be low enough so that excess pore pressure dissipates or large enough so water cannot exit.

In the case of the *CD* test, the shear rate R_f can be calculated based on ASTM D3080 [99]:

$$R_f = \frac{d_f}{t_f} \tag{2.13}$$

where: d_f (mm): estimated relative lateral displacement at failure. It can be 10 mm for normal or lightly overconsolidated.

t_f (minute): total estimated elapsed time to failure. It can be 24 hours for *MH*, *CH* soil.

In the case of the *CU* test, the shear rate could be approximated for saturated specimens performed at about 1.3 mm/min [100]

In this research, the shear rates for *CD* and *CU* were 0.004 mm/minute and 1.3 mm/minute, respectively.

Nominal normal stress τ and nominal shear stress can be calculated as follows:

$$\tau = \frac{Q}{A} \text{ và } \sigma = \frac{P}{A} \tag{2.14}$$

Where: *Q*, *P* (N) is vertical load and shear force

A (cm^2) is soil area.

Figure 2.11: Direct shear apparatus

The relationship between shear strength τ and normal stress σ:

$$\tau = \sigma tg\ \varphi + c \tag{2.15}$$

Where: φ (^{0}): soil internal friction.

c (kN/m^2): soil cohesive.

According to TCVN 4199:1995 [101], to determine φ, c at least 3 different values of σ and τ. At that time, c, φ are computed by:

$$tg\varphi = \frac{n\sum_1^n(\tau_i\sigma_i)-\sum_1^n\tau_i\sum_1^n\sigma_i}{n\sum_1^n\sigma_i^2-(\sum_1^n\sigma_i)^2} \tag{2.16}$$

$$c = \frac{\sum_1^n\tau_i\sum_1^n\sigma_i^2-\sum_1^n\sigma_i\sum_1^n(\tau_i\sigma_i)}{n\sum_1^n\sigma_i^2-(\sum_1^n\sigma_i)^2} \tag{2.17}$$

2.3. MODIFIED SHEAR BOX FOR FRICTION BETWEEN THE SOIL AND STEEL

The direct shear test was conducted by conventional direct shear equipment with a shear box of 60 mm x 60 mm. In addition, a modified shear box was developed to evaluate the shear strength of the interface between untreated or cement-treated soil and stainless steel. As shown in Figure 2.12, the upper shear box is filled with soil, while the original lower shear box has been replaced with a stainless steel plate. The modified shear box's schematic mirrored that proposed by Tsubakihara et al. [102].

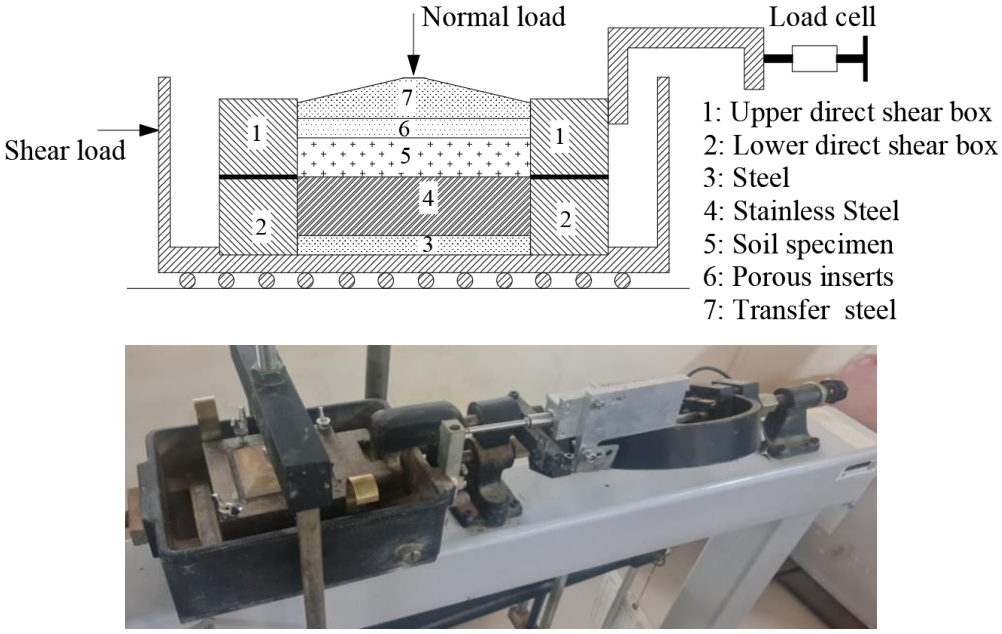

Figure 2.12: Modified shear box for interface shear strength

2.4. MODIFIED OEDOMETER APPARATUS FOR SIDE FRICTION PRESSURE MEASUREMENT

A modified oedometer apparatus was developed to measure the side friction between the soil and the consolidation ring during the progress of consolidation tests. There were two types of consolidation rings, of which the diameters were 50 mm and 75 mm. The initial height of specimens, H_0, varied from 10 mm to 50 mm, equivalent to the ratio of D/H_0 ranging from 1 to 7.5.

The schematic of the modified one-dimensional consolidation apparatus is shown in Figure 2.13. A load cell located at the base measured the reaction force at the bottom of the specimens. The total friction pressure would be evaluated by comparing the compression pressure on the top and the reaction pressure on the bottom of the soil specimens.

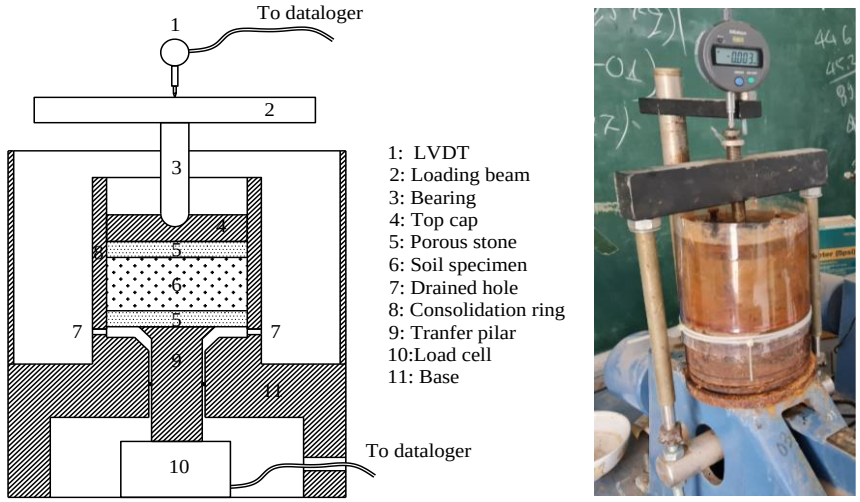

Figure 2.13: Modified oedometer apparatus for side friction pressure measurement

Similar methods to measure side friction during consolidation tests were also found in previous studies [15–17]. However, being different from those studies, the two porous stone disks allowed the pore water pressure to dissipate from the top and bottom of the specimens, which was the same drainage condition as the traditional one-dimensional consolidation test [13]. Lovisa et al. [22] also proposed a similar design with upper and lower drainage boundaries to evaluate the consolidation behavior of tall specimens. Although the modified consolidation apparatus could not

measure the pore water pressure at the bottom of the samples, it helped to significantly shorten the consolidation time by creating the upper and lower drainage boundaries. The test outcome displayed that the proposed apparatus allowed to complete the primary consolidation of a load increment for the specimens with a height of up to 50 mm within 24 hours. Last, the settlement of the soil was measured by a linear variable differential transformer (LVDT) attached to the top of the loading beam.

Therefore, the friction force (F_{fric}) (kN) can be calculated as:

$$F_{fric} = (P - R)\pi D^2/4 \quad (2.18)$$

where: *P*, *R*: compressive pressure at the top and bottom of the soil (kPa), which is measured from the load cell.

D: soil diameter (m)

CHAPTER 3: BEHAVIOR OF SILTY SOIL WITH AND WITHOUT GEOTEXTILE UNDER CBR, UU, AND CONSOLIDATION TESTS

3.1. INTRODUCTION

When the silt's moisture content rises, its swelling and its bearing ability decrease. In addition, due to its low permeability, clay consolidation requires a great deal of time. Thus, the use of soft clay as backfill necessitated an appropriate drainage system and construction methods to ensure its operation [10, 31, 103]. Numerous studies have utilized geosynthetics as reinforcement to increase strength and overcome obstacles due to their high permeability, which considerably enhanced the stability and bearing capacity of reinforced soil structures [104]. The capacity of soil improved with 1 or 2 geogrid layers [39]. The tensile strength of reinforced specimens increases with the number of reinforced layers. So, geotextiles with high permeability were identified as a possible reinforcement material for the marginal backfill soil.

Although there was much research about geotextile, the swellings, *CBR* value, shear capacity due to wetting, and consolidation behavior of reinforced soil were not fully determined, especially for the soil in the Mekong Delta. The research objectives of this chapter are:

- Effect of nonwoven geotextile on silt's swelling and *CBR* value in unsaturated and saturated conditions by the CBR test.
- Effect of nonwoven geotextile on the UU shear strength in unsaturated and saturated conditions by triaxial test to evaluate the silt capacity.
- Effect of side friction on the consolidation behavior of silt. A modified Taylor's method is presented to predict the friction pressure and determine the void ratio distribution without requiring the specimen height at the end of the tests. Furthermore, the study proposed an analytical equation to evaluate the *COV* values, quantifying the degrees of uniformity of the void ratio along the depth of the specimens in the one-dimensional consolidation experiments.
- Effect of geotextile under the one-dimensional consolidation test.

Each objective corresponds to a type of test.

3.2. EXPERIMENTAL PROGRAM

3.2.1. *CBR* specimens

After at least 24 hours in an oven, dry silt powder was combined with water at a water content of 24.5%. This mixture was enclosed in a plastic bag for at least two days in a temperature-controlled chamber to guarantee consistent water in the soil.

For the sample reinforced by geotextiles, following the compaction and leveling of every soil layer, the soil surface was scarified, and a horizontal layer of dry geotextiles with a diameter of 152.4 mm was placed on the surface. The required quantity for the subsequent stratum was then poured and compacted. The method used to finish the surface of samples with geotextiles was comparable to that used for unreinforced specimens.

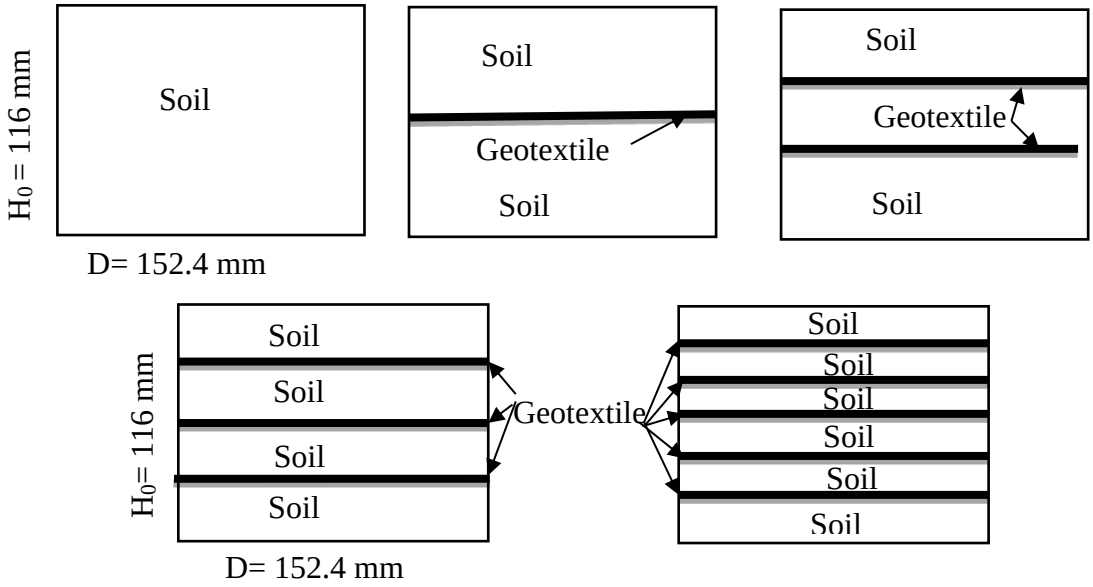

Figure 3.1: Geotextile layers in reinforced and unreinforced *CBR* specimens.

There was a total of 10 specimens for soaked and unsoaked conditions:

- *Unsoaked condition:* silty soil samples and geotextile-soil samples were performed with the *CBR* test.

- *Soaked condition:* Before performing the *CBR* test, the compacted samples were immersed for 96 hours. The samples' surface was loaded with an additional bulk of 4.54 kg. A weight of 2.27 kilograms was positioned to prohibit the soil's movement

into the surcharge hole. The expansion of samples was frequently recorded every 1-2 hours during the soaking procedure.

In every group, there were unreinforced samples and geotextile-reinforced samples with 1, 2, 3, and 5 layers.

3.2.2. Unconsolidated-Undrained shear strength samples in the triaxial test

After at least 24 hours in an oven, dry soil powder was combined with water at a content of 24.5%. A sample of 50 mm in diameter and 100 mm in height was made at 1.531 g/cm^3 of dry-weight soil. The samples were made by pressing each part at a height of 10 mm to achieve uniformity of density and mass in the sample.

Unconsolidated-undrained (*UU*) shear strength was determined by testing a total of 20 samples, including unreinforced samples, 1-layer, 2-layer, and 3-layer reinforced samples, with two initial conditions and compression pressure:

- *Unsaturated samples*: samples will be tested at lateral pressures of 50 kPa, 100 kPa, 150 kPa, and 200 kPa, respectively.
- *Saturated samples*: samples will be saturated at 500 kPa pressure and tested at 300 kPa lateral pressure.

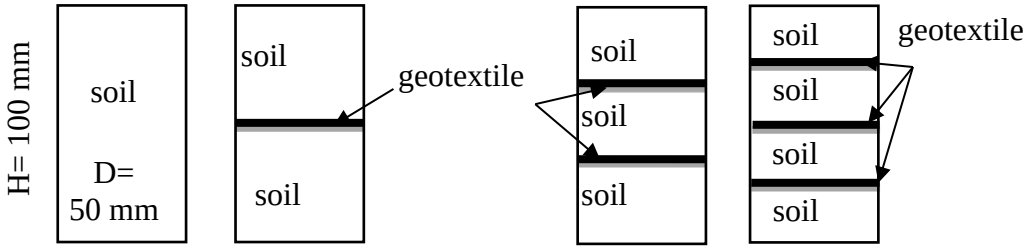

Figure 3.2: Geotextile layers in reinforced and unreinforced samples in the *UU* test.

a) Unreinforce sample b) 1-geotextile c) 2-geotextile d) 3-geotextile

Figure 3.3: Uninforced and geotextile-reinforced samples in UU the test

3.2.3. Consolidation samples

a) <u>Samples to investigate the soil consolidation behavior under the effects of side friction:</u>

The remolded clay samples were made by using clay powder at 54.7% water content. Before preparing the soil specimens, the inner side of the consolidation rings was lubricated using silicon grease to minimize the interface friction. The clay specimens were prepared with the initial heights, H_0 = 10 mm, 20 mm, 30 mm, 40 mm, and 50 mm using consolidation rings with diameters of 50 mm and 75 mm. The samples were soaked in water for 24 h to ensure saturated conditions before applying the consolidation pressure at the top of the specimens. The consolidation pressure was loaded incrementally at 24.8, 49.7, 99.5, 199.1, and 398.3 kPa. Each loading stage remained for 24 h before increasing the load. The settlement at the top and the reaction force at the bottom of the specimens were measured by an LVDT and a load cell, respectively. Both parameters were recorded in time by a data acquisition system.

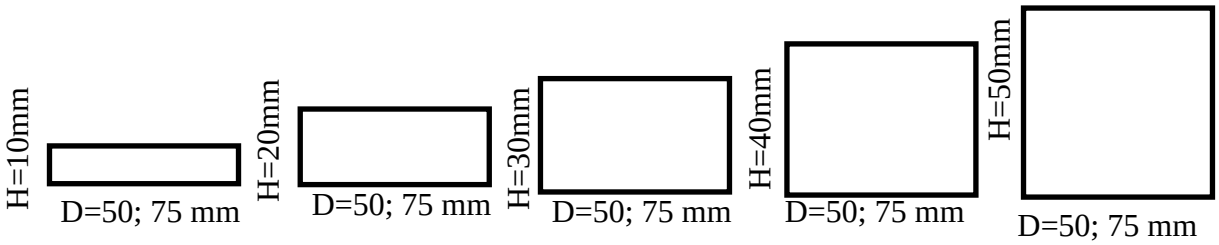

Figure 3.4: Samples to investigate side friction

b) <u>Samples to investigate the effect of nonwoven geotextile on the soil consolidation process.</u>

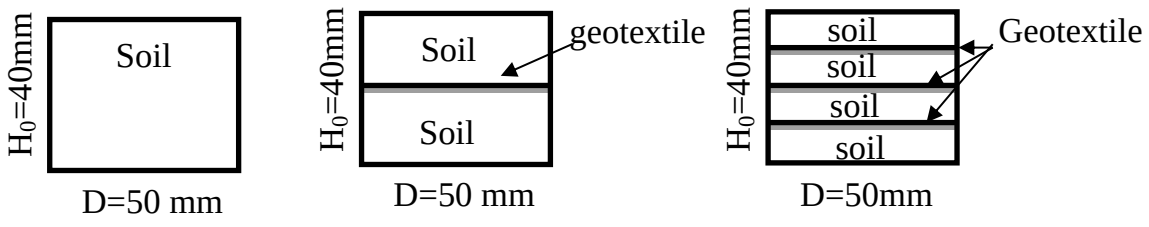

Figure 3.5: Samples reinforced by geotextile in one-dimension consolidation

A series of one-dimensional consolidation tests were performed with the 50 mm diameter and 40 mm height samples, including unreinforcement and soil reinforced

by 1 and 3 layers. All specimens were made at 54.7% water content, and the top pressures were 49.7 kPa, 99.5 kPa, 199.1 kPa, and 398.3 kPa.

3.3. BEHAVIOR OF SILTY SOIL WITH AND WITHOUT GEOTEXTILE UNDER THE SWELLING AND CBR TEST

3.3.1. Influence of the geotextile on the behavior of the soil swell

The swell proportion, denoted as *S* (%) throughout the soaking process, is calculated by equation (2.1). It is the proportion between the vertical expansion and the initial soil's height.

In general, the swelling percentage of specimens with and without geotextiles increased with immersion time. However, the swelling process did not achieve stability during a period of 96 hours.

Initially, the percentage expansion of specimens without geotextiles was less than that of specimens with geotextiles. However, after approximately 40 hours, the unreinforced specimens showed increased swelling. After 96 hours, the number of reinforcement layers decreased the swelling of the reinforced specimens.

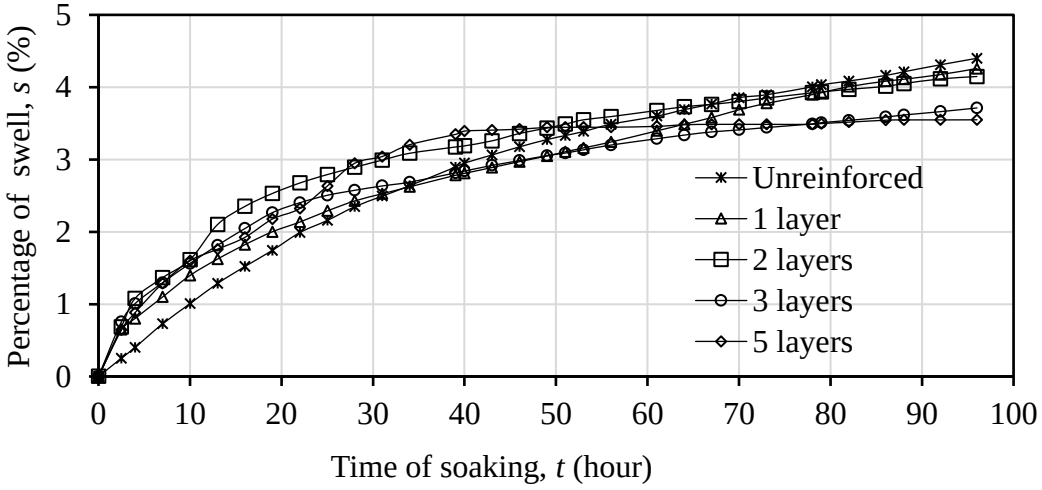

Figure 3.6: Percent swelling of soil and geotextile-soil specimens during soaking

The swelling velocity demonstrates the effect of the geotextile on the swelling behavior as a function of time. It is defined as the percentage of specimens that expand within one hour. During 10 hours of immersion, the reinforced samples exhibit a higher velocity increase compared to their unreinforced counterparts. Specifically, the surge velocity of reinforced specimens in the first 2.5 hours is

approximately 0.25 to 0.3%/hour. This number is about 2.5 to 3 times higher than that of specimens without reinforcement (about 0.1%/hour).

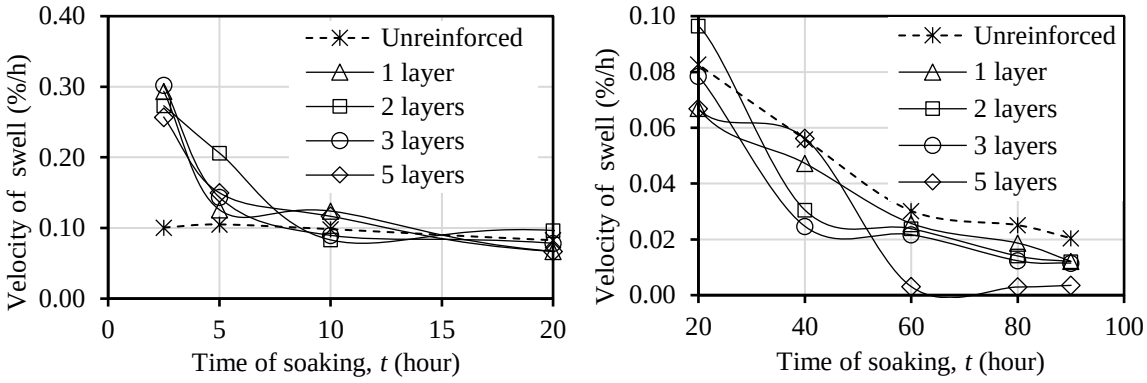

a) The swell velocity in the initial 20 hours b) The swell velocity after 20 hours

Figure 3.7: The swell velocity (a) during the initial 20 hours and (b) after 20 hours

The reinforced clay experiences an increase in drainage paths due to the high permeability of the geotextile. This leads to an increase in swelling in the reinforced samples in the first 20 hours. After that, it is unclear how the number of reinforcements affects the expansion velocity of reinforced samples. The growth rate of specimens increases in direct proportion to the quantity of geotextile layers after 60 hours. With an increase in the number of reinforcing layers, the surge velocity decreases. In other words, owing to wetting, specimens with greater geotextile layers return to stability more quickly than those with fewer geotextile layers.

It is important to observe that while the soil specimens are being soaked, there is no difference in their dry weight. However, there is an increase in volume caused by the swelling influence. Consequently, the dry density of specimens decreases at the end of the soaking process. The percentage decrease in soil dry density over the duration of 96 hours immersed in water, $\%\Delta\gamma_d$, is defined as

$$\%\Delta\gamma_d = \frac{\gamma_{d\_unsoaked} - \gamma_{d\_soaked}}{\gamma_{d\_unsoaked}} \times 100\% \quad (3.1)$$

Where $\gamma_{d\_unsoaked}$ and γ_{d_soaked} represent the dry unit weights of the samples before and after 96 hours of soaking, respectively.

Without considering variations in the thickness of geotextile layers caused by soaking (which appear significantly smaller in comparison to the soil's). The

reduction in the dry unit weight of soil is determined by measuring the percentage increase in volume after the soaking process, S_{96h}.

$$\%\Delta\gamma_d = 1 - \frac{1}{S_{96h}+1} \tag{3.2}$$

Table 3.1 demonstrates that the decrease in dry unit weight of clay samples with a nonwoven geotextile layer, is less than that of soil without reinforcement. Therefore, when the density of the clay is the same after compaction, the soil in samples with reinforcement will be denser than the soil without reinforcement after soaking. This is because of the strength of the nonwoven geotextile.

Table 3.1: The swell and dry unit weight reduction percentages after soaking

Circumstance	S_{96h} (%)	$\%\Delta\gamma_d$ (%)
Unreinforced	4.64	4.43
One layer	4.36	4.18
Two layers	4.15	3.98
Three layers	3.71	3.58
Five layers	3.55	3.43

3.3.2. CBR behavior of unreinforced and reinforced silty soil by geotextile in un-soaked and soaked conditions

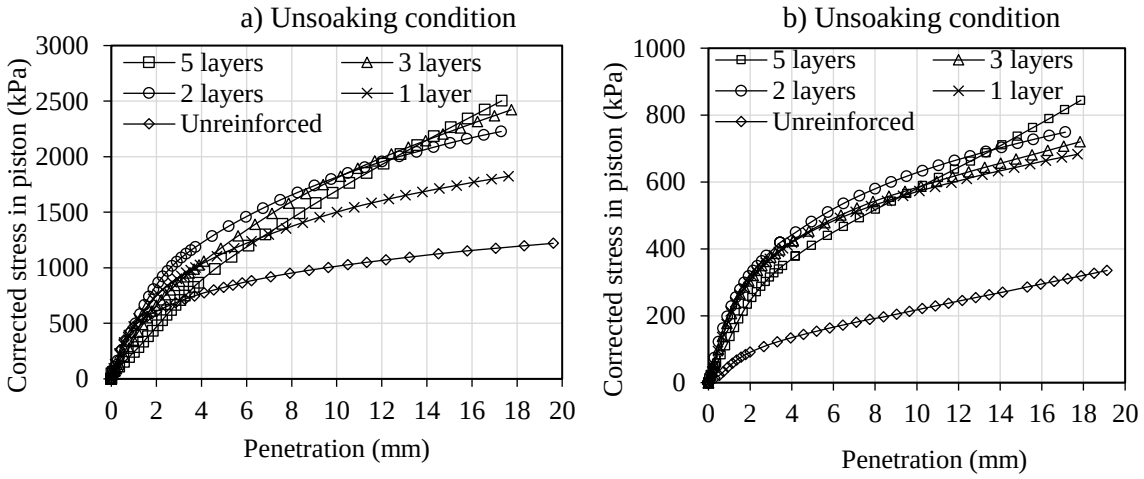

Figure 3.8: The piston stress vs. penetration.

Figure 3.8 depicts the stress of the piston vs. the penetration of specimens with and without geotextiles. For both unsoaked and soaked specimens, the highest strength of soil is considerably enhanced when added by geotextiles. Increasing the quantity of reinforcements directly correlates with an increase in the bearing capacity

of specimens with geotextiles. This result agrees with prior outcomes on reinforced soil attained by Abduljauwad et al. [105], Koerner et al. [106], Kamel et al. [107], Choudhary et al. [36], Rajesh et al. [37], Carlos et al. [38], Keerthi and Kori [108], and Singh et al. [109]. The researchers determined that the addition of reinforcement layers resulted in an enhanced *CBR* value for the soil that was reinforced.

The improved bearing capacity of samples with geotextiles is quantified by using the strength ratio R_{CBR}, specified as the proportion of the *CBR* of the specimen with geotextiles to that of the sample without geotextiles. Figure 3.9 illustrates the variations in the strength ratio with the geotextile spacing. The specimen without a geotextile is equal to the geotextile spacing of 116.5 mm. Because of geotextiles, the strength ratio of the specimen without soaking varied from 1.1 to 1.5, while that of the soaked specimen was 2.7 to 3.3. The nonwoven geotextile demonstrated a more efficient enhancement of the bearing capacity of soaked clay compared to unsoaked clay samples.

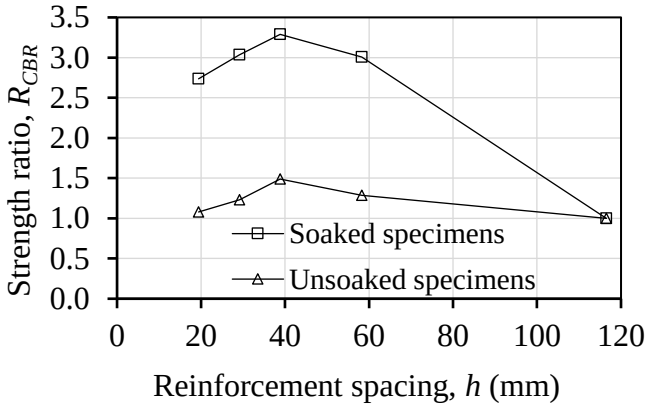

Figure 3.9: The relationship between strength ratio and geotextile spacing

Additionally, for both soaked and unsoaked samples, when growing the reinforcement spacing, h_{geo} (i.e., reducing the number of geotextile layers), the strength ratio at first rose and achieved the highest value at h_{geo} = 40 mm (equivalent to the sample with 2 geotextile layers), then decreased until the specimens without geotextiles. The optimum ratio between geotextile spacing and the load piston's diameter, $D_{pistion}$, for the greatest strength ratio was 0.8. This number was stated in earlier studies. Koerner et al. [106] found that the minimum soil thickness needed to

cover a geosynthetic clay liner should be equal to or greater than the diameter of the load piston (i.e., $h_{geo}/D_{pistion} = 1$). The same conclusion was found by Choudhary et al. [36] and Keerthi and Kori [108] when doing the *CBR* test on expansive soil subgrades with one reinforcing layer. Besides, Kamel et al. [107] stated that the geogrid layer was put at a depth of 1.0-1.2 times the load plate's diameter to achieve the maximum capacity of reinforced specimens. The optimal position of reinforcement was found in the case of a single layer. The ideal reinforcement spacing determined in this research, $h_{geo}/D_{pistion} \approx 0.8$, is close to the result from prior research.

The observation can be explained by the mechanism of reinforced soil under the load of the piston. The improvement in bearing capacity was attributed by the soil-reinforcement interaction. Reinforcements can restrain the lateral deformation or the potential tensile strain of the soil (confinement effect). In addition, deformed reinforcements can develop an upward force (membrane effect). These effects will result in an increase in bearing capacity. At low penetration of the piston, the deformation of reinforcement is small, and the confinement effect would contribute to the improvement of bearing capacity, which much depends on the depth of the punching failure surface, and this surface is limited by the depth of the top reinforcement layer. The specimens with the top reinforcement layer at the optimum depth would have the highest bearing capacity than others (i.e., the specimen reinforced by 2 reinforcement layers in this study). When the penetration is large enough, the tensile strength is mobilized not only from the top reinforcement layer but also from the lower ones. As a result, more bearing capacity improvement could be achieved with a higher number of reinforcement layers. The observation from Figure 3.9 is consistent with the aforementioned analysis. The bearing capacity of the specimen, which had been strengthened with 5 layers of reinforcement, reached its highest value when the penetration exceeded 13 mm.

3.3.3. The effect of soaking on CBR behavior

The percent *CBR* reduction due to soaking is evaluated as follows:

$$\%\Delta CBR = \frac{CBR_{unsoaked} - CBR_{soaked}}{CBR_{unsoaked}} \times 100\% \quad (3.3)$$

in which $CBR_{unsoaked}$ and CBR_{soaked}: the *CBR* values of unsoaked and soaked specimens, respectively.

For specimens without reinforcement, after soaking, the *CBR* value noticeably dropped from 9.5 to 2.2, which is equal to a 76.9% decrease in the *CBR* value. Compared to the reinforced samples, the geotextile reduced the bearing capacity reduction to below 50%. After soaking, the *CBR* of the reinforced sample was 6-7.2, compared to 2.2 for the unreinforced samples. The dramatic reduction in the bearing capacity of expansive clay is affected by the wetting and swelling influences during soaking. The wetting effect would decrease the friction among soil particles as well as the bond between soil and reinforcements. The swelling influence reduces the soil density, which also decreases the bearing capacity of the samples. The geotextile layer not only reduced the swell percentage but also developed the bearing capacity due to the soil-reinforcement interaction and membrane force, which are from the tensile strength mobilization in the reinforcement layers. Nguyen et al. [110] investigated the interface shear strength between clay and geotextiles. These materials are the same as those used in this research. The result showed that in the interaction between soil and geotextile, the friction angle in the *OMC* and saturated conditions was the same: 23.1^{o} and 21.5^{o}, respectively. In contrast, the internal friction angle of soil decreased dramatically from 27.8° to 4.7° when the soil was saturated. In other words, in both *OMC* and saturated conditions, the interaction between soil and geotextile was good enough to maintain the capacity of soil-geotextile.

Table 3.2: *CBR* and *CBR* reduction owing to soaking and sand cushion samples:

Circumstance	*CBR* of unsoaked specimens	*CBR* of soaked specimens	Percentage of *CBR* reduction ΔCBR (%)
Unreinforced	9.5	2.2	76.9
1 layer	12.3	6.6	46.1
2 layers	14.2	7.2	49.1
3 layers	11.7	6.7	43.1
5 layers	10.3	6.0	41.5

3.4. BEHAVIOR OF SILTY SOIL WITH AND WITHOUT GEOTEXTILE ON UU SHEAR STRENGTH UNDER TRIAXIAL TEST

3.4.1. The shear strength behavior of silty soil unreinforced and reinforced by geotextiles in the unsaturated condition

a) Shear strength behavior of silty soil unreinforced and reinforced by geotextiles in the unsaturated condition

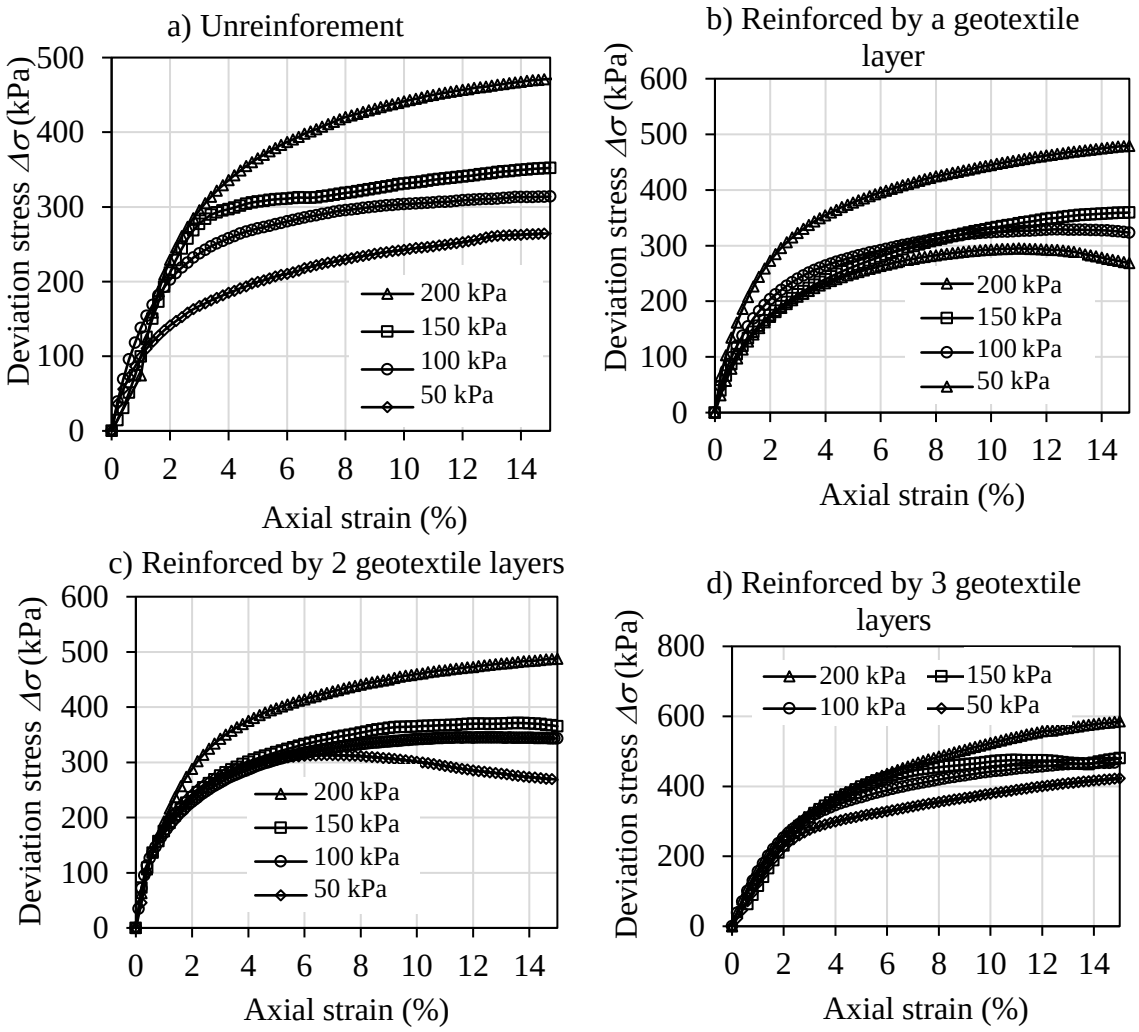

Figure 3.10: Deviation stress versus axial strain of unreinforcement and reinforcement with geotextile in the unsaturated condition

The relationship of deviation stress ($\Delta\sigma = \sigma_1 - \sigma_3$) versus axial strain of soil and soil reinforced by geotextile layers was shown in Figure 3.10. The results indicated that the deviation stress increased as the lateral pressure σ_3 and the number of geotextile layers increased.

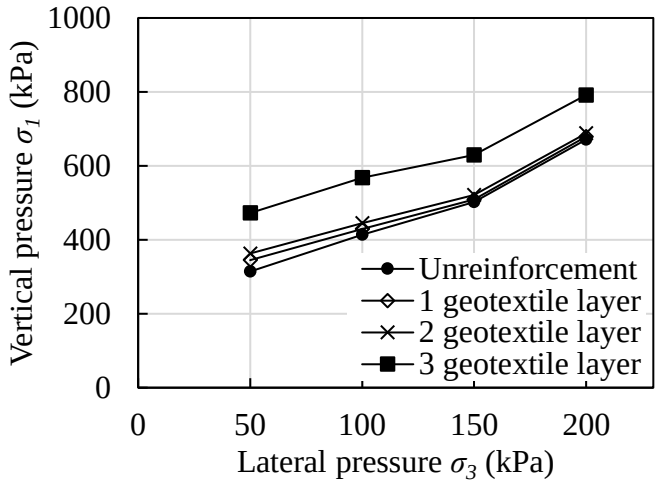

Figure 3.11: The vertical versus lateral pressure of silty soil and geotextile soil at failure in unsaturated condition.

The relationship between vertical and lateral pressures of soil and geotextile soil is shown in Figure 3.11 when the specimen failed at 15% strain.

Table 3.3: The cohesive (c) and internal friction angle (φ) of soil and geotextile-soil at failure of this and previous studies

Condition	Type of reinforcement	φ (°)	c (kPa)	Reference
UU	Unreinforced	65.6	19.8	Yang et al. [11]
UU	1 layer	68.3	13.9	Yang et al. [11]
UU	2 layers	65.0	183.6	Yang et al. [11]
UU	3 layers	68.0	226.0	Yang et al. [11]
CU	Unreinforced	15.3	57.6	Yang et al. [42]
CU	1 layer	15.0	68.2	Yang et al. [42]
CU	2 layers	13.4	80.7	Yang et al. [42]
CU	3 layers	13.4	112.8	Yang et al. [42]
CU	Unreinforced	29.9	11.8	Al-Omari et al. [41]
CU	1 layer	29.4	44.9	Al-Omari et al. [41]
UU	Unreinforcement	23.4	60.9	This study
UU	1-geotextile layer	21.6	74.8	This study
UU	2-geotextile layers	20.8	83.3	This study
UU	3-geotextile layers	23.5	110.5	This study

Table 3.3 displays the results of calculating the total cohesive force (c) and the total internal friction angle (φ) for the unreinforced and reinforced cases in the UU condition because excess pore water pressure cannot be assessed. The table provides the cohesion and internal friction angles from prior investigations. The results showed

that in most cases, the cohesion of reinforced soil increased dramatically, whereas the internal friction angle changed without a general trend. In this study, the soil-geotextile was considered a heterogeneous material. Thus, the values *c* and φ can change without a general trend. UU shear strength should be used to evaluate the capacity of the soil-geotextile instead of *c* and φ. In all cases, the UU shear strength of reinforced soil increased dramatically as the number of geotextile layers increased.

b) The shear strength increasement R_{uf} in the unsaturated condition:

The shear strength increasement R_{uf} in the unsaturated condition was determined:

$$R_{uf} = \frac{\Delta\sigma_{reinforcement}}{\Delta\sigma_{unreinforcement}} \qquad (3.1)$$

Where: $\Delta\sigma_{reinforcement}$; $\Delta\sigma_{unreinforcement}$: deviation at the failure of reinforced soil and soil.

Results indicated that R_{uf} was greater than 1 at all lateral pressures, showing that the reinforcement layers can increase the soil's strength. The R_{uf} value decreased as the lateral pressure increased. The R_{uf} value increased as the number of fabric layers increased. It is consistent with the conclusion that adding geotextile layers increases shear strength [11].

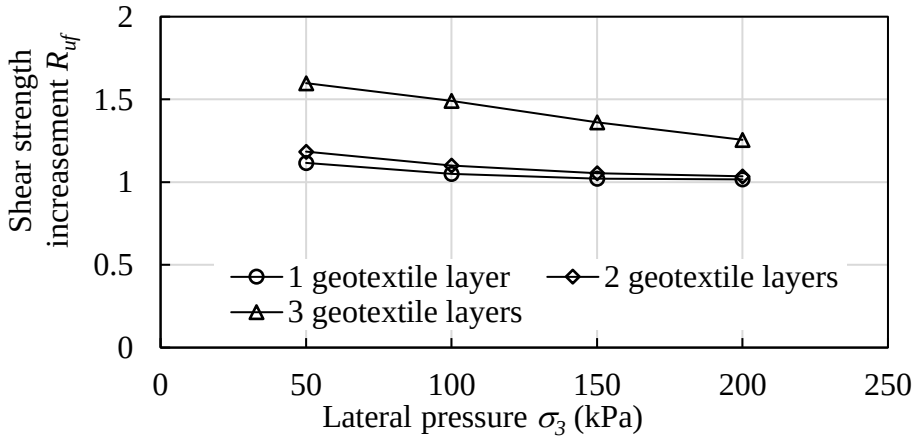

Figure 3.12: Shear strength increasement versus lateral pressure in the unsaturated condition.

3.4.2. The shear strength behavior of silty soil unreinforced and reinforced by geotextiles in the saturated condition.

a) *Shear strength behavior of silty soil unreinforced and reinforced by geotextile in the saturated condition*

The results indicated that deviation stress increased when the axial strain and the number of geotextile layers increased.

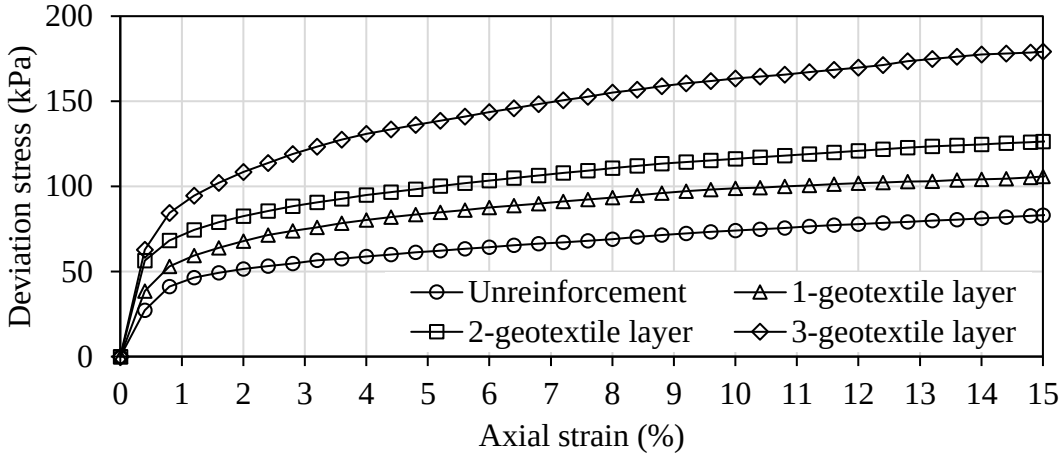

Figure 3.13: The deviation stress and axial strain of soil and soil reinforced by geotextile in the saturated condition

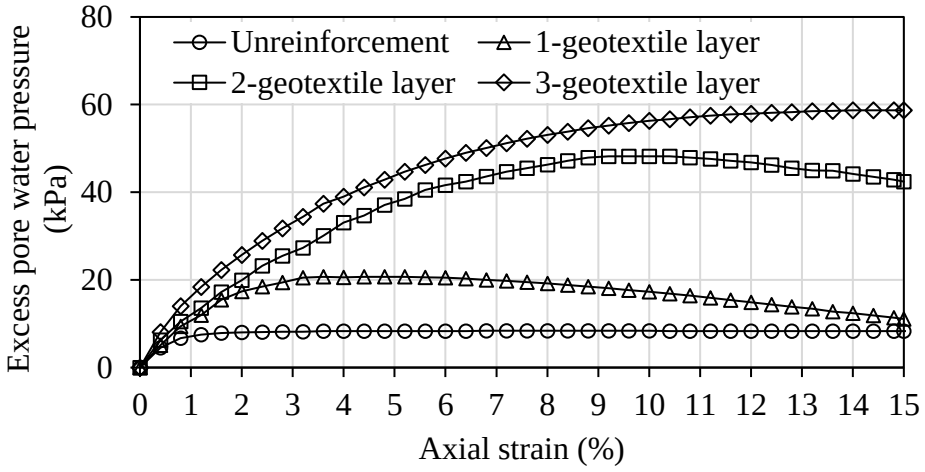

Figure 3.14: The excess pore water pressure and axial strain of soil and soil reinforced by geotextile in the saturated condition

Figures 3.13 and 3.14 illustrated the deviation stress and excess pore water pressure with the axial strain of unreinforced and geotextile-reinforced saturated samples, respectively, in UU conditions. The saturated sample's undrained shear strength, S_u is determined to be fifty percent of the deviation stress at the failure. The sample's total shear resistance is calculated when $c_u = S_u$ and $\varphi_u = 0$. As the number

of geotextile layers increased, the UU shear strength and the excess pore water pressure increased.

Table 3.4: The excess pore water pressure and deviation pressure of soil and soil reinforced by geotextile in the saturated condition

Case	Deviation pressure (kPa)	Excess pore water pressure Δu (kPa)
Unreinforcement	83.02	8.30
1-geotextile layer	105.80	11.10
2-geotextile layers	126.26	42.40
3-geotextile layers	179.09	58.70

Yang et al. [11] confirmed that the excess pore water pressure increases as geotextiles can prevent lateral displacement or the potential tensile strain of the soil, thus raising the pore water pressure. In the strain range of 1% to 3%, the sample with reinforcement generated a higher water pressure than the unreinforced sample, as the geotextile restrained the lateral deformation of the sample; thereby, the pore water pressure surged. As the strain increased, the soil sample developed lateral strain (sliding between the soil and geotextile) (1- and 2-layer reinforcement samples), which decreased the pore water pressure, and the excess water pressure dissipated due to the geotextile's high permeability.

b) <u>The shear strength increasement R_f in the saturated condition:</u>

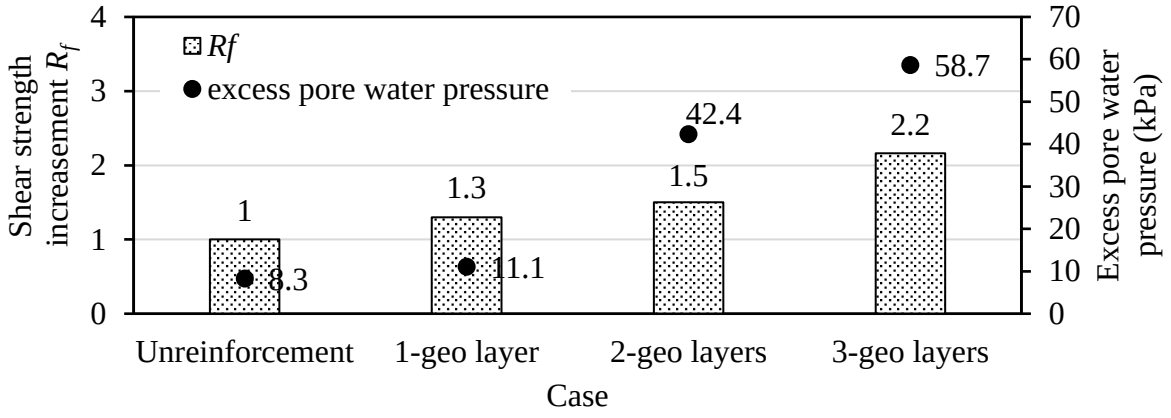

Figure 3.15: The shear strength increasement R_f and excess pore water pressure of soil and soil reinforced by geotextile in the saturated condition.

The shear strength increasement R_f in the saturated condition:

$$R_f = \frac{S_{u\ \text{reinforcement}}}{S_{u\ unreinforcement}} \quad (3.4)$$

In which: $S_{u\ reinforcement}$; $S_{u\ unreinforcement}$: the shear strength of the saturated soil and soil reinforced with geotextile in UU conditions.

Figure 3.15 showed that R_f was larger than 1, indicating the effect of geotextile on the reinforcement in the saturated condition. The R_f index increased as the number of layers surged.

3.4.3. Shear strength reduction of silty soil and geotextile soil due to saturation

Shear strength reduction T_{shear} due to saturation was determined as

$$T_{shear} = \frac{\Delta\sigma_{unsaturation} - \Delta\sigma_{saturation}}{\Delta\sigma_{unsaturation}} \quad (3.5)$$

In which $\Delta\sigma_{unsaturation}$; $\Delta\sigma_{saturation}$ (kPa): deviation stress of unsaturated and saturated samples.

The results showed that the shear strengths of saturated samples were much lower than those of unsaturated ones, about 57% - 83%.

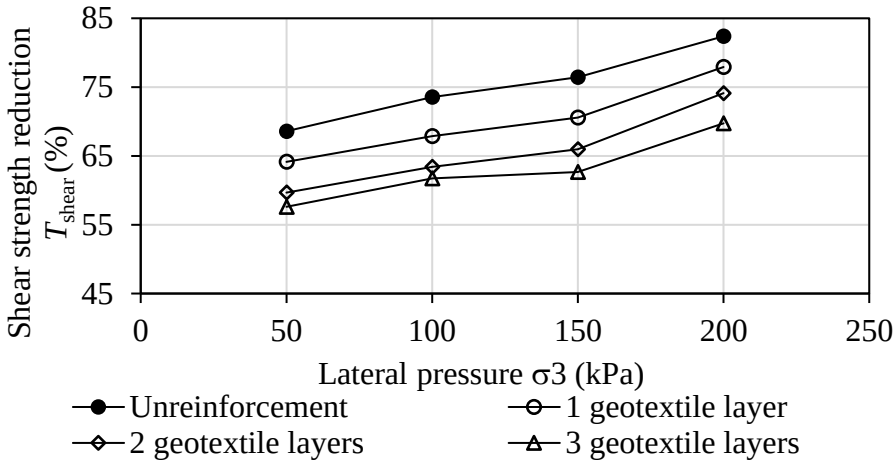

Figure 3.16: Shear strength reduction T_{shear} due to saturation of silty soil with and without geotextile

3.5. CONSOLIDATION BEHAVIOR OF SILTY SOIL UNDER EFFECTS OF SIDE FRICTION

The author also experimented with considering the effect of the side friction on the one-dimensional consolidation tests of the high-height samples by comparing the

results of the one-dimensional test and triaxial consolidation tests without horizontal expansion [111]. The 50 mm diameter, D, and 40 mm height, H_o, of the experimental samples included soil, soil reinforced by one layer of geotextile, and soil reinforced by a 10 mm thick sand cushion. The procedure to find the horizontal expansion coefficient K_0 and the triaxial consolidation process without horizontal expansion were proposed in the experiment [111]. The K_0 is the ratio between the horizontal and vertical pressure, so that the soil sample is compressed only in the axial direction but not in the horizontal direction. The results showed that with clay dredged from Cai Lon River, Kien Giang province, a value of $K_0 = 0.527$ was found, and consolidation time with soil and reinforced soil samples in one-dimensional consolidation was shorter by 0.68 to 0.88 times than that of the triaxial consolidation time without horizontal expansion K_0. This can be explained by the friction between the soil, the reinforcing layers (sand), and the ring in the one-dimensional consolidation test, which reduced the compressive consolidation pressure, making the test sample achieve consolidation faster. Therefore, the effect of friction in the one-dimensional consolidation test should be considered when the sample size is large.

3.5.1. The one-dimensional consolidation behavior under the effects of side friction pressure

a) The strain of specimens:

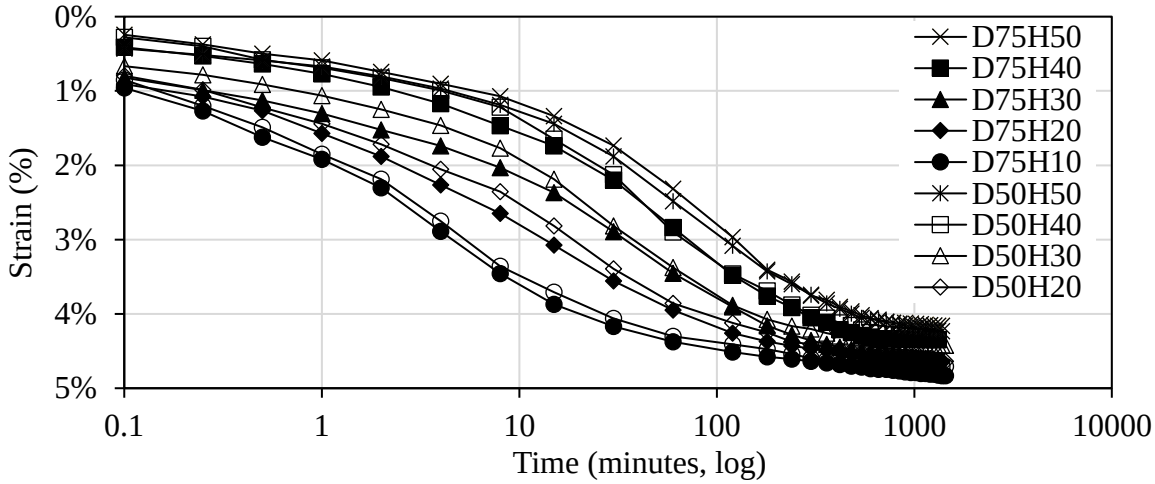

Figure 3.17: Axial strain vs. time under 99.5kPa of compression pressure (The specimens' names exhibit the diameter, D, and the initial height, H_0, in mm)

The temporal variation of the axial strain of the soil specimens under the compression pressure, P = 99.5 kPa, was presented in Figure 3.17. The smaller axial strain was observed in the soil specimens with the higher initial height and the smaller diameter. As discussed previously, the side friction caused a decrease in the consolidation pressure. As a result, the axial strain of the specimens would be smaller due to the rise of side friction. Based on the test results, the lowest axial strain was observed in the specimens with D = 50 mm and H_0 = 75 mm, of which the side friction reached the highest level after 24h of the consolidation period.

The required time to complete the primary consolidation of the specimens, T_{100}, was determined using the method of the log time-deformation curve as recommended in ASTM D2435 [13]. As presented in Figure 3.18, the value of T_{100} was proportional to the square of the maximum drainage distance, which was consistent with Terzaghi's one-dimensional consolidation theory. This finding agrees with the results of several studies [17, 22]. The results also verified the adequacy of a 24h period to complete the primary consolidation of a load increment.

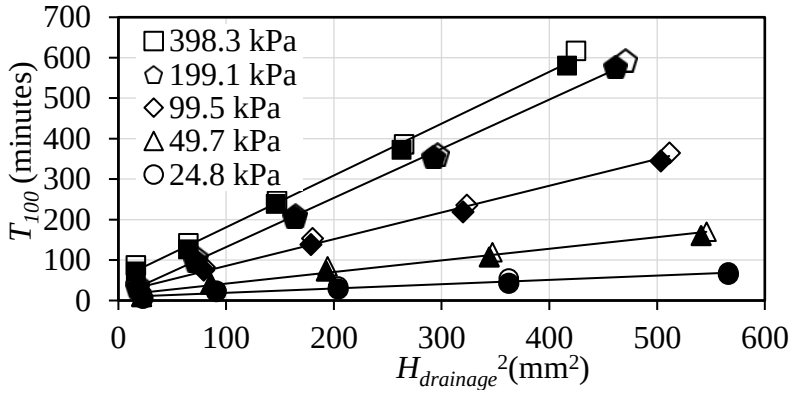

Figure 3.18: Variation of time corresponding to 100% primary consolidation, T_{100}, with square maximum drainage distance, $H_{drainage}^2$, under different compression pressures. The empty and solid symbols indicate the specimens with a 50 mm and 75 mm diameter, respectively.

b) <u>The coefficient of consolidation</u>

Figure 3.19 shows the variation of the coefficient of consolidation, C_v, of the clay specimens with the average consolidation pressure, $P_{average}$. It was defined as the

average value of the compression pressure and the reaction pressure acting on the top and bottom of the soil specimens, respectively [17].

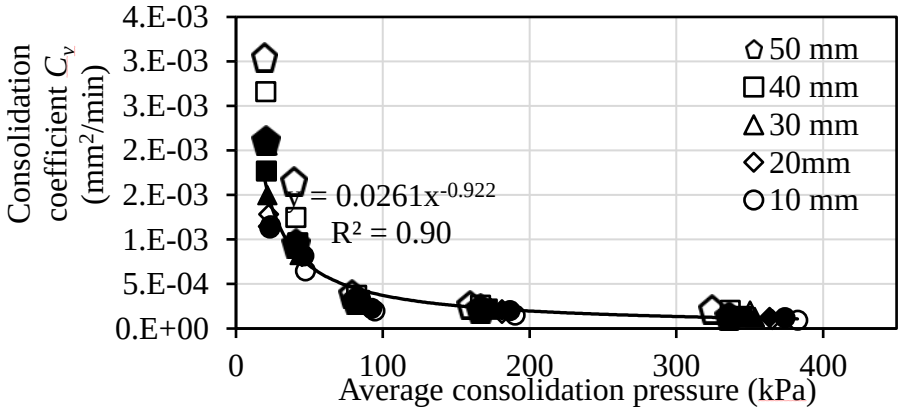

Figure 3.19: Consolidation coefficient value with the average consolidation pressure. The empty and solid symbols indicate the specimens with the diameters, D = 50 mm and 75 mm, respectively.

It is observed that the greater the average consolidation pressure, the smaller the coefficient of consolidation. The relationship between C_v and consolidation pressure has been reported differently in previous studies. Raju et al. [112] illustrated the smaller C_v value of the normally consolidated clay under higher overburden pressure. Besides, Retnamony [113] concluded that C_v decreased with a higher pressure for the montmorillonite mineral, in which physicochemical factors governed the compression behavior. In contrast, C_v would increase with consolidation pressure for kaolinite, illite, and powdered quartz, whose compressibility behavior was controlled by mechanical factors. For the remolded clay, Sridharan et al. [12] proposed that the decreasing trend of C_v vs. consolidation pressure preferred to occur for more plastic soils due to the mobilization of the diffuse double layer repulsive force acting against the external loading. That finding was supported by the results of C_v of the high plasticity silt (i.e., LL = 91.5 and PI = 46.6) in this study. In contrast, for low plasticity clay (CL), C_v increased with the increment in consolidation pressure [22].

The correlation between the two parameters is given below with a high coefficient of determination, R^2 = 0.90:

$$C_v = 0.0261 P_{average}^{-0.922} \quad (3.6)$$

c) <u>The void ratio at the end of the primary consolidation (EOP):</u>

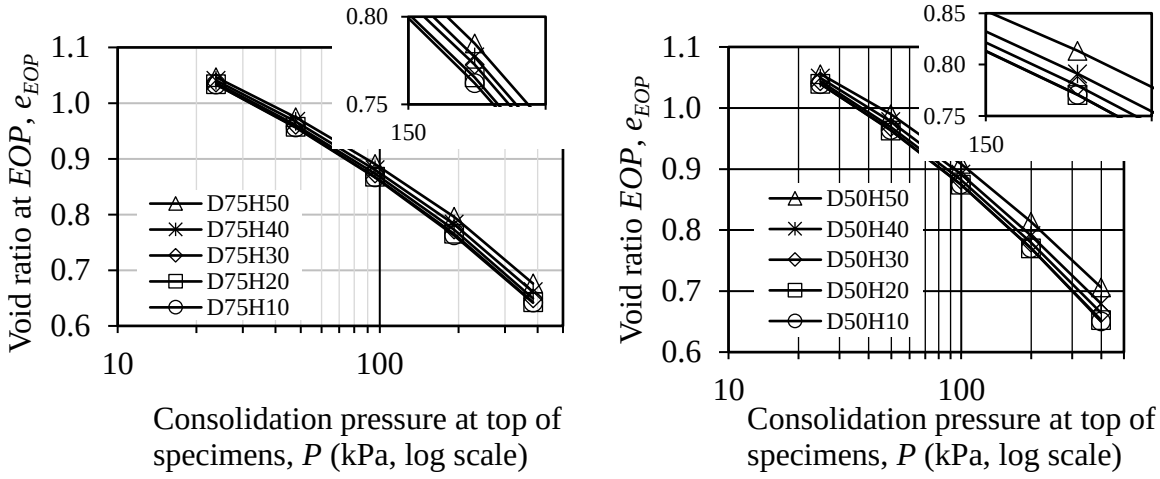

a) Diameter, D = 75mm b) Diameter, D = 50mm

Figure 3.20: Compression curves (e_{EOP}-log$P$) without pressure correction for friction pressure loss.

As expected, the compression curves of the soil specimens with initial heights of H_0 = 10 mm and 20 mm were identical, illustrating that the side friction marginally affected the test results. So, the influence of the frictional pressure loss on the 20 mm thick specimens was negligible [17].

In contrast, the void ratio at *EOP* of the specimens with the initial height, $H_0 \geq$ 30 mm, was significantly higher than those with a lower H_0. It illustrates that for the cases of $H_0 \geq 30$ mm, the friction between the soil and the inner side of the consolidation ring was high enough to cause a significant reduction in the actual consolidation pressure. In addition, the effects of friction loss were more visible for soil specimens with a smaller diameter. Several studies also provided a similar observation, which introduced that the side friction effect on one-dimensional consolidation test results was pronounced on the diameter-to-height ratio of the sample [18, 21].

d) <u>Coefficient index</u>

Based on the variation in the void ratio with the average consolidation pressure at the end of the primary consolidation, the results illustrated that the compression curves of all the soil specimens converged into a unique curve and were independent

of the dimensions of the samples and the friction pressure. It was because the effects of side friction on reducing the compression pressure were eliminated when using the average consolidation pressure to correct the compression curves (e-log$P$). In other studies [17, 18], this correction method was also applied to the consolidation test results to reveal the true e-log$P$ curves of soils with no friction pressure loss. The soil specimens exhibit normal consolidation behavior with the coefficient index of the soil, $C_c \approx 0.32$.

Since the clay specimens were remolded at a very high water content and void ratio, the pre-consolidation pressure would be too small to determine from the one-dimensional consolidation tests. However, it could be evaluated using the consolidation curves shown in Figure 3.21.

$$P_0 = \frac{P_{average}}{10^{\frac{e_0 - e_{EOP}}{C_c}}} \tag{3.7}$$

in which e_{EOP} and $P_{average}$ are the void ratio and equivalent average consolidation pressure of all the specimens at *EOP*.

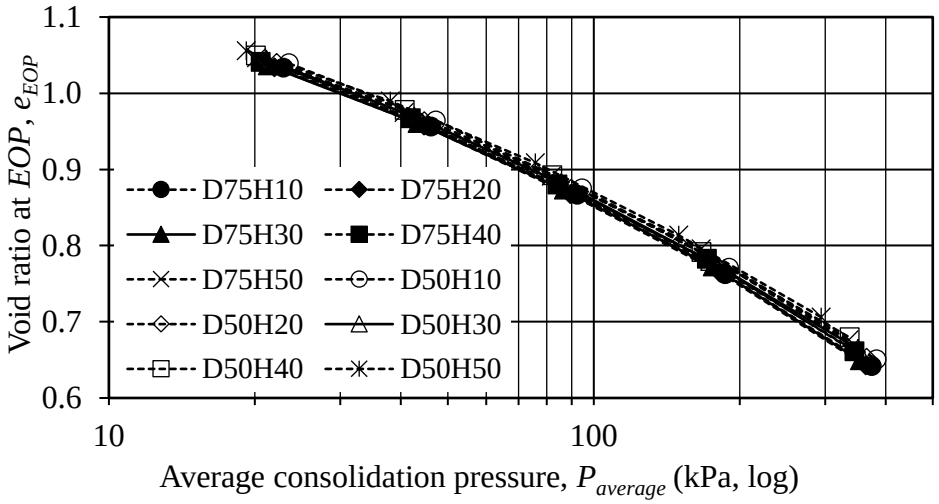

Figure 3.21: Compression curves (e_{EOP}-log$P_{average}$) of soil specimens after pressure correction for friction pressure loss.

The results of P_0 are shown in Figure 3.22, in which the average pre-consolidation pressure, $P_{0\_average}$, and the standard deviation, $\sigma_{sd\_P,}$ are 7.92 kPa and 1.68 kPa, respectively. The evaluation of the $P_{0\_average}$ value would be verified when predicting the height of specimens and the friction pressure loss ratio.

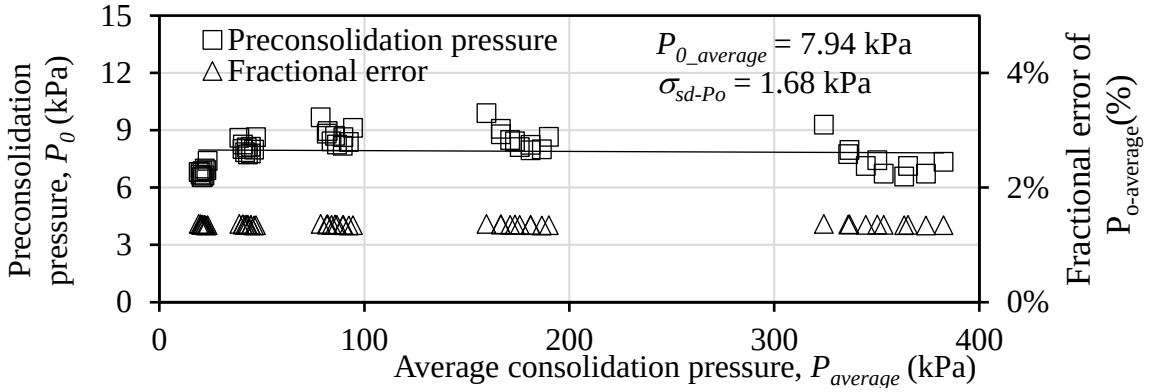

Figure 3.22: The estimated pre-consolidation pressure with fractional error σ_α/α

3.5.2. The total friction pressure and the friction pressure loss ratio

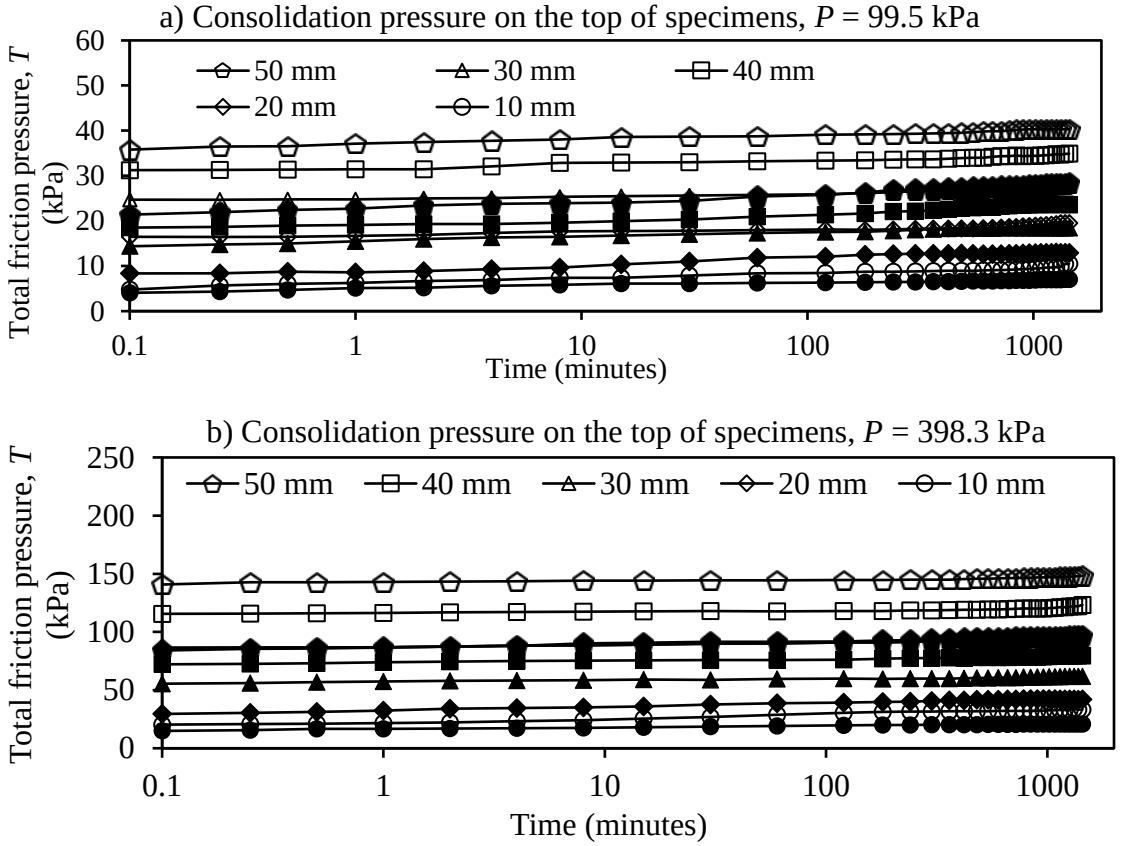

Figure 3.23: The temporal variation of total friction pressure.

The empty and solid symbols indicate the specimens with the diameters, D = 50mm and 75 mm, respectively.

The total friction pressure during the one-dimensional consolidation tests was defined as the difference between the compression pressure on top, P, and the reaction pressure measured at the bottom of the specimens, R.

$$T = P - R \tag{3.8}$$

Examples of the temporal total friction pressure with different initial heights are shown in Figure 3.23. The test results show that the value of *T* slightly increased with the soil specimens' consolidation time. Sivrikaya et al. [16] and Watabe et al. [17] also reported a similar trend for the temporal variation of *T*. It would be due to the increase in effective stress caused by water pressure dissipation. As a result, the effective lateral earth pressure rose and induced an increment in the total friction pressure, *T*. Besides, during the secondary consolidation period, the frictional pressure slightly increased in the normal consolidation range [17]. Last, a higher total friction pressure was obtained for specimens with higher thicknesses and smaller diameters. This experimental observation supports the correlation between the friction pressure and the ratio *D/H* presented in the previous studies [15, 20, 21]. As previously discussed, de Lima and Keller [19] concluded that the side friction reduced the vertical stress from the top to the bottom of soil samples. The samples with a smaller diameter would experience a greater decrease in vertical stress at the bottom (i.e., a smaller *R*) and generate a greater total friction pressure.

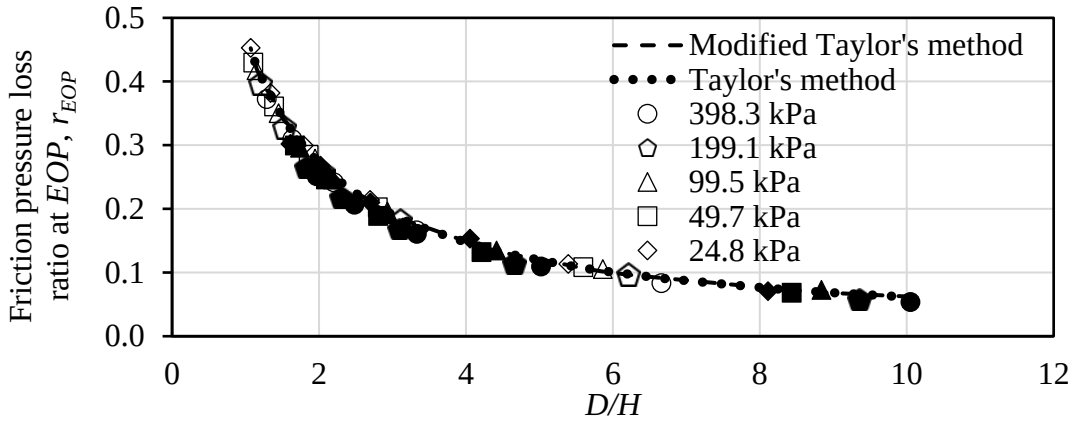

Figure 3.24: The friction pressure loss ratio at the end of the primary consolidation. The empty and solid symbols indicate the specimens with the diameters, D = 50mm and 75 mm, respectively.

The reduction due to side friction could be quantified using the friction pressure loss ratio, *r*, which is the ratio of the total friction pressure and the compression pressure, calculated as follows:

$$r = \frac{P-R}{P} \tag{3.9}$$

The result indicated that the value of r_{EOP} was strongly correlated with the *D/H* value. The higher the ratio of *D/H*, the smaller the friction pressure loss ratio. The r_{EOP} values were also reduced when the compression pressure on the top of the specimens was increased. Those findings agreed with the test results presented in other studies [15, 16, 21]. Based on the test results, a *D/H* ratio higher than 2.5 was recommended to ensure the friction pressure loss ratio is less than 0.2, which is consistent with the minimum specimen diameter-to-height ratio in ASTM D2435 [13]. For the case of *D/H* > 6, the value of r_{EOP} would be very small (i.e., less than 0.1). The ratio of *D/H*>6 also induced little friction pressure (less than 6% of the consolidation pressure) when coating the inner side of the consolidation ring with Reflon and grease [114].

3.5.3. Friction between silty soil and steel, measured by a modified shear device:

The interface shear strength between the soil and the inner surface of the consolidation ring played an important role in the friction loss in the one-dimensional consolidation test [14, 15, 20]. This interface shear strength can be determined by a modified shear device.

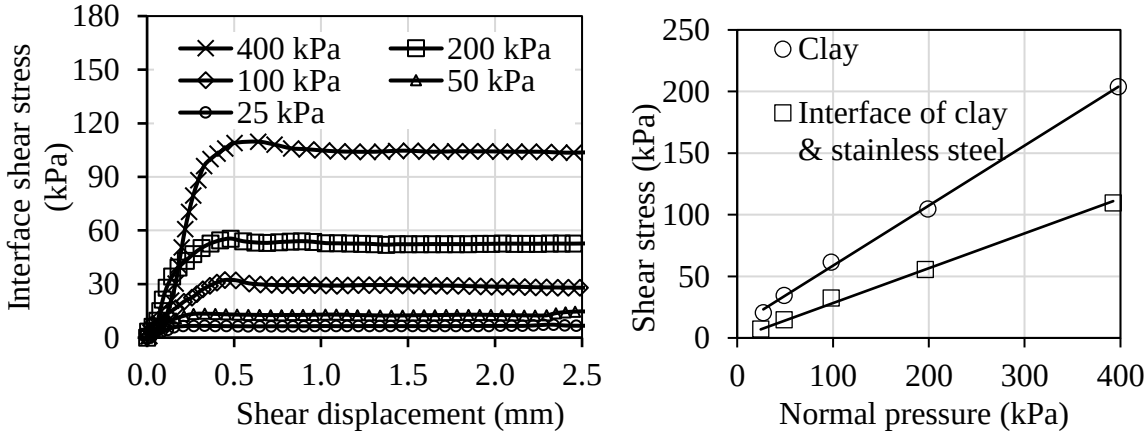

a) Interface shear strength behavior b) Failure envelops

Figure 3.25: Interface shear strength behavior and failure envelopes of shear strength and interface shear strength under different normal pressures.

In this test, the soft clay samples were made by remolding the soil from the riverbed. The dry unit weight and the water content of the remolded clay samples

were 1.621 g/cm^3 and 54.7%, respectively. The specimens were consolidated under normal pressures varying from 25 kPa to 400 kPa for 24h. They were then sheared at a shear rate of 0.004 mm/minute, as suggested in ASTM D3080 [99] for CH clay, to ensure that an insignificant excess pore pressure existed at failure.

As shown in Figure 3.25, the interface shear stress between the clay and the stainless steel surface reached the peak interface shear stress at a very small shear displacement (i.e., 0.2-0.5mm) and then remained unchanged when increasing the shear displacement. The failure envelopes were evaluated using the peak values of the shear stress and the interface shear stress. The effective friction angle of the clay, and the interface friction angle between the clay and the stainless steel, ϕ'_{int}, were 27.6^0 and 16.5^0, respectively. Those parameters were utilized to evaluate the friction pressure between the clay and the inner side of the rings in the next section.

The effective shear strength of the clay was comparable to that of the normally consolidated Kawasaki clay reported by Tsubakihara et al. [102]. Compared to the effective interface friction angle of Kawasaki clay and the polished steel surface (i.e., $\phi'_{int} \approx 22^0$), that of the clay and the stainless steel surface in this study was smaller. The difference in lubricated conditions might be crucial between the two studies. In this study, the surface of the stainless steel was lubricated with silicone grease to reduce the interface friction angle. In contrast, there was no lubrication between the surface of the polished steel and Kawasaki clay. These results encouraged silicone lubrication to minimize the interface friction between clay and steel surfaces.

3.5.4. Modified Taylor's method to evaluate friction pressure loss ratio

The side friction reduced the effective consolidation pressure and increased the void ratio of the soil at the end of the primary consolidation. By dividing the soil specimens into an infinite number of soil layers (Figure 3.26), and evaluating the side friction distribution over height *dz*, the average consolidation pressure at height z at the end of the primary consolidation could be evaluated as proposed by Taylor [14]:

$$P_z = Pe^{-\frac{4Z}{D}K_0 \tan \phi' int} \quad (3.10)$$

in which the coefficient of earth at rest, $K_0 = 1 - \sin\phi'$ for the normally consolidated clay.

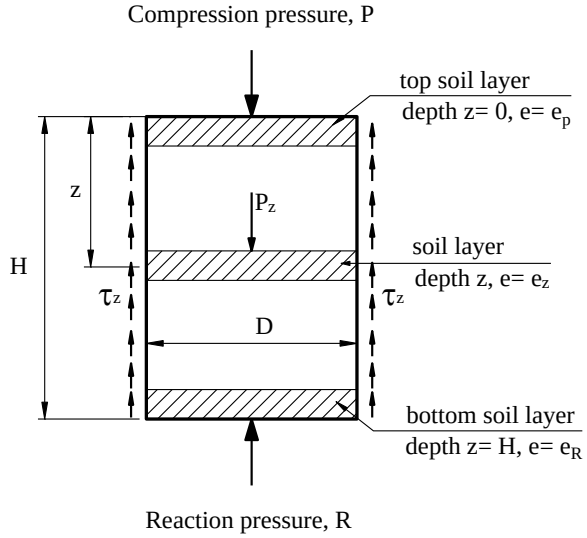

Figure 3.26: Non-uniform void ratio condition caused by side friction at *EOP*

Besides, the total friction pressure at *EOP* was calculated as follows:

$$T = P\left(1 - e^{\frac{-4H}{D}K_0 \tan\phi'_{int}}\right) \quad (3.11)$$

In which *H*: the height of the soil at EOP

Thus, Taylor's equation to evaluate r_{EOP} could be written as

$$r_{EOP} = 1 - e^{\frac{-4H}{D}K_0 \tan\phi'_{int}} \quad (3.12)$$

Since the height of soil specimens at *EOP*, *H*, was not predetermined before tests, the application of Taylor's equation is limited.

To improve, an analytical method was developed to evaluate the *H* value based on the initial height of samples, H_0:

$$H = \alpha H' \quad (3.13)$$

in which H' is the height of specimens at EOP without side friction effects. For normal consolidated soil, the value of H' could be calculated as

$$H' = \left(1 - \frac{C_c}{1+e_0} log\frac{P}{P_0}\right) H_o \quad (3.14)$$

And α is the height factor that accounts for the effects of side friction:

$$\alpha = \frac{1}{1 - \frac{C_c}{1+e_0}\frac{2H_0}{D\ ln\ 10}K_0 \tan\varphi'_{int}} \quad (3.15)$$

in which e_0: the void ratio at the pre-consolidation pressure, P_0.

It should be noted that the value of α is higher than 1 as the side friction reduced the consolidation pressure from the compression pressure on the top, *P*, to the average consolidation pressure. As a result, the height of specimens at *EOP*, *H*, should be higher than that without side friction effects (i.e., H> *H'*). The value of *H* could be obtained from the equation:

$$H = \alpha \left(1 - \frac{C_c}{1+e_0} log \frac{P}{P_0}\right) H_o \tag{3.16}$$

The error of *H* due to the evaluation of P_0 was evaluated by considering the pre-consolidation pressure as a variable in the equation of P_0. By applying the derivation of the function *H*, factional error σ_{SD_H}/H can be evaluated based on the fractional error $\sigma_P/P_{0\_average}$.

$$\frac{\sigma_{SD\_H}}{H} = \frac{\frac{C_c}{(1+e_0)\,ln\,10}}{1-\frac{C_c}{1+e_0} log \frac{P}{P_0}} \frac{\sigma_{SD\_P}}{P_{0\_average}} \tag{3.17}$$

The results of the fractional σ_{SD_H}/H of all the cases are less than 1.8%, which illustrates that the proposed method was applicable for evaluating the pre-consolidation pressure.

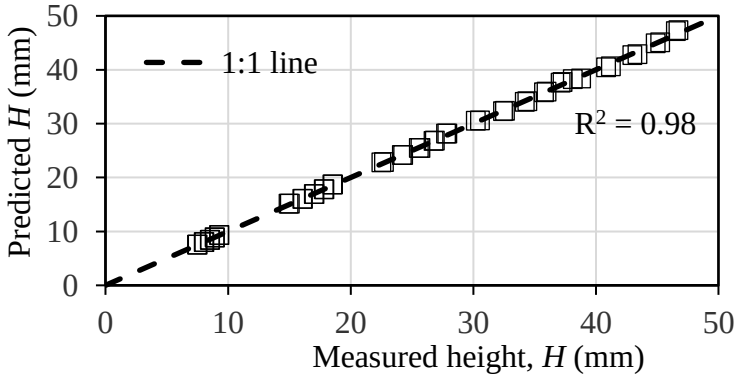

Figure 3.27: Comparison between the experimental and predicted height of soil specimens at *EOP* using the height factor

The results of the predicted *H* illustrated that the proposed equations were a good prediction method with a determination coefficient of $R^2 = 0.98$ (Figure 3.27).

Therefore, Taylor's equation would be modified to evaluate r_{EOP}

$$r_{EOP} = 1 - e^{\frac{-4H_0}{D}\alpha\left(1-\frac{C_c}{1+e_0}log\frac{P}{P_0}\right)K_0\,tan\,\varphi'_{int}} \quad (3.18)$$

The predicted results of r_{EOP} using Taylor's method and modified Taylor's method were verified and demonstrate that good agreement exists between the measured values and prediction results, of which the coefficients of determination, R^2, are equal to 0.95 and 0.97 (i.e., very close to 1), respectively. In other words, in the one-dimensional consolidation tests, those two methods would be able to accurately predict the friction pressure loss ratio of the clay specimens at the end of primary consolidation. Sivrikaya et al. [16] also reported that the measured values of side friction parameters were consistent with those calculated using Taylor's method. However, the modified Taylor's method is more applicable since it does not require the determination of *H*, which might be difficult to determine before tests. It should be noted that the two methods are only suitable for predicting the value of r_{EOP} for the clay in the normal consolidation range.

3.5.5. The non-uniform density in the specimens caused by side friction:

The non-uniform soil density was caused by the side friction. Due to the greater side friction pressure, specimens with a lower ratio of *D/H* exhibited a more uneven soil condition. Based on the consolidation index for normally consolidated clay, the void ratio of soil at depth z could be determined. Due to the fact that the self-weight of the soil samples was less than 30 times the consolidation pressures, its value was omitted from the equation below:

$$e_z = e_P + \frac{4z}{D\,ln\,10}K_0\,tan\,\phi'_{int}C_c \quad (3.19)$$

in which e_P: the void ratio under the compression pressure *P* acting on the top of the specimen.

The above equation would be verified using the void ratio of the soil specimens at the end of the primary consolidation, which was the average value of the void ratio:

$$e_{EOP\_predicted} = e_P + C_c\frac{2H_0}{D\,ln\,10}\alpha K_0\,tan\,\phi'_{int} \quad (3.20)$$

Comparing measurement and prediction results, in which the solid line is the 45^0 line, exhibited a degree of equality between those two results.

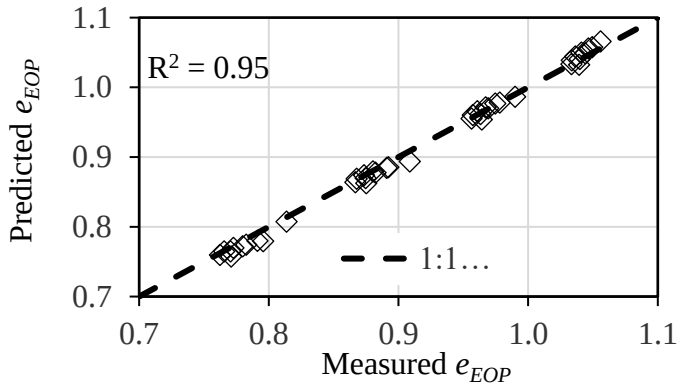

Figure 3.28: Comparison between the measured and predicted void ratio

When considering constants K_0 and $tan\phi'_{int}$, the void ratio would increase proportionally with the depth. The linear distributions of the void ratio and the ratio *z/H* were evaluated. The soil with the smallest void ratio (i.e., the densest condition) is located on the top, while the loosest soil (i.e., the highest void ratio) is found at the bottom of the soil specimens.

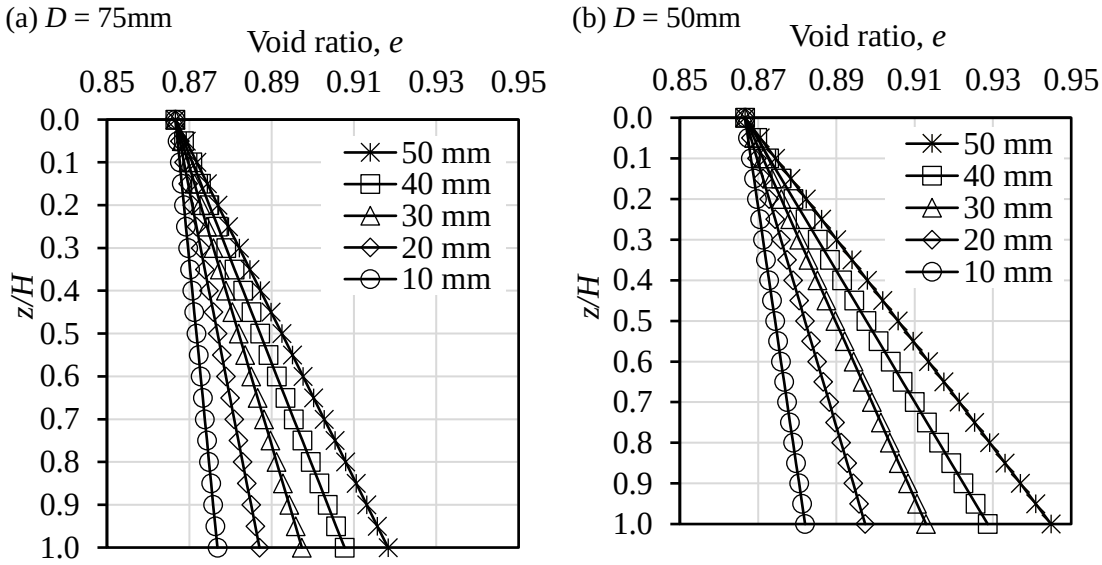

Figure 3.29: The variation of void ratio with the depth with the diameter (a) *D* = 75mm and (b) *D* = 50m under the compression pressure, *P* = 99.5 kPa

3.5.6. The coefficient of variation, *COV*:

Similar to the study conducted by Mir et al. [26]**,** the degree of uniformity of the void ratio in the soil samples at *EOP* was quantified using the coefficient of variation, *COV*. The greater the coefficient of variation, the less uniformity of void ratio along the depth of soil specimens at *EOP*. On the basis of the variation of void

ratio with the depth of the soil specimens, the value of *COV* was determined by dividing a soil sample into n layers along its depth.

$$COV = \frac{\sigma_{SD\_e}}{e_{EOP}} \tag{3.21}$$

in which σ_{SD_e} and e_{EOP} are the standard deviation and the average void ratio at *EOP*, respectively. The σ_{SD_e} could be evaluated by using the value of the void ratio:

$$\sigma_{SD\_e} = \sqrt{\frac{\sum_{z=0}^{H}(e_z - e_{EOP})^2}{n}} \tag{3.22}$$

Thus, the COV value could be evaluated by applying an infinite value to *n*:

$$COV = \frac{2H}{\sqrt{3}\, ln\, 10 D e_{EOP}} K_0\, tan\, \varphi\,'_{int} C_c \tag{3.23}$$

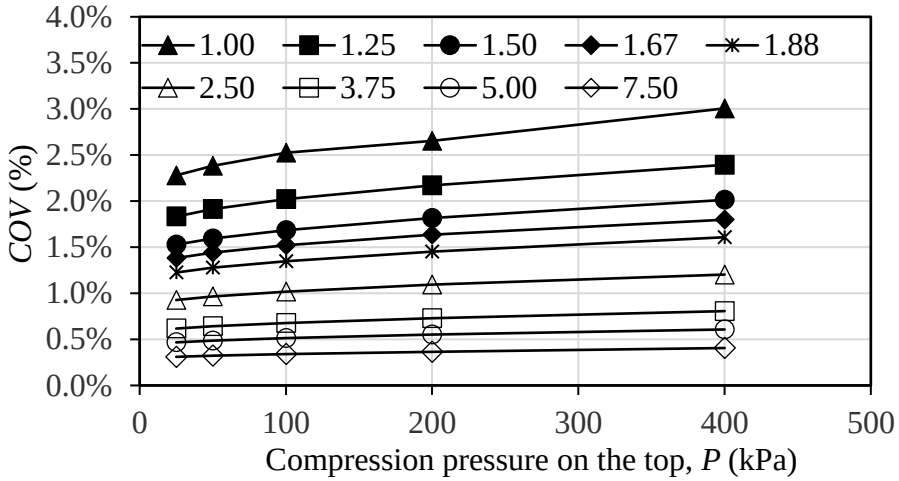

Figure 3.30: Variation of *COV* with the compression pressure on the top of soil specimens with different ratio D/H_0

From the above equation, the value of *COV* increased proportionally with the coefficient of side friction, the ratio *D/H*, and the soil compression coefficient, C_c. In addition, as shown in the following figure, specimens subjected to a higher compression pressure, *P*, would exhibit a greater coefficient of variation (i.e., a lower degree of uniformity). For specimens with $D/H_0 \geq 2.5$, the *COV* values were less than 1.2%, indicating that the void ratio of soil was distributed uniformly in the specimens at *EOP*. This result supported the requirement of the specimen size (i.e., $D/H_0 \geq 2.5$) in the current standard practice to eliminate the effect of wall friction in one-dimensional consolidation experiments [13]. This *COV* value (1.2%) was marginally

less than the variation in water content across the radius of triaxial soil specimens subjected to undrained loading followed by consolidation (1.5%) [24]. In addition, the value of *COV* for the variation of the void ratio of specimens with D/H_0 = 3.75 was less than 0.8% (Figure 3.30), which concurred with de Lima and Keller's [19] suggestion that the error in bulk density caused by neglecting soil-wall friction was approximately 1% for D/H_0 = 3.00.

In addition, the correlation between *COV* value and friction pressure loss was determined using the results of one-dimensional consolidation experiments reported in Table 1.1 from additional studies. As shown in Figure 3.31, a higher friction pressure loss ratio generally induced a higher *COV* of void ratio. The consolidation pressure loss ratio at *EOP* was less than 0.21 for samples with a *COV* lower than 1.2%. In other words, the requirement of $D/H_0 \geq 2.5$ not only ensures the homogeneity void ratio in the specimens (i.e., *COV*<1.2%), but it also limits the loss of consolidation pressure at *EOP* due to side friction to less than 21%.

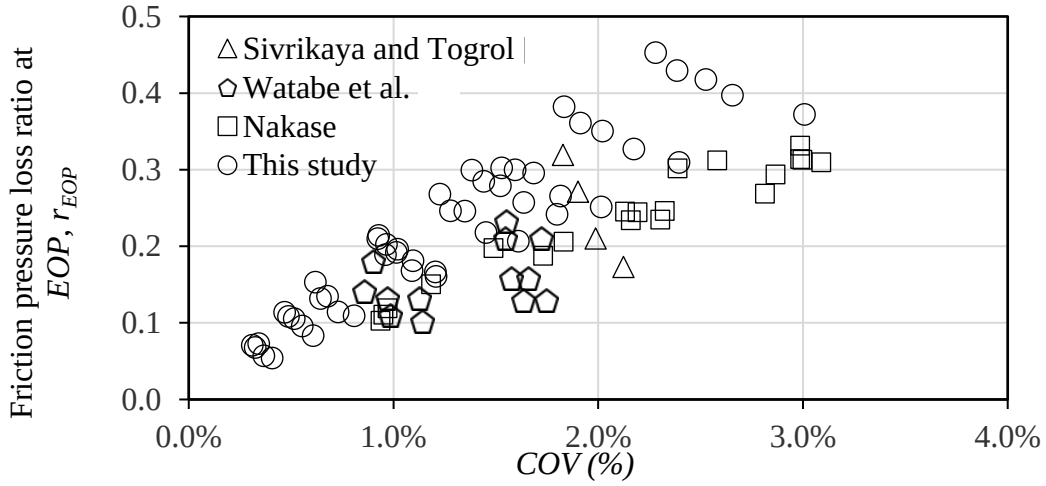

Figure 3.31: Variation of *COV* with the friction loss ratio at *EOP* of soil specimens obtained from different studies.

3.6. BEHAVIOR OF SILTY SOIL WITH AND WITHOUT GEOTEXTILE UNDER ONE DIMENSIONAL CONSOLIDATION TEST

3.6.1. Primary consolidation

The test samples were 50 mm in diameter and 40 mm tall, including an unreinforced sample and 1, 3- geotextile layer samples. Figure 3.32 depicted the

required time to attain 90% consolidation (T_{90}) and 100% consolidation (T_{100}). The consolidation time decreased from unreinforced to reinforced samples with 1 layer and 3 layers of geotextile. Consolidation time was reduced by approximately 1.5 to 2 times when adding a layer of geotextile.

As a result, geotextile enhanced the process of dissipating the excess pore water pressure. Although the geotextile has not adhered to the external drainage boundary, the results demonstrated that consolidation was accelerated in the reinforced sample. In this instance, the geotextile was regarded as a drainage boundary, thereby decreasing the drainage path.

Due to the side friction, the load compression decreased with the depth of the samples. Therefore, the average compression pressure, which was measured by the modified oedometer apparatus in Section 2.4, was ultilized instead of the load compression.

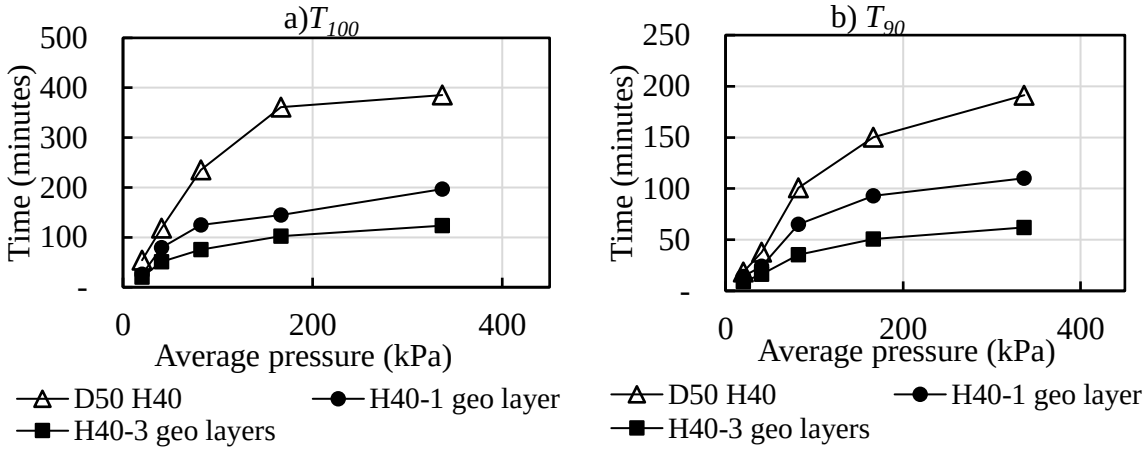

Figure 3.32: The required time to obtain a) 100% (T_{100}) and b) 90% (T_{90}) consolidation of geotextile samples

3.6.2. Consolidation coefficient C_v:

When the clay was reinforced with geotextile, the consolidation coefficient C_v increased due to its enhanced permeability, causing the consolidation process to occur more rapidly. However, as the load developed, the C_v reduced.

Due to side friction, the consolidation coefficients C_v vs. average pressures were displayed in Figure 3.33:

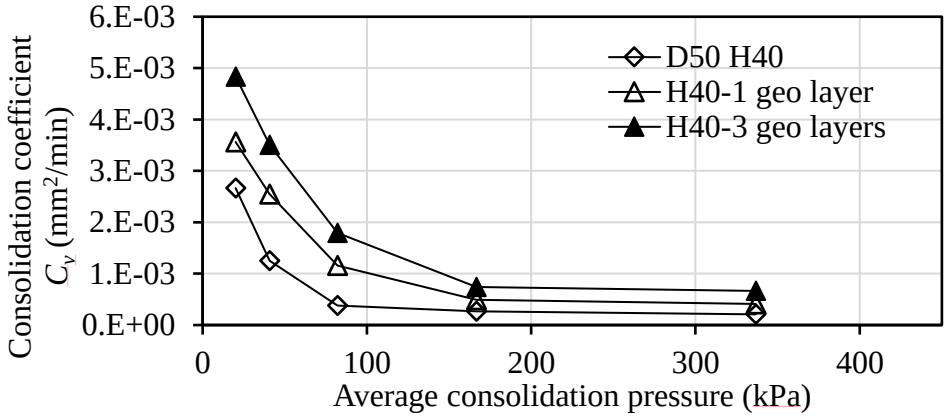

Figure 3.33: The consolidation coefficients C_v vs. average pressure of geotextile soil samples

3.7. CONCLUSION

A series of tests, including *CBR*, *UU* triaxial, and consolidation tests, were performed to investigate geotextile's effect on soil improvement due to the soaking process. The results illustrated the critical role of reinforcement inclusion in enhancing bearing capacity and consolidation in both soaked and unsoaked conditions. The additional conclusions are:

a) Behavior of soil and geotextile-soil under swelling and the CBR test:

1. The permeable reinforcement induces swell faster by adding more drainage paths into the reinforced specimens. It also reduces the percent swell and soil density reduction after soaking. The higher the number of reinforcement layers in the reinforced specimens is, the lower the swell percentage is. The dry unit weight reduction due to soaking decreases from 4.43% (for unreinforced clay) to 3.43% (for a 5-layer reinforced specimen).

2. The nonwoven geotextile significantly improves the *CBR* behavior of expansive clay in both soaked and unsoaked conditions; however, the effect of reinforcement is activated more effectively when the soil is soaked. Compared to the *CBR* value of unreinforced clay, the highest strength ratios are 1.5 and 3.3 for the unsoaked and soaked specimens reinforced by 2 reinforcement layers, respectively.

3. The *CBR* behavior of reinforced specimens is dependent on the changes in piston penetration, and it requires sufficient deformation to mobilize the shear

strength from soil-reinforcement interaction and the membrane force from reinforcement tension. When the penetration is less than 2 mm, there is no significant bearing capacity improvement. Up to 5.08 mm of penetration, the specimens reinforced with 2 reinforcement layers (i.e., h_{geo} /D_{piston} ≈ 0.8) reach the highest bearing capacity. When the penetration is beyond 13 mm, the specimens reinforced with a higher number of reinforcement layers will have a higher bearing capacity due to the full activation of all the reinforcement layers.

4. Both the unreinforced and reinforced specimens significantly reduced their bearing capacity after soaking. However, the nonwoven geotextile remedies the *CBR* reduction of reinforced specimens. While the unreinforced specimens decreased by 76.9% of their *CBR* value, the value of the reinforced specimens is only less than 50%. After soaking, the *CBR* of the reinforced specimen is up to 7.2%, and the *CBR* value of the unreinforced specimens is very low, only 2.2%.

b) Behavior of silty soil with and without geotextile on UU shear strength under the triaxial test:

1. The soil strength diminished from 68% to 83% when the soil was saturated. However, the shear strength reduction of reinforced samples was about 65% to 78% for the 1-layer specimen and 57% to 69% for the 3 geotextile layers.

2. Unsaturated soil's shear strength increased with the number of geotextile layers, up to 1.6 times for 3 geotextile layer samples. The cohesion and the angle of internal friction can change without a general trend. However, the shear strength increased in all reinforced soils.

3. When the strain was from 1% to 3%, a higher excess pore water pressure was found than in the unreinforced samples because the geotextile prevented the soil from lateral expansion. As the strain increased, there was a sliding phenomenon between the soil and the geotextile, reducing the pore water pressure, and the pore water pressure dissipated through the geotextile's high permeability.

Thus, geotextiles prevented horizontal movement and enhanced the soil's shear strength, especially in the saturated condition.

c) Consolidation behavior of silty soil under the effects of side friction:

A modified consolidation apparatus was introduced to investigate the side friction between the soil and the inner side of the consolidation ring. The following are the findings of this investigation:

1. Despite side friction, Terzaghi's one-dimensional consolidation theory about the proportional relation between the consolidation time for the primary consolidation and the squared maximum drainage distance is still valid. The coefficient of consolidation was highly dependent on the average consolidation pressure.

2. The total side friction pressure increased marginally with increasing consolidation time, but this resulted in a substantial decrease in the average consolidation pressure at *EOP*.

3. The friction pressure loss ratio at the end of primary consolidation decreases as D/H_0 increases. It also decreased when the applied compression pressure was increased. In particular, the friction pressure loss ratio for $D/H_0>2.5$ and $D/H_0>6$ was less than 0.2 and 0.1, respectively.

4. The proposed analytical method can accurately predict the values of r_{EOP} and e_{EOP} for clay under the normal consolidation pressure range without requiring the height of specimens after tests.

5. Side friction induces the condition of a non-uniform void ratio in clay specimens. In particular, the void ratio at the end of primary consolidation increases proportionally with depth. Using *COV* values of the void ratio, the degree of uniformity of soil samples at the *EOP* was measured. The greater the friction pressure loss ratio, the greater the *COV* values. The results also prompted the use of specimens with $D/H_0>2.5$ for one-dimensional consolidation experiments to ensure a uniform void ratio with a *COV* of less than 1.2%.

It should be remembered that the data relates to one-dimensional consolidation tests on remolded clay at *EOP* under normal consolidated pressure. The conducted tests were intended to simulate the compression conditions of the intact soil, although

its mechanical properties (such as shear strength and compression behavior) deviate considerably from those of the remolded soil. Despite these differences, the test data are expected to provide valuable and insightful information for understanding the effects of side friction on the one-dimensional consolidation behavior of clay. Furthermore, the proposed analytical equations could be applied to predict the friction pressure loss and the *COV* values of the void ratio of soil specimens in the one-dimensional consolidation tests.

d) Behavior of silty soil with and without geotextiles under consolidation test:

Geotextiles accelerated the silty soil consolidation process by 1-2 times compared to unreinforced soil. Moreover, the consolidation coefficient increased as the number of geotextile layers increased and decreased as the consolidation pressure increased.

The significant drop in the bearing capacity of both unreinforced and reinforced expansive clay suggests that a good drainage system is crucial for the unreinforced and reinforced clay structures to maintain their bearing capacity and stabilization. Additionally, the geotextile acts as a drainage path, forcing the consolidation process of the soil sample to happen faster.

CHAPTER 4: BEHAVIOR OF SILTY SOIL WITH AND WITHOUT SAND CUSHION UNDER CBR, UU, AND CONSOLIDATION TEST

4.1. INTRODUCTION

Riverbed silty soil was difficult to reuse because of the massive property changes caused by changing its water content. When saturated, it becomes looser and softer, causing a significant reduction in bearing capacity. To improve those disadvantages, the clay was reinforced by a nonwoven geotextile with a sandwich sand layer [31, 44]. These results showed that a thin sand cushion improves the interface friction between clay and geotextile, increasing the strength of clay. This sand cushion was also a drainage boundary, decreasing the pore pressure with increasing loads [46–48].

Although there were many studies to investigate the behavior of clay reinforced by a sand cushion, the swellings, *CBR* value, shear capacity due to wetting, and consolidation of reinforced soil were not fully determined, especially for the clay in the Mekong Delta. The research objectives of this chapter are:

- Effect of sand cushion on silty soil's swelling and *CBR* value in unsaturated and saturated conditions by the *CBR* test.
- Effect of sand cushion on the *UU* shear strength in unsaturated and saturated conditions by triaxial test to evaluate the soil capacity when constructed fast.
- Effect of sand cushion under the one-dimensional consolidation test.

Each objective corresponds to a type of test.

4.2. EXPERIMENTAL PROGRAM

4.2.1. *CBR* specimens

Similar to *CBR* specimens reinforced by geotextile, 8 specimens were reinforced with cushion sand for soaked and unsoaked conditions. The thickness of the sand cushion varied from 10mm to 15mm, 20mm, and 40 mm.

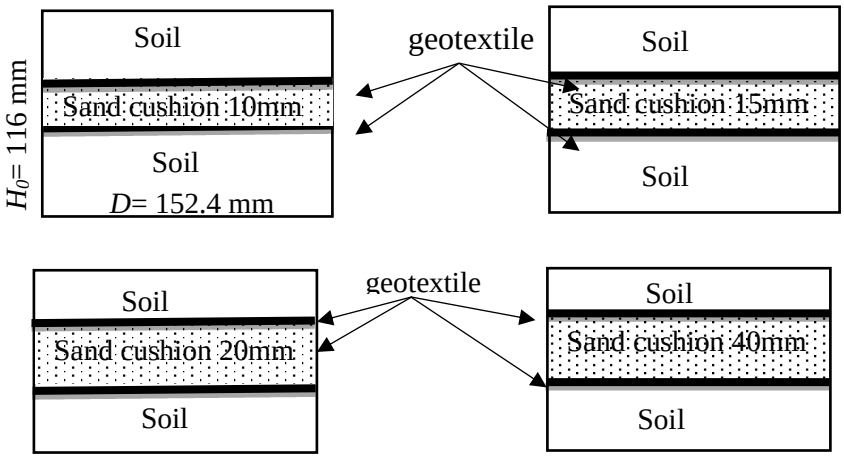

Figure 4.1: The arrangement of the sand cushion with varied thickness reinforced CBR specimens in unsoaked and soaked conditions.

4.2.2. Unconsolidated-Undrained shear strength samples in the triaxial test

Similar to the specimens reinforced by geotextile, there were 15 sand cushion samples with sand thicknesses ranging from 5mm to 10 mm and 20 mm. There were 2 types of tests, as follows:

- *Unsaturated samples*: samples will be tested at lateral pressures of 50 kPa, 100 kPa, 150 kPa, and 200 kPa.
- *Saturated samples*: samples will be saturated at 500 kPa pressure and tested at 300 kPa lateral pressure.

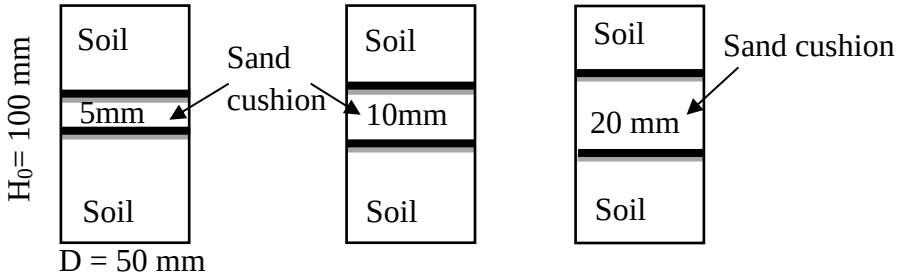

Figure 4.2: The arrangement of sand cushions in the UU test.

a) 5 mm sand cushion b) 10 mm sand cushion c) 20 mm sand cushion

Figure 4.3: The sand cushion specimens in the UU test.

4.2.3. Consolidation samples

To investigate the consolidation of reinforcement soil, 10 mm and 20 mm of sand were placed between geotextiles in the middle of the soil. All specimens were created with 54.7% water content, and the pressure was 49.7 kPa, 99.5 kPa, 199.1 kPa, and 398.3 kPa, respectively. The total height of the specimens was 40mm.

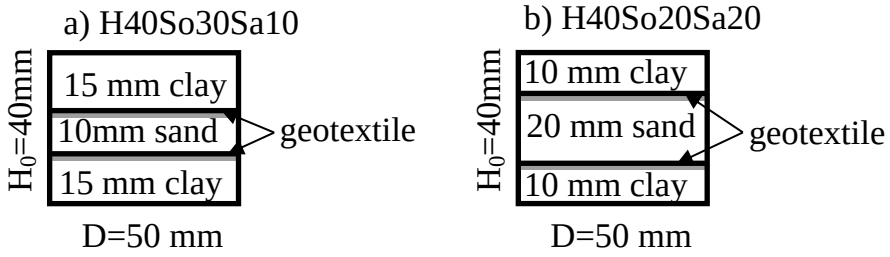

Figure 4.4: Samples reinforced by sand cushions in one-dimensional consolidation

The results of the sand cushion samples would be compared to the soil with a height of 30 mm and 20 mm, namely H30 and H20, respectively.

4.3. BEHAVIOR OF SILTY SOIL WITH AND WITHOUT SAND CUSHION UNDER THE SWELLING AND CBR TEST

4.3.1. Influence of the sand cushion on the swell behavior

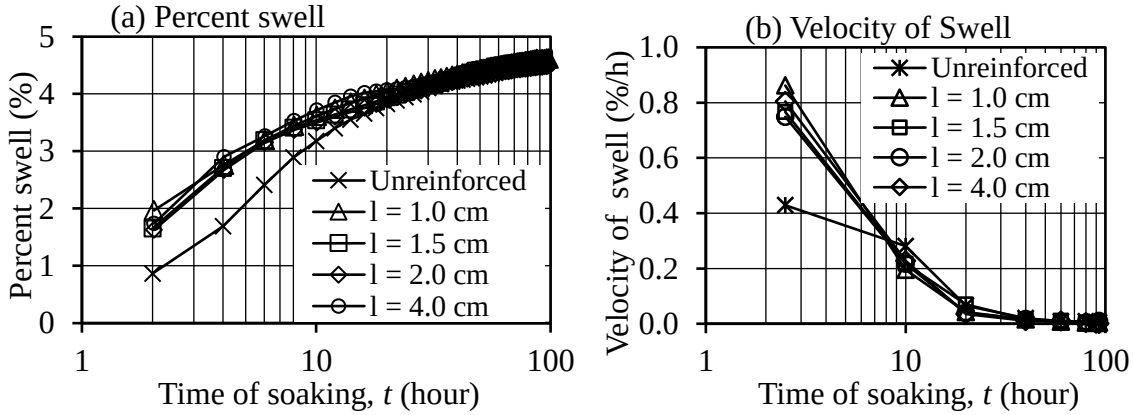

Figure 4.5: Swell behavior with time of unreinforced and reinforced specimens (a) percent swell and (b) velocity of swell

The percentage swell of unreinforced and reinforced specimens (*S*) in time is given in Figure 4.5. Generally, it increased with time during the soaking process. The swell of the specimens reached equilibrium after 96 hours of soaking.

In the first 30 hours, the percentage swell of reinforced specimens is higher than that of unreinforced specimens. However, in the end, the swells of the reinforced

specimens were slightly smaller than those of the unreinforced specimens. The effect is due to the local lateral confinement from soil-reinforcement interaction. It can be explained that the expansion develops in all directions and mobilizes the interfacial frictional force between soil and reinforcement [35]. This frictional force tends to counteract the swelling pressure in a direction that parallels the reinforcement and consequently reduces the heave. A similar observation was found by Keerthi [108].

Regarding the swelling velocity, which was evaluated as the percent swell per hour of soaking, in the first 10 hours of soaking, the reinforced specimen's swell velocity was significantly higher than that of unreinforced specimens. It could be explained by the high permeability of nonwoven geotextile layers and sand cushions, which enhance the velocity of swell in reinforced specimens. After 20 hours, the influence of the reinforcement layers on the swell behavior of the reinforced specimens was diminished. The swell velocity of unreinforced and reinforced specimens was reduced to less than 0.005%/h after 96h of soaking.

To conclude, the sand cushion with high permeability induced swell faster at the initial soaking but a lower final percentage of the swell.

Table 4.1: Percent swell and dry unit weight reduction after 96h of soaking of sand cushion- soil

Thickness of sand cushion layer (mm)	Sand/Clay dry mass ratio	Final percent swell S_{96h} (%)	Dry unit weight reduction $\%\Delta\gamma_d$ (%)
0	0.00	4.64	4.43
10	0.10	4.63	4.41
15	0.16	4.60	4.40
20	0.23	4.49	4.30
40	0.58	4.51	4.32

During the soaking process, there are no changes in the dry weight of soil specimens, but there is an increase in the volume of the specimens, resulting in a decrease in the dry density of the clay layers. As shown in the table, the reduction in dry unit weight of the clay in the reinforced specimens was slightly smaller than that of the unreinforced specimen. In other words, when compacted by the same density at initial, after soaking, the clay in the reinforced specimens would be higher than that

in the unreinforced specimens, which contributed to the higher bearing capacity of the reinforced specimens than that of the unreinforced specimens after soaking.

4.3.2. The CBR behavior of unreinforced and reinforced specimens

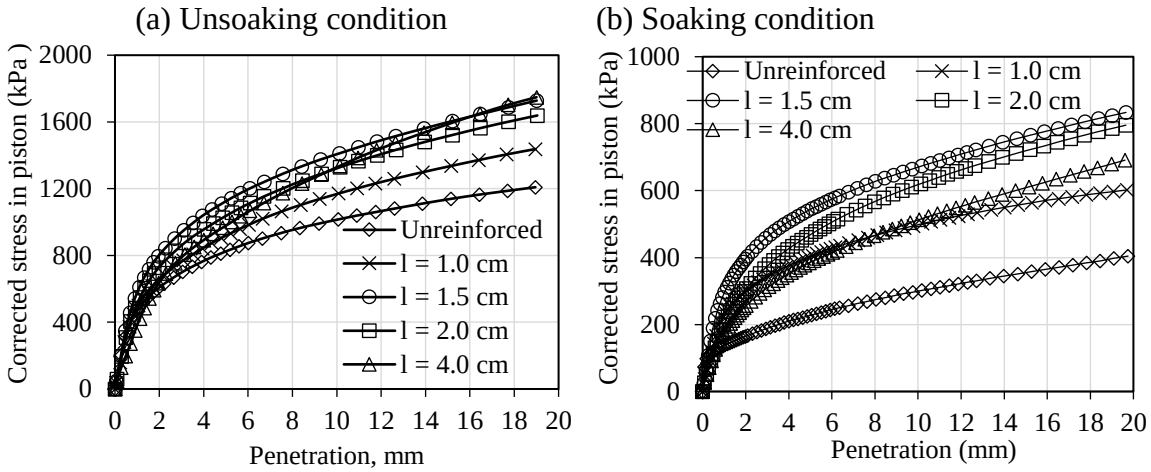

Figure 4.6: Corrected stress in the piston of the specimen (a) without soaking and (b) soaking condition

Due to the reinforcement, the *CBR* value of reinforced specimens was higher than that of unreinforced specimens.

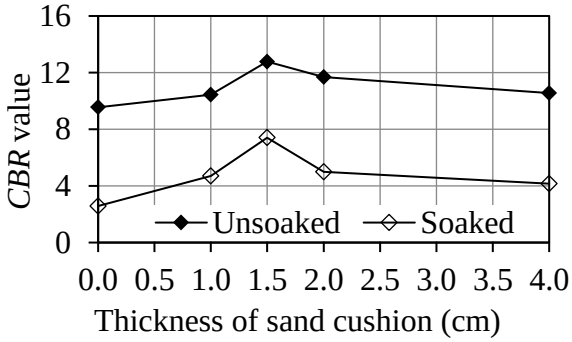

Figure 4.7: The *CBR* of the soaked and unsoaked specimens with the thickness of the sand cushion layer

Interestingly, the bearing capacity of the specimens was the highest for the specimens reinforced by 2 layers of geotextile with a 1.5 cm thickness of the sand cushion, of which the ratio of the height of the topsoil layer and the diameter of the penetrated piston, D_{piston}, was equal to 1. This optimum value agreed with those in previous studies. Koerner et al., [106] found that the thickness of soil required to cover a geosynthetic clay liner should be at least equal to the diameter of the load

piston. A similar conclusion was presented when performing the *CBR* test on the expansive soil subgrades reinforced with a single reinforcement layer [36, 108].

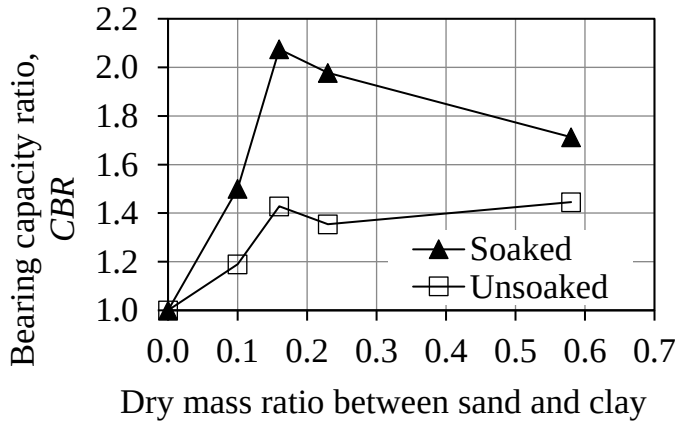

Figure 4.8: The correlation between the strength ratio and the dry mass ratio

When increasing the ratio between sand and clay dry mass, the *CBR* also went up in both cases. For the case of un-soaking, the *CBR* value increased approximately 1.2 times and up to 1.4 times when the ratios were 0.1 and 0.16, respectively, compared to the un-reinforced specimen. However, the increase in the *CBR* value was not apparent when continuing this ratio (about 1.3 to 1.4 times when the ratio was 0.23 and 0.58). Similarly, with a larger scale for the case of the soaking process, the *CBR* jumped up to 1.5 and over 2 times when raising this ratio to 0.1 and 0.16 in the same order. Interestingly, for both cases, the maximum increase occurred when the ratio between sand and clay dry mass was 0.1. It can be concluded that using sand and geotextile can significantly improve the bearing capacity of soil when the soil was wet, and the optimal dry mass ratio between sand and clay was 0.1.

4.3.3. Influences of soaking on the *CBR* behavior of unreinforced and reinforced specimens

Compared to the unsoaked specimens, the *CBR* value of the soaked specimens was much smaller, which demonstrated the extreme reduction of the strength of clay when saturated. The figure below shows the ratio of *CBR* of un-soaking and soaking specimens, which exhibited the strength reduction of specimens due to soaking. For the unreinforced specimens, the ratio reached the highest (about 3.7) and decreased to less than 2.6 for the reinforced specimens. The lowest strength reduction was 1.73

for the specimen reinforced by the 1.5cm thickness of the sand cushion layer. Robert G. Nini [115] also had similar observations about the significant *CBR* reduction when performing *CBR* tests after soaking for two days.

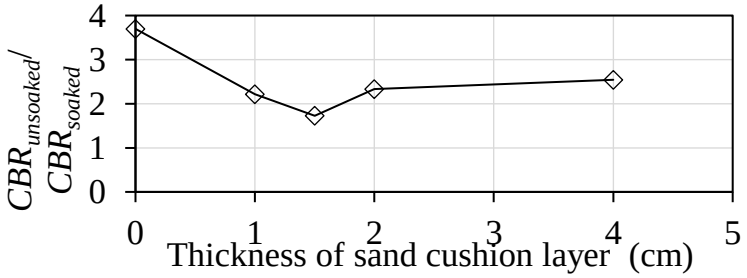

Figure 4.9: The influence of the thickness of the sand cushion layer on the ratio of *CBR* of specimens before and after soaking.

In short, sand cushions not only enhanced the bearing capacity of clay soil under both soaked and unsoaked conditions but also minimized the strength reduction of the clayey soil after soaking.

4.4. BEHAVIOR OF SILTY SOIL WITH AND WITHOUT SAND CUSHION ON UU SHEAR STRENGTH UNDER THE TRIAXIAL TEST

4.4.1. The shear strength behavior of silty soil reinforced with a sand cushion in the unsaturated condition.

a) <u>Shear strength behavior of unsaturated soil reinforced by a sand cushion:</u>

The relationship of deviation stress ($\Delta\sigma = \sigma_1 - \sigma_3$) versus axial strain of soil reinforced by a sand cushion was shown in the below figure. The results indicated that the deviation stress increased as the lateral pressure σ_3 and the thickness of the sand cushion increased.

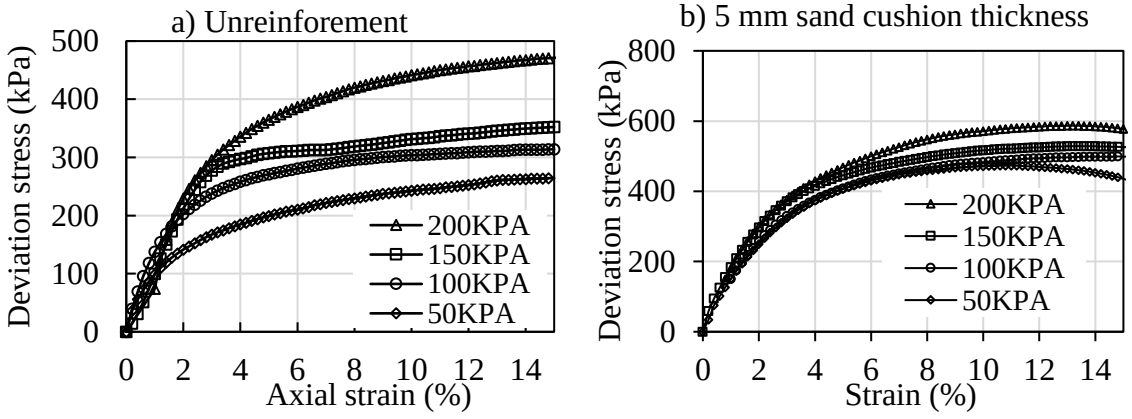

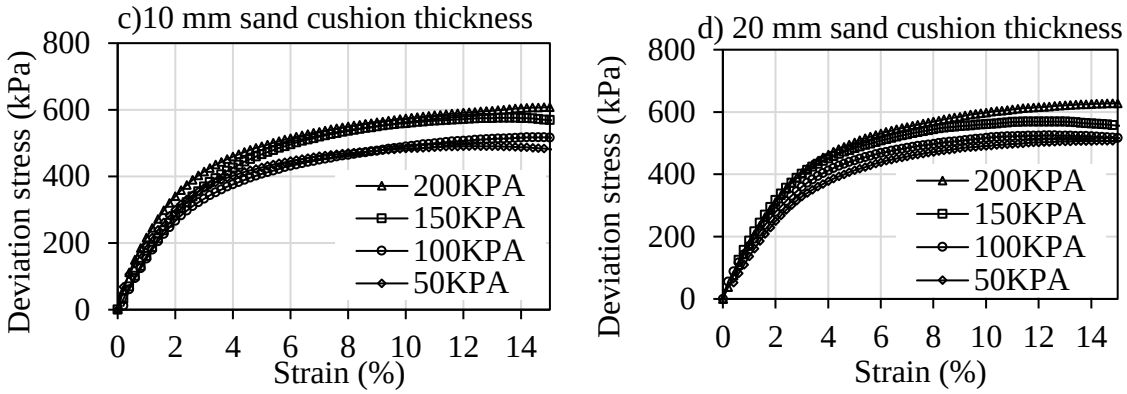

Figure 4.10: Deviation stress versus axial strain of sand cushion samples in the unsaturated condition

The relationship between vertical and lateral pressures of soil and sand cushion-soil was shown in Figure 4.11 when the specimen failed at 15% strain.

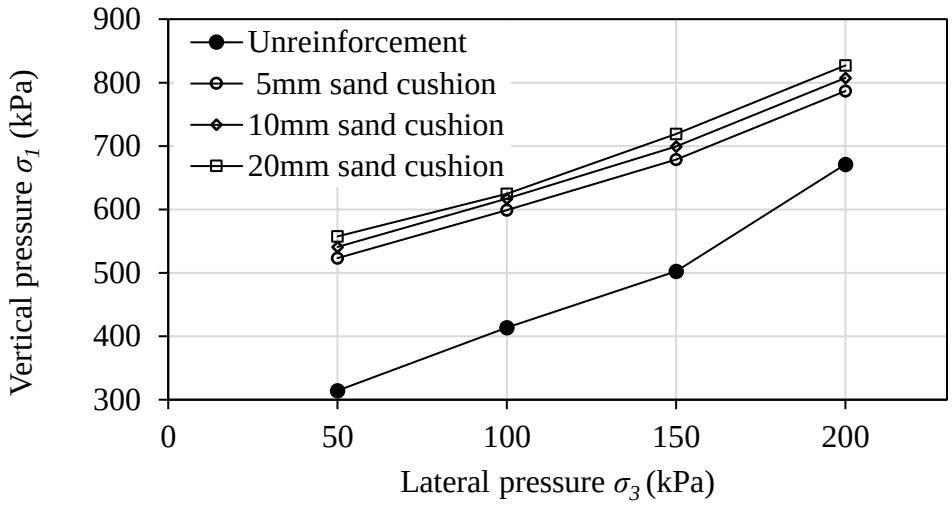

Figure 4.11: The vertical versus lateral pressure of soil and sand cushion-soil at failure in unsaturated condition

Reinforcing the *UU* with the sand cushion increased its shear strength substantially at failure. With a 5mm sand cushion, the sample's strength was approximately 1.2 to 1.4 times greater than without reinforcement. When the thickness of the sand increased, its strength increased slightly.

Table 4.2 displays the results of calculating the total cohesive force (c) and the total internal friction angle (φ) for the reinforced cases in the *UU* condition because excess pore water pressure cannot be measured.

Table 4.2: The cohesive (c) and internal friction angle (φ) of sand cushion-soil at failure of this and previous studies

Condition	Type of reinforcement	φ (°)	c (kPa)	Reference
UU	Unreinforcement	65.6	19.8	Yang et al. [11]
UU	5 mm sand cushion	63.8	69.8	Yang et al. [11]
UU	10 mm sand cushion	67.5	50.0	Yang et al. [11]
UU	15 mm sand cushion	67.2	74.7	Yang et al. [11]
UU	20 mm sand cushion	70.2	47.6	Yang et al. [11]
UU	Unreinforcement	23.4	60.9	This study
UU	5 mm sand cushion	15.7	162.8	This study
UU	10 mm sand cushion	16.0	167.8	This study
UU	20 mm sand cushion	16.7	169.7	This study

In this study, when the 5 mm sand cushion was present, the c value increased rapidly (about 2.7 times), whereas the φ value decreased slightly. When the thickness of the sand cushion increased, these numbers increased slightly. However, Yang et al. [11] showed that these numbers changed without a general trend. In this study, the sand cushion soil was considered a heterogeneous material. Thus, UU shear strength should be used to evaluate the capacity of the sand cushion soil instead of c and φ. In all cases, the UU shear strength of reinforced soil increased dramatically as the thickness of the sand cushion increased.

b) The shear strength increasement R_{uf} in the unsaturated condition.

The shear strength increasement R_{uf} was the ratio between the deviation at the failure of reinforced soil and unreinfroced soil. The shear strength increasement R_{uf} of sand cushion soil was shown in Figure 4.12:

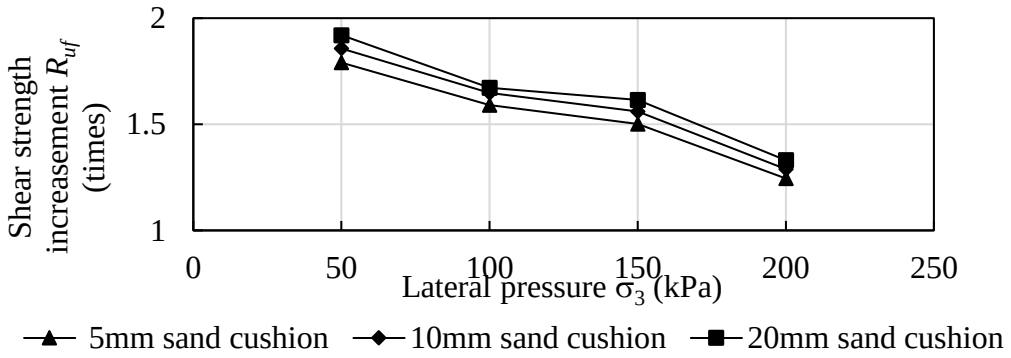

Figure 4.12: The shear strength increasement versus lateral pressure in the unsaturated condition of sand cushion samples.

Results indicated that R_{uf} was greater than 1 at all lateral pressures, showing that the reinforcement can increase the soil's strength. The R_{uf} value decreased as lateral pressure increased. The R_{uf} value increased as the thickness of the sand increased.

4.4.2. The shear strength behavior of silty soil reinforced by a sand cushion in the saturated condition.

a) Shear strength behavior of the saturated soil reinforced by the sand cushion.

The results indicated that deviation stress increased when the axial strain and the thickness of the sand cushion increased. The larger the strain and the sand thickness were, the higher the deviation was.

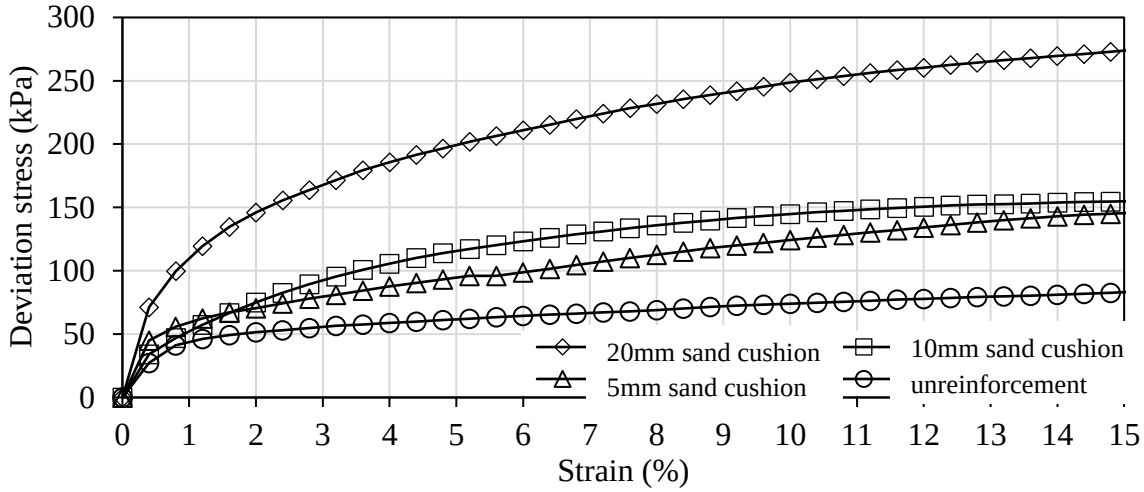

Figure 4.13: The deviation stress and axial strain of soil and soil reinforced by the sand cushion in the saturated condition.

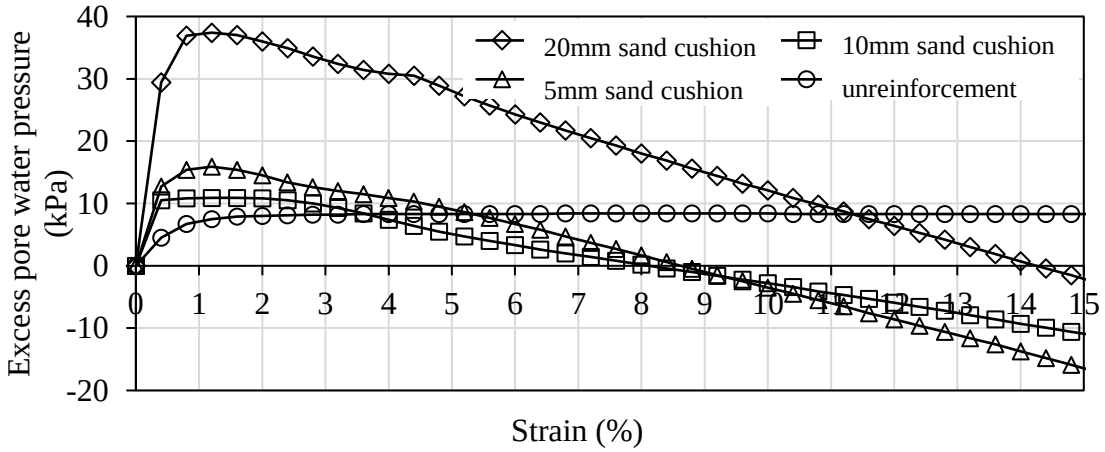

Figure 4.14: The excess pore water pressure and axial strain of soil and soil reinforced by a sand cushion in the saturated condition

As the thickness of the sand cushion increased, the *UU* shear strength and the excess pore water pressure increased. In the strain from 1% to 3%, the reinforced sample generated a higher water pressure than the unreinforced sample, as the sand cushion prevented lateral expansion of the sample; thereby, the water pressure surged. As the strain increased, the soil sample developed lateral strain (sliding between the soil and geotextile) (1- and 2-layer reinforcement samples), which decreased the water pressure, and the excess pore water pressure dissipated due to the sand cushion's high permeability. The excess pore water Δu was changed in the pore water pressure at the sand cushion. The excess pore water was negative, indicating that there was a decrease in the pore water pressure (16.5, 10.9, 2.1 kPa) compared to the initial one. In other words, the lateral expansion and the high permeability of sand dissipated the pore water pressure.

Table 4.3: The excess pore water pressure and *UU* shear strength S_u of soil and soil reinforced by a sand cushion in the saturated condition.

Case	Deviation pressure (kPa)	Excess pore water pressure Δu (kPa)	UU shear strength S_u (kPa)
Unreinforcement	83.02	8.30	41.51
5 mm sand cushion	145.53	-16.50	72.77
10 mm sand cushion	154.83	-10.90	77.42
20 mm sand cushion	273.83	-2.10	136.91

b) <u>The shear strength increasement R_f in the saturated condition.</u>

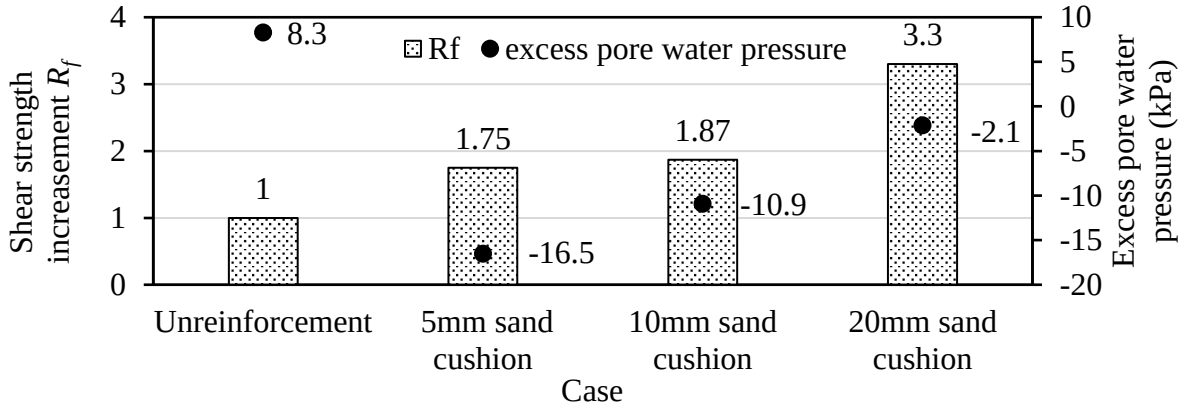

Figure 4.15: The shear strength increasement R_f and excess pore water pressure of soil and soil reinforced by sand cushion in the saturated condition.

The strength increasement index R_f was the ratio between the deviations of the sand cushion and the unreinforced samples at failure in the saturated condition. The results showed that the strength increase index R_f increased as the thickness of the sand increased when comparing the strength of unreinforced and reinforced soil.

4.4.3. Shear strength reduction of soil and sand cushion soil due to saturation:

Shear strength reduction T_{shear} was defined as equation 3.5. When comparing the strengths of unsaturated and saturated soil, the shear strength reduction, T_{shear}, was smaller than 1. It indicated that, after soaking, the shear strength decreased. The larger the lateral stress and thickness of the sand were, the higher the strength reduction was.

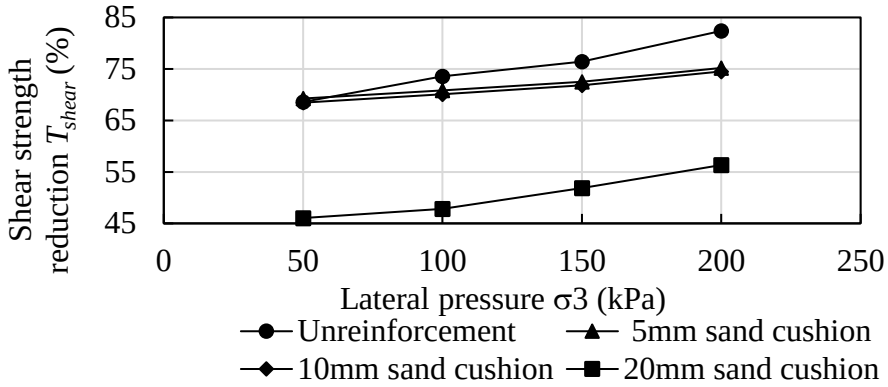

Figure 4.16: Shear strength reduction T_{shear} due to saturation of soil and soil reinforced by a sand cushion.

4.5. BEHAVIOR OF SILTY SOIL WITH AND WITHOUT SAND CUSHION UNDER ONE – DIMENSIONAL CONSOLIDATION TEST

4.5.1. Estimate the height and the bottom of the sand cushion under load:

Based on Section 3.5.4, the height (h_{sand}) and the bottom pressure (P_{b_sand}) of the sand cushion under compression load P_{t_sand} were predicted by the below equations:

$$h_{sand} = \frac{1-\frac{C_{c\_sand}}{1+e_{0\_sand}} log\frac{P_{t\_sand}}{P_{0\_sand}}}{1-\frac{C_{c\_sand}}{1+e_{0\_sand}}\frac{2H_{0\_sand}}{D\,ln\,10}K_{0\_sand}\,tan\,\phi'_{int\_sand}} H_{o\_sand} \quad (4.1)$$

$$P_{b\_sand} = P_{t\_sand} e^{-\frac{4h_{sand}}{D}K_0\,tan\,\phi'_{int}} \quad (4.2)$$

In which C_{c_sand} = 0.162: compression index of the sand, P_{o_sand} = 0.2 kPa: pre-consolidation pressure corresponding to the void ratio e_{0_sand} = 1.078. These values were obtained by one-dimensional consolidation with 20 mm of the sample height.

H_{o_sand} the initial height of the sand cushion.

D = 50 mm: diameter of sand cushion in one dimensional consolidation.

K_{0_sand} = 0.426, the coefficient of sand cushion at rest

ϕ'_{Int_sand} = interface friction angle between sand and ring, which was measured by the modified shear box in Section 2.3.

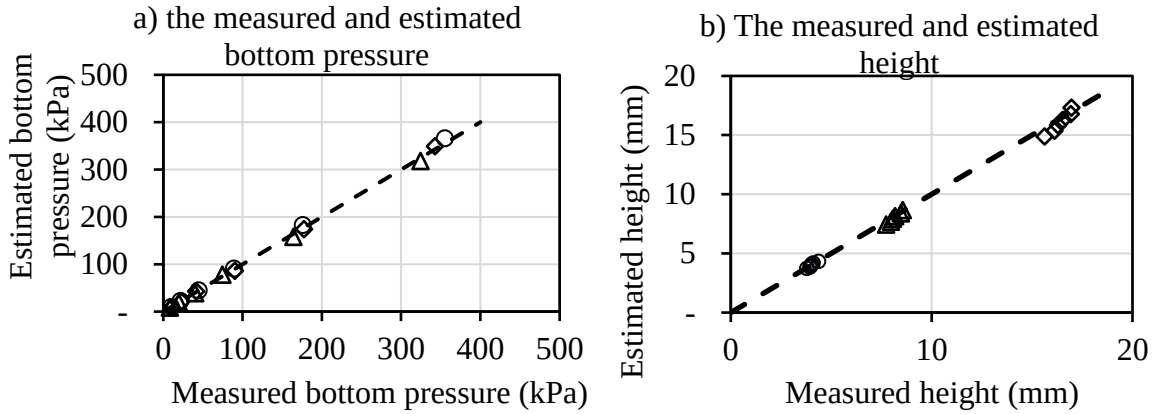

Figure 4.17: The measured and estimated a) bottom pressure and b) height of a sand cushion under top pressure

Figure 4.17 showed the similarity between measured and estimated values under the top pressures of 24.2, 48.7, 97.7, 195.7, and 391.74 kPa of the sand cuhsion's thicknesses of 5mm, 10mm, and 20 mm. The results showed they were the same, with an error under 7%. Thus, the above equations were used to predict the sand cushion's height and bottom pressure with varied top pressure.

4.5.2. The average pressure in soil and sand cushion

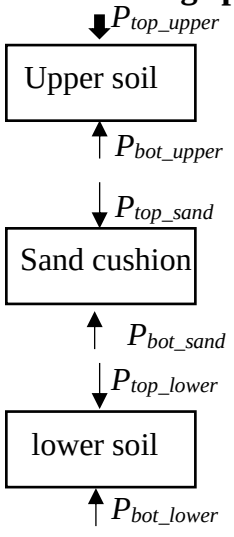

P_{top_upper} = compression load

$P_{bot\_upper} = P_{top\_sand}$

$P_{bot\_sand} = P_{top\_lower}$

$$P_{ave\_upper} = \frac{P_{top\_upper} + P_{bot\_upper}}{2}$$

$$P_{ave\_lower} = \frac{P_{top\_lower} + P_{bot\_lower}}{2}$$

$$P_{ave\_soil} = \frac{P_{ave\_upper} + P_{ave\_lower}}{2}$$

Figure 4.18: Dividing the samples into 3 parts

P_{ave_upper}, P_{ave_lower}, and P_{ave_soil} were the average pressures at the center of the upper, lower, and all the soil.

Due to the side friction between the soil, specifically sand, and the ring, the lost compression pressure in the sample must be considered. The average compression pressure was required for the consolidation procedure to be carried out. To determine the average pressure in soil, divide the samples into 3 parts, with the top and bottom pressures shown in Figure 4.18.

The pressure on the top of the upper soil was equal to the compression pressure, whereas the pressure at the bottom of the lower soil was estimated and compared to the measured value by the oedometer apparatus for side friction (item 2.4).

Based on 4.5.1, the values of P_{bot_upper}, P_{bot_sand}; P_{bot_lower}, P_{ave_upper}, P_{ave_lower}, and P_{ave_soil} were estimated. To ensure that these values were corrected, the height of the total soil and the P_{bot_lower} were compared to the measured values.

The values of the top, bottom, and average pressure of each layer, errors of sample height, and bottom pressure of the sand cushion were presented in Table 4.4.

Table 4.4: The value of pressure and errors of sample height and bottom pressure of sand cushion specimens. The names of samples included the height of samples (*H*), total soil (*So*), and sand cushion (*Sa*), respectively.

Parameters	Pressure (kPa)				
	24.2	48.7	97.7	195.7	391.74
H40So30Sa10					
P_{top_sand} (estimated) (kPa)	20.2	41.1	83.1	167.9	339.0
P_{top_lower} (estimated) (kPa)	17.2	35.1	71.4	144.9	293.9
P_{bot_lower} (estimated) (kPa)	14.4	29.5	60.5	123.9	253.4
P_{bot_lower} (measured) (kPa)	14.1	28.6	63.6	127.6	250.9
Error P_{bot_lower} (%)	2.0%	3.0%	-5.0%	-3.0%	1.0%
P_{ave_upper} (kPa)	22.22	44.90	90.43	181.83	365.36
P_{ave_lower} (kPa)	15.65	31.89	67.50	136.29	272.39
P_{ave_soil} (kPa)	18.94	38.40	78.96	159.06	318.87
Total estimated sample height (mm)	36.8	35.23	33.65	32.08	30.50

Error of estimated sample height (%)	1.31%	2.19%	0.29%	0.56%	2.04%
H40So20Sa20					
P_{top_sand} (estimated) (kPa)	21.5	43.5	87.8	176.8	355.8
P_{top_lower} (estimated) (kPa)	15.6	31.8	64.8	131.7	267.6
P_{bot_lower} (estimated) (kPa)	13.8	28.3	58.0	118.6	242.3
P_{bot_lower} (measured) (kPa)	13.2	26.6	59.8	123.4	244.7
Error P_{bot_lower} (%)	4.0%	6.0%	-3.0%	-4.0%	-1.0%
P_{ave_upper} (kPa)	22.84	46.10	92.74	186.25	373.77
P_{ave_lower} (kPa)	14.41	29.23	62.29	127.55	256.15
P_{ave_soil} (kPa)	18.63	37.67	77.51	156.90	314.96
Total estimated sample height (mm)	35.786	34.41	33.04	31.68	30.31
Error of estimated sample height (%)	3.12%	2.29%	5.08%	5.51%	5.00%

The results revealed that the bottom pressure and height errors of the estimated and measured values were less than 5%. Consequently, the equations in item 3.5.4 were accurate. Besides, the average pressure of the upper soil layer (P_{ave_top}) was higher than that of the lower soil layer (P_{ave_lower}) due to the side friction, which decreased the compression pressure.

The loss pressure ($\lambda_{loss\ pressure}$) of soil was calculated as follows:

$$\lambda_{loss\ pressure} = \frac{P \quad - P_{ave\_soil}}{P} \tag{4.3}$$

The figure below showed the loss pressure under varied compression pressure:

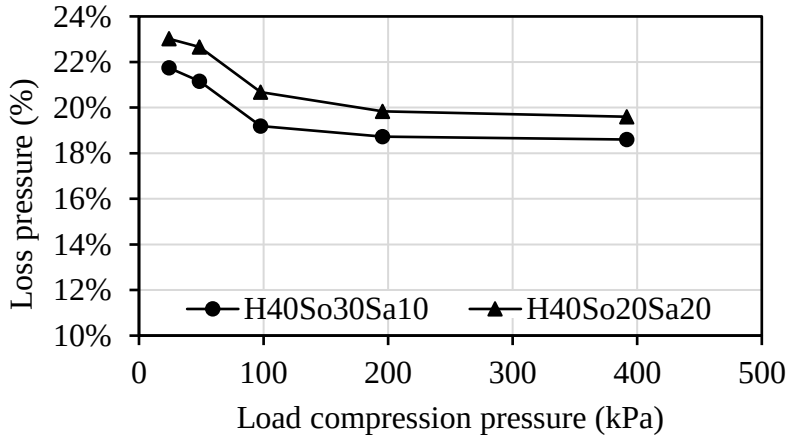

Figure 4.19: The loss pressure of the 40-mm-height samples with 10 mm of sand cushion (H40So30Sa10) and 20 mm of sand cushion (H40So20Sa10)

And the average friction pressure F_{fri} between the soil/ sand cushion and the ring can be calculated by:

$$F_{fri} = \frac{(P_{top}-P_{bot})A}{\pi Dh} = \frac{(P_{top}-P_{bot})D}{4h} \quad (4.4)$$

where P_{top}; P_{bot} the top and bottom pressures of layer,

A, h, D: section area, height, and diameter of the sample, respectively.

Figure 4.20 shows that the friction pressure in the sand cushion layer was much higher than that of the upper and lower soil, up to 1.9 times, leading to a high loss pressure in the average compression pressure of about 20%. The significant difference was due to the different materials.

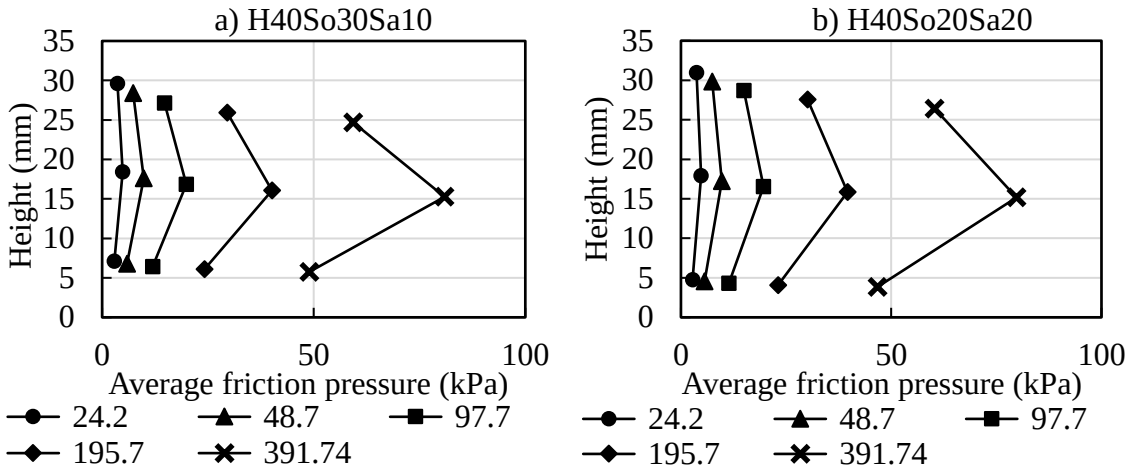

Figure 4.20: The average friction pressure at the middle of each layer of the 40-mm-height samples with a) 10 mm of sand cushion (H40So30Sa10) and b) 20 mm of sand cushion (H40So20Sa10)

4.5.3. The effect of the sand cushion on the silty soil consolidation process

a) <u>Primary consolidation</u>

50 mm in diameter and 40 mm in height, the test included an unreinforced sample and samples of 10- and 20-mm sand cushions called H40So30Sa10 and H40So20Sa20. The graph below depicts the time to achieve 90% (T_{90}) and 100% (T_{100}) consolidation versus the average soil compression. Consolidation time decreased from unreinforced samples to those reinforced with 10- and 20-mm sand cushions. The addition of sand cushions decreased consolidation time. Comparing

the soil sample with a 30 mm height, the time to consolidate the soil sample with a 10 mm sand cushion in the middle (sample H40So30Sa10) decreased up to 3.5 times. When the sand cushion height increased, the time for consolidation decreased. However, the time to consolidation of sample H40So20Sa20 was greater than that of soil with 10 mm.

It can be concluded that the sand cushion enhanced the dissipation process of pore water pressure. Although the sand cushion had not adhered to the external drainage boundary, the results indicated that consolidation was accelerated in the sample that was reinforced. In this instance, the sand cushion was considered a drainage boundary, reducing the drainage path.

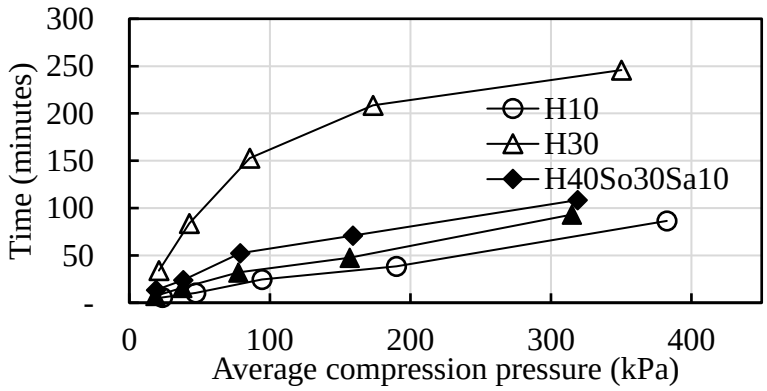

Figure 4.21: The time to obtain 100% (T_{100}) consolidation of sand cushion samples.

b) *Consolidation coefficient C_v:*

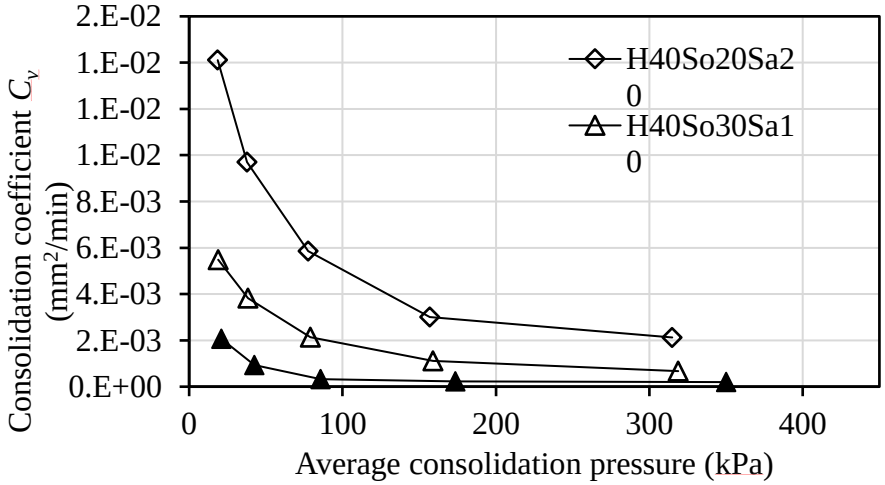

Figure 4.22: The consolidation coefficients C_v vs. average compression pressure of sand cushion samples.

When the clay was strengthened with geotextile, the consolidation coefficient C_v rose due to its increased permeability, leading the consolidation process to occur more quickly. As the load increased, the C_v decreased. As a result of side friction, the consolidation coefficients C_v versus average pressure were plotted in Figure 4.22.

4.6. CONCLUSION:

A series of tests, including *CBR, UU* triaxial, and consolidation tests, were performed to investigate the sand cushion's effect on soil improvement due to the soaking process. The results illustrated the critical role of reinforcement inclusion in enhancing bearing capacity and consolidation in both soaked and unsoaked conditions. The other conclusions are the following:

a) Behavior of silty soil with a sand cushion under swelling and the CBR test

1. The permeable geotextile and sand cushion forced the swell to happen faster by allowing extra drainage paths into the reinforced specimens. Additionally, the density reduction fell slightly. Similarly, the percentage swell went down by over 4%. It also slightly decreased the percent swell.

2. The geotextile-sand cushion significantly improved the strength of soft clay in both unsoaked and soaked conditions. Based on the results, the optimum thickness of the sand cushion was 15 mm, which was equivalent to the ratio between the top clay's height and the penetrated piston's diameter,

3. When increasing the dry mass of sand, the *CBR* value soared, particularly in the case of the soaking process. Moreover, the optimal dry mass ratio between sand and soil was 0.16 for the highest bearing capacity of the reinforced specimen under both soaked and unsoaked conditions.

b) Behavior of silty soil with a sand cushion on UU shear strength

1. The sand cushion-soil strength widened approximately from 1.2 to 1.9 times compared to the soil's strength in the unsaturated condition. And this number was about 1.75 to 3.3 times that for the saturated condition. After soaking, the shear strength reduction was about 68% to 82% for the soil. And this figure was about 45% to 56% for the 20-mm-sand cushion-soil sample.

2. The cohesion and the angle of internal friction can change without a general trend. However, the shear strength increased in all reinforced soils.

3. When the strain was between 1% and 3%, more excess pore water pressure was observed than in the unreinforced samples because the sand cushion prevented the soil from expanding laterally. As the strain increased, a sliding phenomenon occurred between the soil and the geotextile, reducing the pore water pressure, which then dissipated due to the high permeability of the sand cushion. Therefore, a sand cushion prevented horizontal movement and increased the shear resistance of the soil.

c) Behavior of silty soil with a sand cushion under the consolidation test

A one-dimensional consolidation test was performed to confirm the effects of sand cushions in the consolidation process. The conclusions were as follows:

1. The height and compression pressure of the sand can be estimated under the one-dimensional test with an error of about 5%. The average friction pressure between the sand and the ring was about 1.9 times higher than that of the soil, leading to a high loss pressure in the average compression pressure, about 20%.

2. Sand cushions accelerated the soil consolidation process by 3.5-5 times compared to unreinforced soil. Moreover, the consolidation coefficient increased as the height of the sand cushion increased and decreased as the consolidation pressure increased.

In summary, a proper drainage system is crucial for the unreinforced and reinforced clay to maintain its stabilization. The sand cushion, as a drainage path, can improve the soil's consolidation process.

CHAPTER 5: BEHAVIOR OF SILTY SOIL REINFORCED BY CEMENT UNDER CBR, UU, CONSOLIDATION, AND SHEAR TEST

5.1. INTRODUCTION

To increase the strength and stiffness of soft soils, cement is frequently used as an addition [52]. The remolding water content plays a crucial role in influencing the strength of cement-treated soils [66]. Due to the hydration process, the water content in the soil decreases, and the primary cementitious materials are formed [60, 61] to improve the soil capacity, the swell, and the settlement. Although there were many studies investigating the soil cement, the effects of the soaking process on the swelling, *CBR* value, *UU* shear strength, interface shear strength, and curing time of the treated soil were not fully determined, especially for the soil in the Mekong Delta.

The research objectives of this chapter are:

- Effect of cement ratio on silty soil's swelling and CBR value in unsaturated and saturated conditions by the *CBR* test.
- Effect of cement ratio on the *UU* shear strength in unsaturated and saturated conditions by triaxial test to evaluate the soil capacity.
- The behavior of cement-treated soil on the one-dimensional consolidation test.
- The effects of cement content and curing time on the shear strength behavior of the cement-treated clay and steel interface. In addition, grain size analysis was conducted on the treated soil samples to reveal the effects of cement treatment on improving their structure, which led to an increase in shear strength. Using the peak and residual strength values, the brittleness of the treated soil was also evaluated. In addition, a correlation equation would be proposed to quantify the rate of shear strength and interface shear strength development in cement-treated soil specimens with curing time.

The cement content is defined as the mass ratio of cement to dry soil expressed as a percentage.

5.2. EXPERIMENTAL PROGRAM

5.2.1. CBR specimens

Similar to the geotextile- and sand-cushion-reinforced *CBR* specimens, three specimens were reinforced with cement under wet conditions. The dried weight ratio of soil to cement was 3%, 5%, and 10%. After mixing the dried soil and cement, the optimal amount of water was introduced to the mixture.

The specimens were compacted using a 152.4 mm in diameter by 116 mm in height mold. Five layers of compaction were used to form a specimen. The compaction energy level was 482 kJ/m3. (10 blows per layer).

There were 3 specimens for soaked conditions: Before performing the *CBR* test on the soaked specimens, the compacted specimens were soaked for 96 hours.

Figure 5.1: Soil cement *CBR* specimens with 3%, 5%, and 10% cement ratios.

5.2.2. Unconsolidated-Undrained shear strength samples in the triaxial test

Similar to the specimens reinforced by geotextile and sand cushions, there were 15 samples reinforced by cement. The dimensions of the samples were 50 mm in diameter and 100 mm in height. The dried weight ratio of cement to soil was 3%, 5%, and 10%. The water was then added to the dried mixture at 24.5% water content and stored in the chamber for 28 days before testing. There were two types of tests, including:

- *Unsaturated samples*: samples will be tested at lateral pressures of 50 kPa, 100 kPa, 150 kPa, and 200 kPa, respectively.
- *Saturated samples*: samples will be saturated at 500 kPa pressure and tested at 300 kPa lateral pressure.

Figure 5.2: Samples reinforced by 3%, 5%, and 10% cement

5.2.3. Consolidation samples

There were 4 specimens for the one-dimensional consolidation test. The soil at 1.25 g/cm^3 of dry density was added by dry cement at 3%, 5%, 7%, and 10% of weight. The mixture and water were blended at 24.5% water content and then poured into the mold, which was 50 mm in diameter and 20 mm in height.

5.2.4. Direct shear and interface shear samples

In this investigation, the powdered soil was mixed with tap water at 54.7% moisture content. A quantity of dry cement, equivalent to the cement content, was then put on the soft soil. The mixture was placed into a 60 mm by 20 mm rectangle mold after 15 minutes of mixing. As recommended by Bushra et al. [116] and Sasaniana et al. [117], trapped air bubbles were removed from the samples by tapping gently on the walls of each mold and employing the thumb-kneading technique. It takes only about 60 minutes to establish each sample (mix and compact), which is less than the first setting time of Portland cement. Other studies prepared cement-treated soil specimens by curing them in plastic wrap and placing them in a temperature-controlled room at a constant 25^{0}C to prevent a change in water content [72, 75, 117]. In this study, the treated soil specimens were cured by soaking in water. The specimens were retained in the molds throughout the process to preserve their original volume. This curing procedure is consistent with the preparation approach provided by Chew et al. [62] for cement-treated soil samples. It was also adapted to the curing state of the cement-treated soil in the deep mixing wall. Although the wall

was coupled with the sheet pile to protect the cofferdam structure, a water leak might cause the treated soil of the wall to become saturated immediately after the completion of the wall's construction.

The consolidated drained conditions were applied to both the direct shear test and the interface direct shear test. Before shearing, samples were properly consolidated in saturated conditions for 24 hours, according to ASTM D3080 [99]. To prevent significant excess pore water pressure at failure, the shearing rate was fixed at 0.004 mm/min. It was evaluated based on the assumption that a CH-type soil would fail at 10% shear strain after 24 hours of shearing, as recommended by ASTM D3080 [99]. For the interface direct shear test, the same shearing rate (i.e., 0.004 mm/min) was also employed, which was similar to that used in earlier research for determining the effective interface shear strength between soil and steel [78]. In this investigation, the tests would terminate when the shear displacement reaches 5 mm, the limit at which the applied shear force remains essentially constant with increasing displacement, as recommended by ASTM D5321 [119]. The repeatability and consistency of the test results were evaluated by conducting several tests on the samples under the same conditions.

Table 5.1: Testing program

Material	Cement content, c_m (%)	Effective normal stress (kPa)	Curing period (days)
Type of test: Direct shear test under consolidated drained condition			
Untreated soil	0%	50, 100, 150, and 200	0
Cement-treated soil	10%	200	3, 7, 14, 28, and 56
Cement-treated soil	3%, 5%, 7%, and 10%	50, 100, 150, and 200	28
Type of test: Interface shear test under consolidated drained condition			
Untreated soil vs. stainless steel	0%	50, 100, 150, and 200	0
Cement-treated soil vs. stainless steel	10%	200	3, 7, 14, 28, and 56
Cement-treated soil vs. stainless steel	3%, 5%, 7%, and 10%	50, 100, 150, and 200	28

Table 5.1 provides an overview of the testing conditions for the direct shear and interface direct shear tests, for which the curing period was extended to 56 days. As discussed previously, the strength development of the treated soil was due to the hydration and pozzolanic reactions in cement [60, 61]. In contrast, the strength would be reduced with the curing period due to the organic matter (such as humic acid) and salt concentration [117]. The study of the uniaxial compression strength of the cubic cement-treated organic soil samples found that their maximum compressive strengths at 84 days would be lower than those at 56 days [117]. In this study, the organic matter in the soil was very small, as its ignition loss was less than 4%. In addition, the soil was retrieved from a freshwater region devoid of salt. Due to the minimum presence of organic and salty matter, the strength of the cement-treated soil in this study would not degrade within 56 days of curing, as indicated in the next section.

5.3. BEHAVIOR OF SILTY SOIL WITH CEMENT UNDER THE SWELLING AND CBR TEST

5.3.1. Influence of cement on the soil's swell behavior

The percent swell of reinforced specimens (*S*) in time (the ratio between the settlement and the initial soil height) is given in Figure 5.3. Generally, it increased with time during the soaking process. The swell of the specimens reached equilibrium after 96 h of soaking.

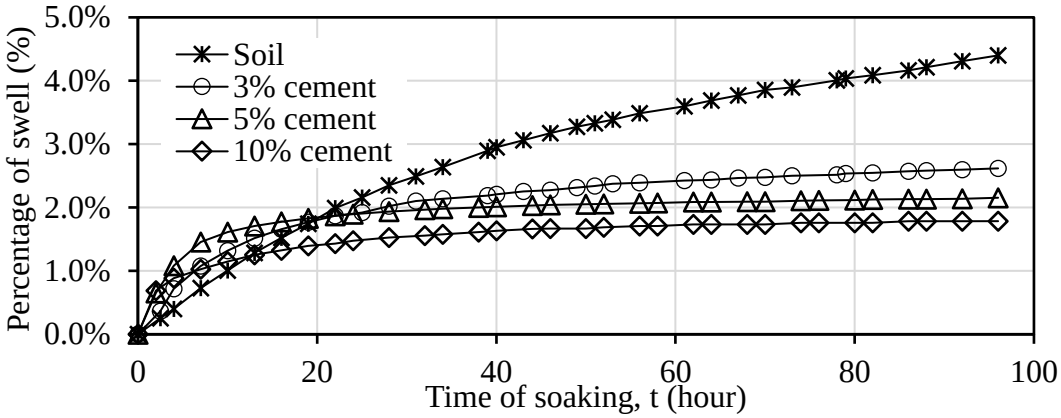

Figure 5.3: Swelling of unreinforced and soil cement specimens during soaking

At the initial time, the percent swell of unreinforced specimens was smaller than that of reinforced specimens. However, after about 20 hours, more swelling was

found in the unreinforced specimens. After 96 hours, the final swell of reinforced specimens was observed to be reduced with the higher ratio of cement. The percent swell of soil with a 3%, 5%, and 10% cement ratio was about 2.62%, 2.15%, and 1.79%, respectively, after 96 hours of soaking.

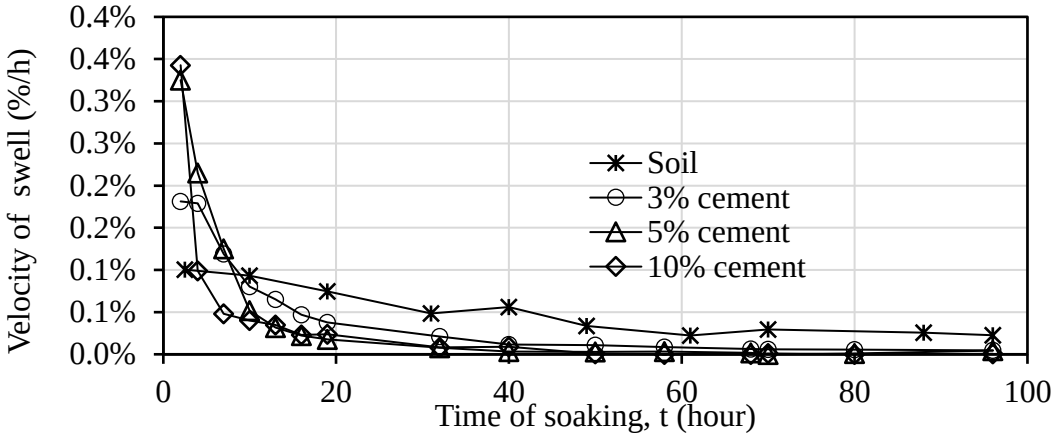

Figure 5.4: Velocity of the swell of soil and soil cement during soaking

The swelling velocity is defined as the percent swell of specimens in an hour. The swell velocity of reinforced specimens is observed to be higher than that of unreinforced specimens after 10 hours of soaking. Especially in the first 2.5 hours, the swell velocity of reinforced specimens is about 0.2-0.4%/hour, which is approximately 2-4 times that of unreinforced specimens (about 0.1%/hour).

It can be explained by the increase in cement content in the soil. The cement sucked water into the soil, enhancing the swell in the reinforcement. Thus, the velocity of the soil with a higher cement content was greater than that of the samples with a lower cement content. At the same time, the hydration process occurred and bound the soil grains together, leading to a decrease in the swell. After 10 hours, the soil cement's velocity was lower than that of the soils, and after 96 h, the velocity of the soil was about 4.8 and 5.1 times higher than that of soil reinforced by 3% and 5% cement content, respectively. Especially, this number was about 40 times compared to the 10% cement ratio. In other words, the soil cement reached equilibrium faster, about 60 h.

The reduction of dry unit weight of soil is evaluated using the percent swell after 96 hours of soaking, S_{96h}:

$$\%\Delta\gamma_d = 1 - \frac{1}{S_{96h} + 1}$$

Table 5.2: Percent swell and percent reduction of dry unit weight of soil-cement specimen after 96 hours of soaking

Cases	S_{96h} (%)	$\%\Delta\gamma_d$ (%)
Unreinforced	4.64	4.43
3% cement	2.62	2.55
5% cement	2.15	2.10
10% cement	1.78	1.75

As shown in Table 5.2, the reduction in dry unit weight of clay specimens reinforced by cement was smaller than that of unreinforced soil. As a result, in the case of having the same density after compaction, after soaking, the clay in reinforced specimens would be denser than that of the unreinforced soil due to the cement.

5.3.2. The CBR behavior of unreinforced and reinforced specimens

The figure below presents the corrected stress in the piston with the penetration of unreinforced and reinforced clay specimens for soaked specimens.

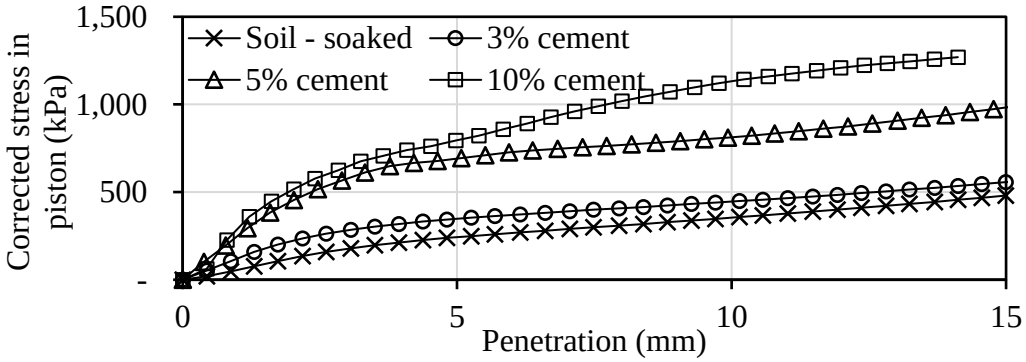

Figure 5.5: Corrected stress in the piston of soil-cement samples under the soaking condition.

For soaked specimens, at 28 days of curing time, the bearing capacity of the soil was significantly improved when reinforced by cement. The higher the cement content was, the higher the bearing capacity of reinforced specimens would be.

The improved bearing capacity of reinforced specimens is quantified by using the strength ratio, defined as the ratio of the *CBR* of the reinforced specimen to that of the unreinforced specimen. The changes in strength ratio with cement content are shown in Figure 5.6. It revealed that the higher the cement content was, the higher

the strength was. When the cement ratio increased to 3%, 5%, and 10%, the *CBR* values went up 1.7, 3.4, and 3.8 times.

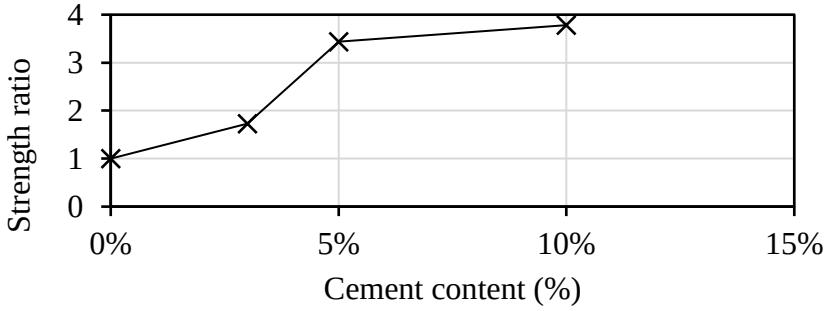

Figure 5.6: The correlation of strength ratio and cement content at 28 days of curing

5.4. BEHAVIOR OF SILTY SOIL WITH CEMENT ON UU SHEAR STRENGTH UNDER THE TRIAXIAL TEST

5.4.1. The shear strength behavior of unsaturated soil reinforced by cement:

a) <u>Shear strength behavior of unsaturated soil reinforced by cement:</u>

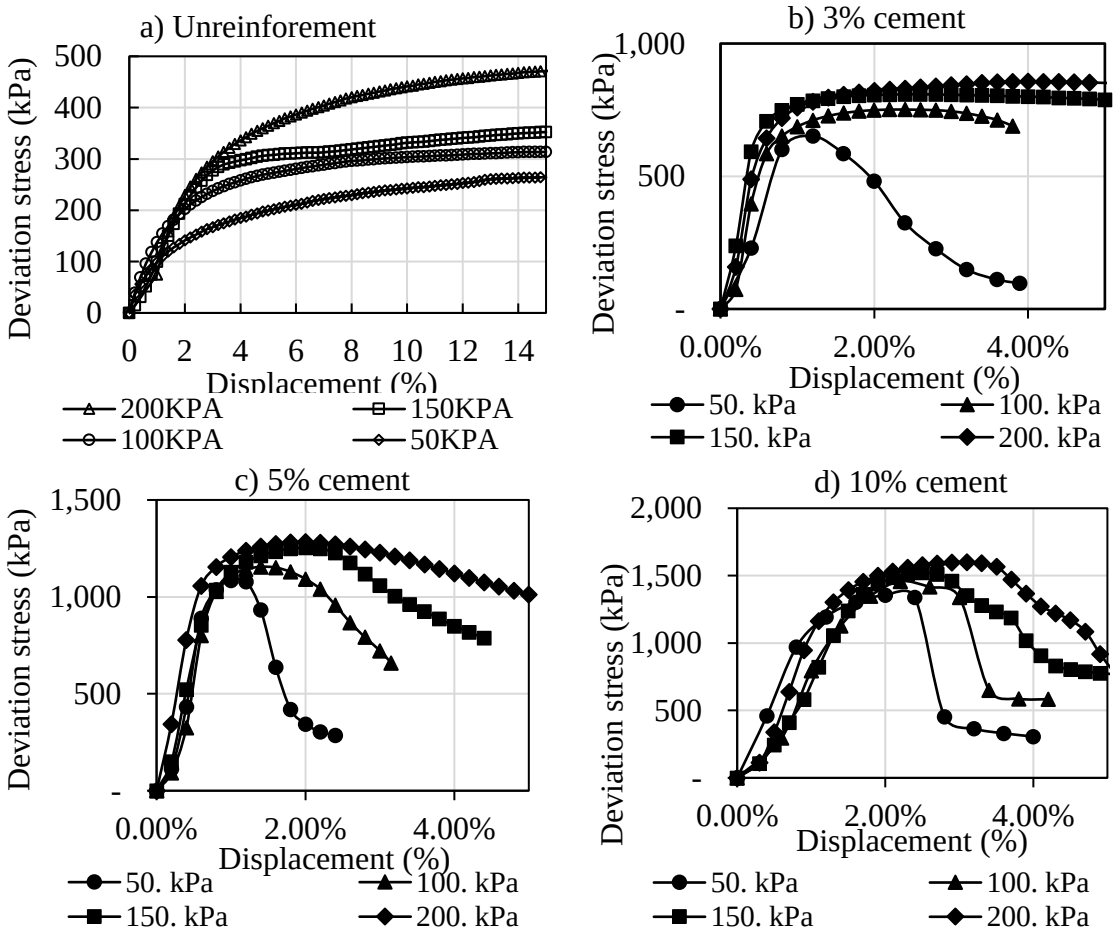

Figure 5.7: Deviation stress versus axial strain of unsaturated cement soil.

The relationship between deviation stress ($\Delta\sigma = \sigma_1 - \sigma_3$) versus axial strain of soil reinforced by cement at 28 days of curing was shown in Figure 5.7. The results indicated that when the cement content increased, the sample exhibited brittle failure with minimal deformation at a horizontal pressure of 50 kPa. As lateral pressure rose, the strain at failure increased.

The relationship between the vertical and lateral pressure of soil and cement soil, as shown in the below figure, when the specimen failed.

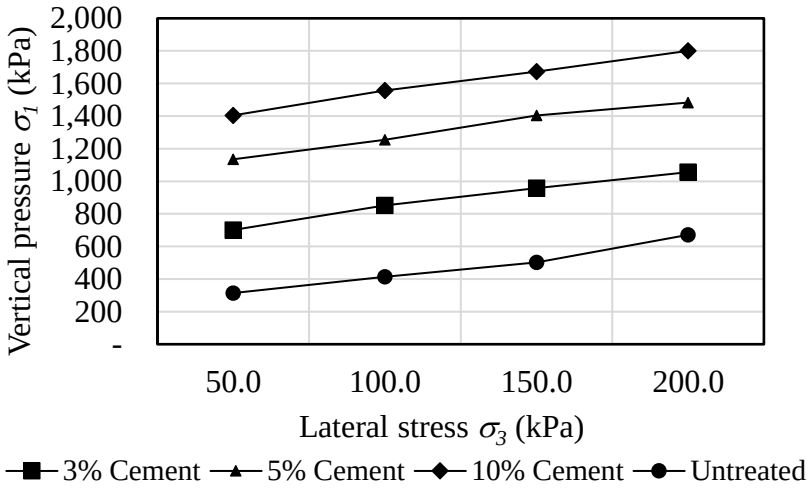

Figure 5.8: The vertical versus lateral pressure of unsaturated soil cement at failure.

Reinforcing the *UU* with cement increased its shear strength substantially at failure. With 3% cement, the sample's strength was approximately 1.6 to 2.2 times greater than without reinforcement. When the cement content increased, its strength increased dramatically.

Table 5.3 displays the results of calculating the cohesive force (c) and the internal friction angle (φ) for the reinforced cases in the *UU* condition. Again, excess pore water pressure cannot be measured, this value represents the sample's total shear resistance.

Table 5.3: The cohesive (c) and internal friction angle (φ) of cement soil at failure in the unsaturated condition

Case	$2c\tan(45^0+\varphi/2)$	$\tan^2(45^0+\varphi/2)$	φ (°)	c (kPa)
Unreinforcement	185.57	2.32	23.4	60.9
3% cement	599.02	2.34	23.7	195.7

Case	$2c\tan(45^0+\varphi/2)$	$\tan^2(45^0+\varphi/2)$	φ (°)	c (kPa)
5% cement	1021.15	2.39	24.2	330.5
10% cement	1283.38	2.60	26.4	397.7

When 3% cement was presented, the cohesive force increased rapidly (about 3.2 times), especially nearly 6.5 times with a 10% cement ratio. Similarly, the angle of internal friction was stable, about 24^0 with 3% and 5% cement, before increasing to 26.4^o at 10% cement.

Figure 5.9: The cemented soil samples at failure

b) <u>The shear strength increasement R_{uf} in the unsaturated condition.</u>

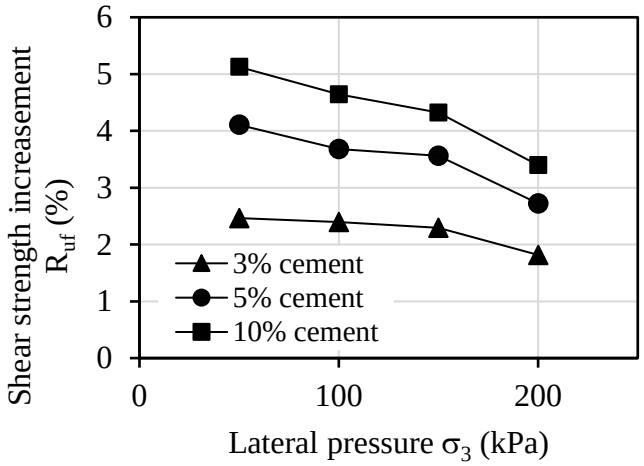

Figure 5.10: The shear strength increasement versus lateral pressure of unsaturated cement soil

Compared to soil, the shear strength increase of the R_{uf} of cement soil was shown in the above figure. Results indicated that R_{uf} was greater than 1 at all lateral pressures,

showing that the reinforcement can increase the soil's strength. The R_{uf} decreased as lateral pressure increased. The R_{uf} increased as the cement content increased.

5.4.2. The shear strength behavior of silty soil reinforced by cement in the saturated condition

a) Shear strength behavior of saturated soil reinforced by cement

The results indicated that deviation stress increased when the axial strain and the cement content increased. The larger the strain and the cement content were, the higher the deviation was.

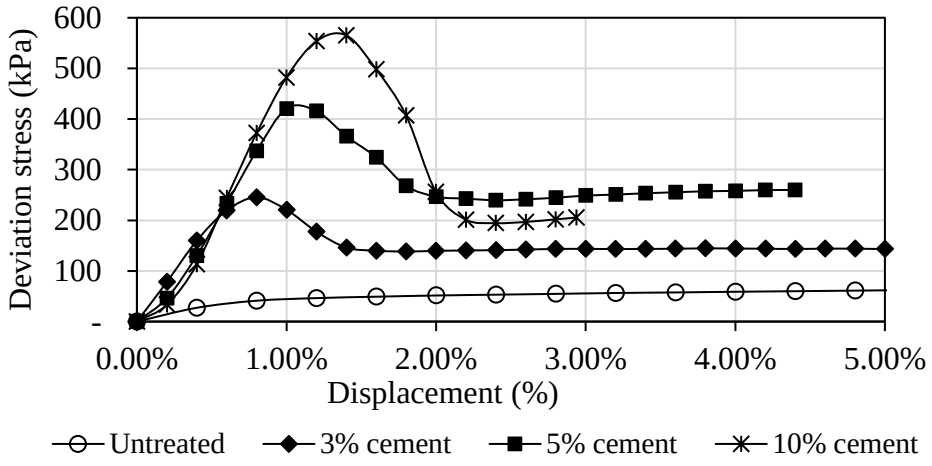

Figure 5.11: The deviation stress and axial strain of soil and soil reinforced by the sand cushion in the saturated condition

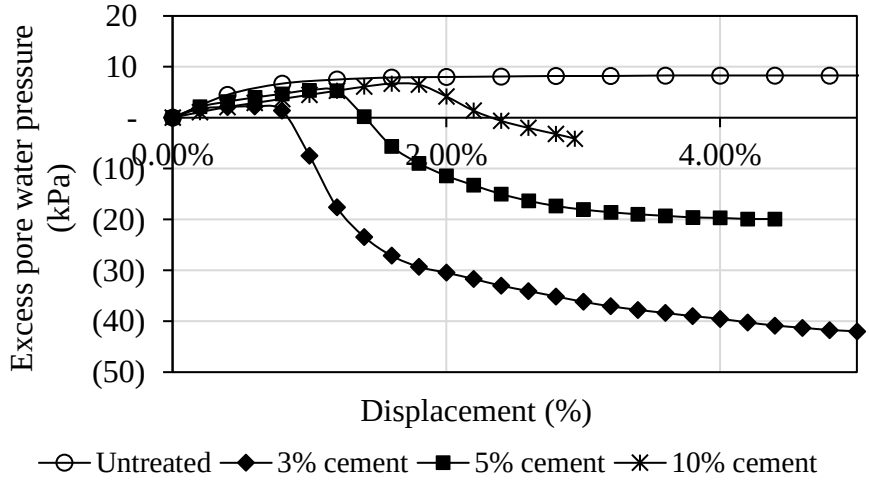

Figure 5.12: The excess pore water pressure versus axial strain of soil and soil reinforced by cement in the saturated condition

Because the soil cement samples failed at minimal strain (1%-2%) with brittle failure, excess pore water pressure went up slightly (about 6.5 kPa) before dropping significantly. When the cement ratio increased, the excess pore water pressure rose slightly from 1.6 (3% of cement) to 6.1 (10% of cement). However, they were smaller than those without reinforcement.

Table 5.4: The excess pore water pressure and *UU* shear strength S_u of soil and soil reinforced by cement in the saturated condition.

Case	Deviation pressure (kPa)	Excess pore water pressure Δu (kPa)	UU shear strength S_u (kPa)
Unreinforcement	83.02	8.30	41.51
3% cement	278.8	1.6	139.40
5% cement	412.4	5.3	206.20
10% cement	565.3	6.1	282.67

b) <u>The shear strength increasement R_f in the saturated condition.</u>

The strength increment index R_f was the ratio between deviations of soil cement and soil at failure. The cement index R_f increased with the cement ratio increment.

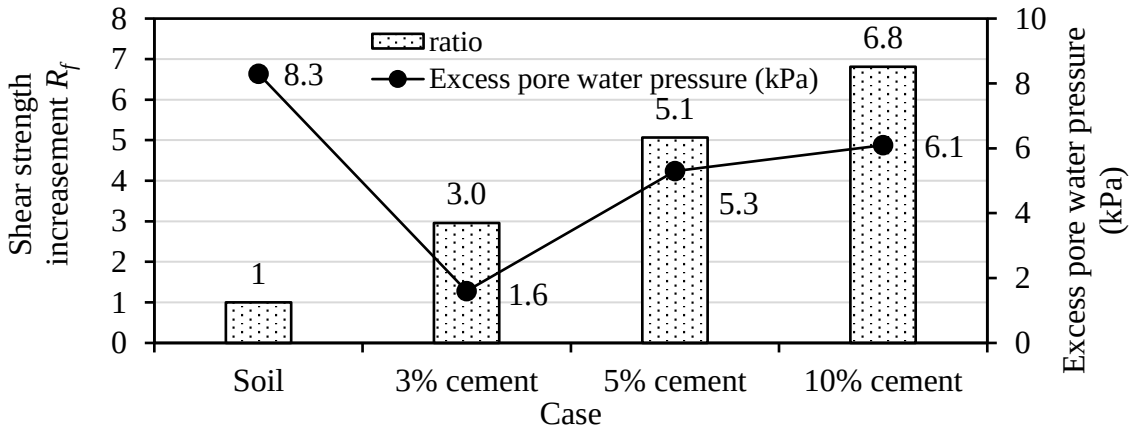

Figure 5.13: The shear strength increasement R_f and excess pore water pressure in soil cement samples

5.4.3. Shear strength reduction of silty soil and cemented soil due to saturation:

Shear strength reduction T_{shear} was defined as equation 3.5. When comparing the strengths of unsaturated and saturated soil, the shear strength reduction T_{shear} was smaller than 1. It indicated that, after soaking, the shear strength decreased, and the

cement improved the shear strength of the mixture. The larger the lateral stress, the higher the strength reduction was.

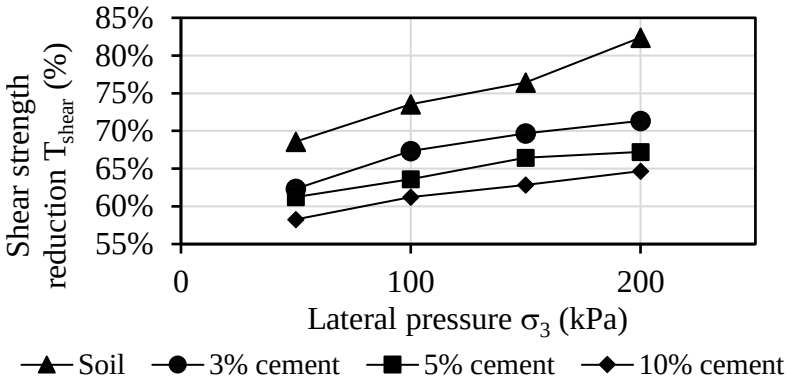

Figure 5.14: Shear strength reduction T_{shear} due to the saturation of the cemented soil.

5.5. BEHAVIOR OF SOIL CEMENT UNDER CONSOLIDATION TEST

Figure 5.15 and Figure 5.16 show the observed total compression of the soil cement versus time under different pressure levels, from 23.74 kPa to 384.30 kPa.

The results showed that the soil-cement settles quickly and stabilizes after approximately 30 minutes. Comparing the settlement of these samples with the same height and diameter, it is not possible to determine the consolidation time and consolidation coefficient C_v according to Taylor and Cassagrade's methods due to the limitations of these methods. Shukla et al., [120] indicated that the Casagrande approach is only applicable to typical S-shaped curves; it is inadequate for other curves. Additionally, it is not appropriate for commercial laboratories because the secondary portion must be firmly demonstrated over a somewhat longer period of time [121]. The Taylor square root of time method specifies that the dial gauge readings should be taken at frequent intervals of time after the specimen has been loaded until 90% consolidation is achieved. Since coarse kaolinite consolidates quickly, for example, it can be challenging to manually record adequate dial gauge readings in the early stages of compression due to the high speed of rotation of the compression dial pointer. For some soils, the curve exhibits continuous curvature rather than an initial linear part, or the curve may have a negative initial compression value. For all such soils, the Taylor technique cannot be successfully employed to obtain accurate values of C_v [120].

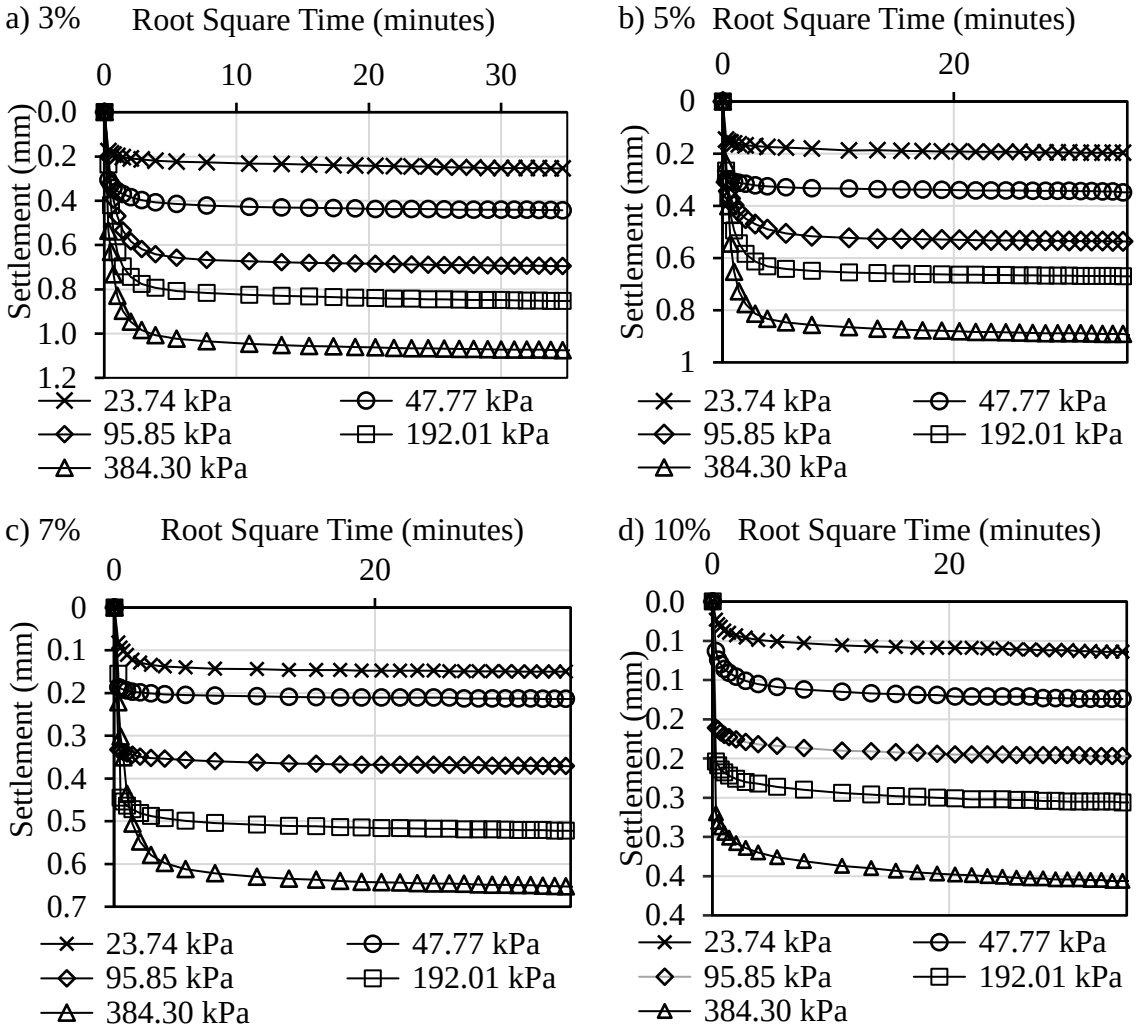

Figure 5.15: Compression of soil cement versus root time under different pressure

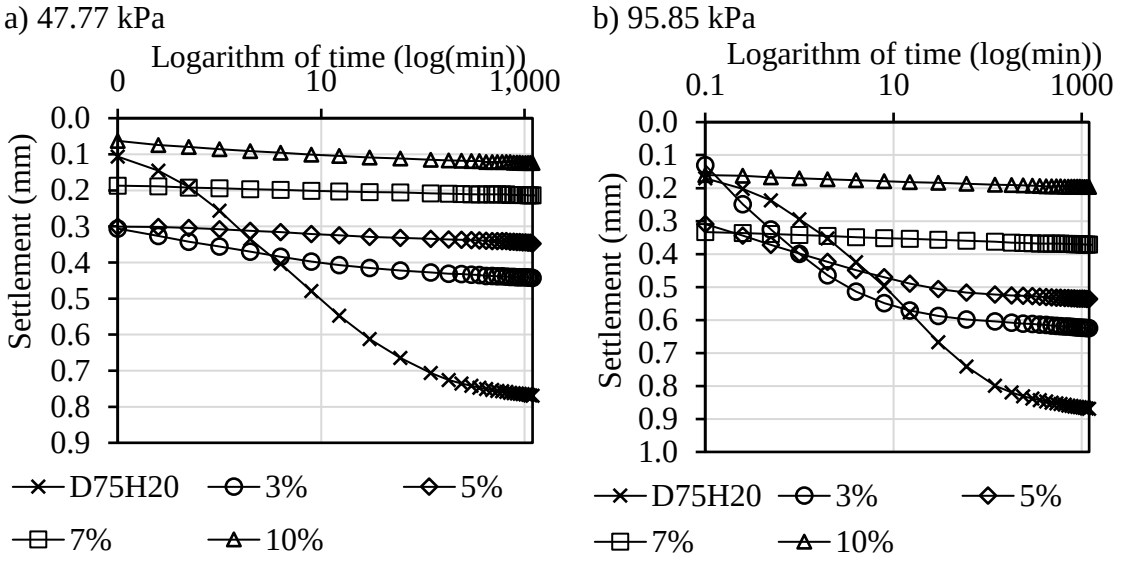

Figure 5.16: Settlement versus log *t* under the pressure of 47.77 kPa và 95.85 kPa.

Sridharan et al. [122] showed many curves of observed total compression δ versus time and their applications:

In Figure 5.17, the ideal curve for which Taylor's approach can be successfully used is represented by curve 1. The other curves indicate various shapes that provide challenges to the procedures that are frequently seen. For some soils, the curve displays continuous curvature rather than an initial linear part (Curve 2). Some soil demonstrates a slight rate of compression early and a quick rate of compression afterward. As a result, the curve may indicate a negative initial compression value, and it may be challenging to identify the 90 percent consolidation point (Curve 3). When testing soils that quickly consolidate, it can be difficult to initially capture the dial gauge readings at regular intervals (such as coarse kaolinite). The curve shows a significant rapid compression, then flattens (Curve 4).

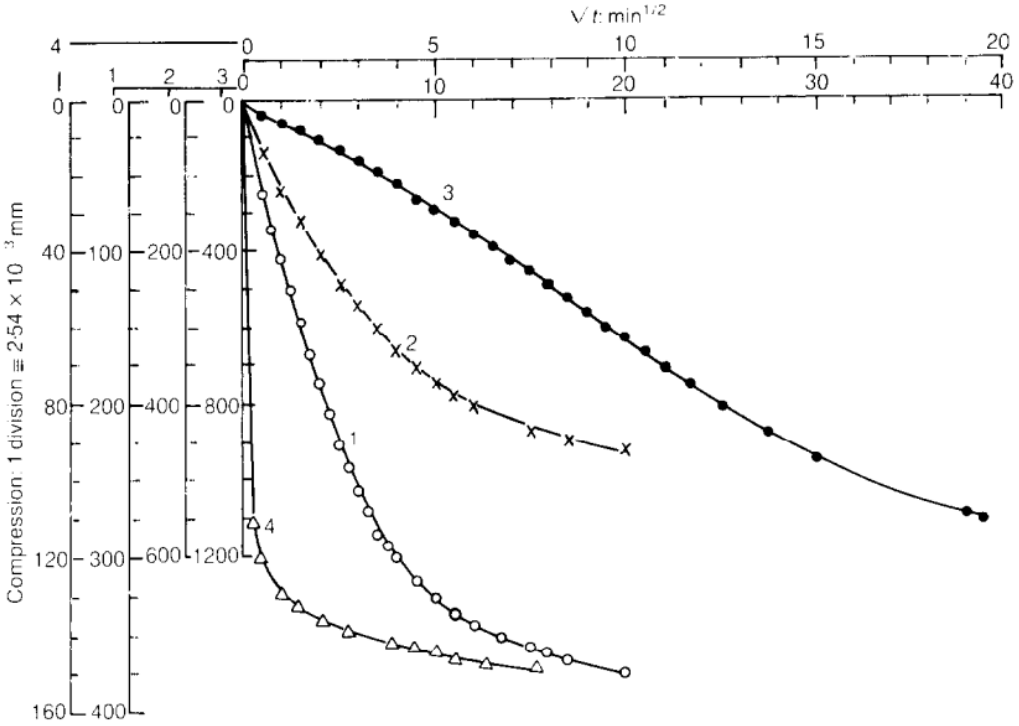

Figure 5.17: Typical δ versus $\sqrt{t}$ curves (remolded soils) [122]

Additionally, Casagrande's method suffers from the following disadvantages:

- When the soil exhibits significant secondary compression, it is sometimes impossible to tell the difference between secondary compression and primary

compression [123]. As a result, finding the T_{100} point on the curve is challenging (Curve 5).

- Although the early part of the curve is a parabola, there may be a small quantity of gas in the soil or other factors that cause the compression to begin later than expected, causing the curve to vary from the predicted parabolic shape (Curve 6).

- In the semilogarithmic plot, it is possible to generate a curve that, after initially displaying a concave-down shape, suddenly displays a sudden drop, indicating a concave-up shape (Curve 7). The shapes of curves 8 and 9 make it difficult to identify the T_{100} of soil.

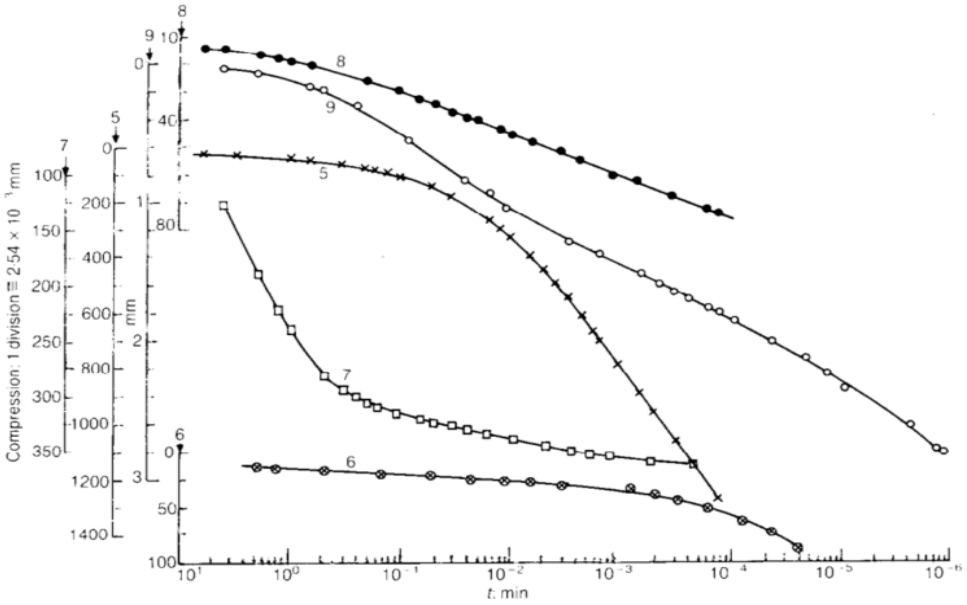

Figure 5.18: Typical δ versus *log t* curves [122]

In this study, soil cement deforms similarly to curve 4. The Taylor and Casagrande methods cannot be used to calculate the consolidation time T_{100} and the consolidation coefficient C_v.

Instead, stress-strain relationships and elastic properties [58] were some of the characteristics of soil cement. The secant modulus of soil cement was displayed in Figure 5.19. It showed that the modulus of soil cement increased slightly, about 2 times, when the cement ratio increased from 3% to 7%, but the modulus in the case of 10% cement was 6 times higher than that of 3% cement at 23.74 kPa. This figure decreased about 3 times when the compression pressure went up to 384.3 kPa.

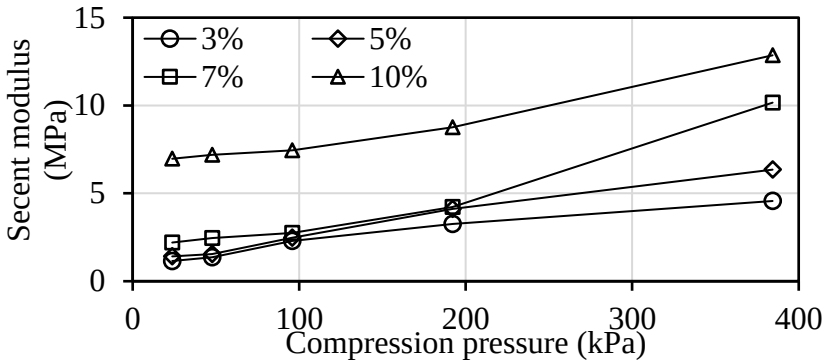

Figure 5.19: The modulus of soil cement under different compression pressures.

The result showed that the modulus of soil cement increased when the dried cement ratio and load pressure increased.

The void ratios versus pressures of soil cement after 24 hours are displayed in Figure 5.20.

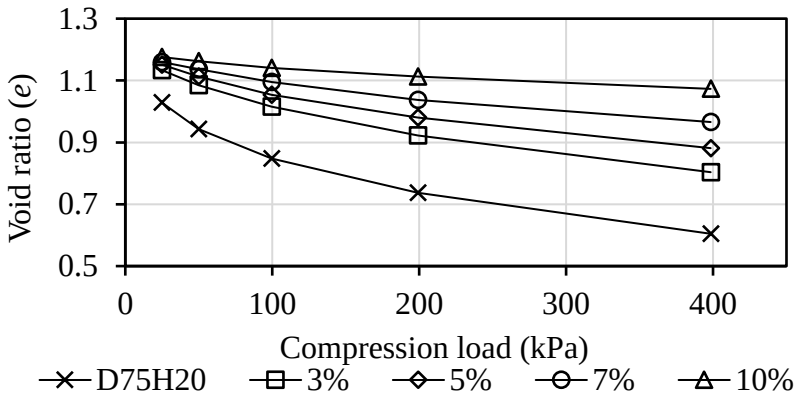

Figure 5.20: The void ratio versus pressure of the soil-cement mixture and soil

The results show that the higher the pressures were, the lower the void ratio was, and when increasing the cement content, the void coefficient increased because the settlement decreased under the same load level. Thus, when cement was added to the soil, it reduced the settlement of the soil. Cement content increased to 3%, and the void ratio increased from 1.1 to 1.33 times compared to unreinforced soil. This value is 1.14 to 1.77 times higher with a cement content of 10%.

5.6. GRAIN SIZE DISTRIBUTION OF SOIL CEMENT MIXTURE

To determine the grain size of cement-treated soil, the SEM (scanning electronic microscopy) method can be used to evaluate the properties of soils improved by cement through electronic microscope scanning and X-ray diffraction testing [124].

However, this method has some disadvantages, including a small sample that cannot be represented for all soils. Additionally, the quantity of grain size distribution for all soils could not be determined. In this study, sieve analysis and hydrometer analysis were performed to determine grain size distribution. Although this method cannot give an image of structural soil or illustrate its properties, a large amount of soil can be used to investigate. So, the quantity of grain size and accuracy can be obtained. Table 5.5 shows the difference between SEM and sieve-hydrometer analysis.

Table 5.5: The difference between SEM and sieve-hydrometer analysis methods

SEM method	Sieve -hydrometer analysis method
- A small sample that cannot be represented for all soils	- A sample with large quantities can be represented for all soils.
- Investigating the soil structure	- Can not investigate the soil structure.
- Can not determine the grain size distribution	- Determine the grain size distribution.

Using particle size analysis, the effects of cement treatment on the structure of the modified soil were examined. After 28 days of curing, sieve analysis and hydrometer analysis were performed on cement-treated soil samples using ASTM C136 [125] and ASTM D4440 [118], respectively. In general, the particle size of the treated soil was larger than that of the untreated soil, as illustrated in Figure 5.21.

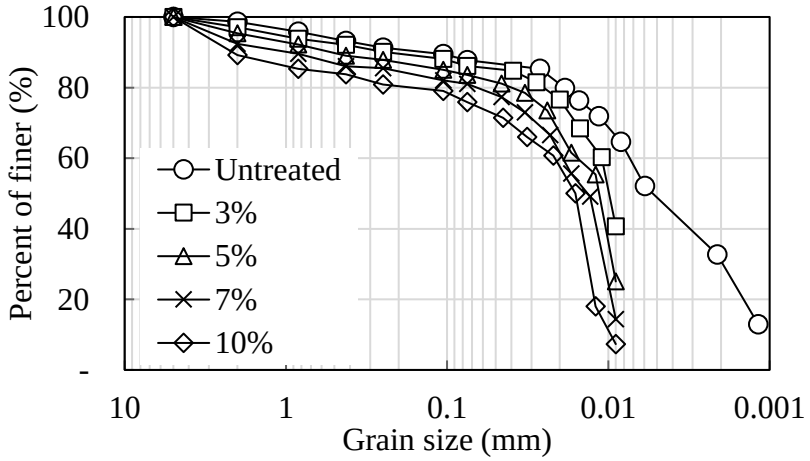

Figure 5.21: The grain size distribution of the untreated soil and the cement-treated soil after 28 days of curing.

The increase in cement content resulted in a greater fraction of sand-size particles and a larger median particle size, D_{50}. Similar results were found for the

particle size distribution of cement-treated clay as measured by the Carlo Erba mercury intrusion porosimeter [62]. It revealed a transition from predominantly clay-sized particles to silt-sized particles. Due to hydration and pozzolanic processes in cement, the creation of fabric and bonding in cement-treated soil induces an increase in particle size. In this investigation, it appears that the later effect predominated and caused the particle size to increase. While it appears that the fabric and bondings did not entirely form due to the low cement content (i.e., less than 10%) and the soaking procedure of the treated specimens. The size improvement in fine particles was also observed in the cement-treated soft Singapore marine clay by Chew et al. [62], who concluded that there was a shift from predominantly clay-size particles to silt-size particles. The increase in sand size fraction of cement-treated soil was quantified further by analyzing the proportion of sand-sized particles and fine contents shown in Table 5.6.

Table 5.6: Percent of sand and fines with median particle size of untreated and treated soil specimens after 28 days of curing

Cement content, c_m (%)	% sand (%)	% fines (%)	Median particle size, D_{50} (mm)	Coefficient β
0% (untreated)	12.3	87.7	0.006	0
3%	13.9	86.1	0.010	0.018
5%	16.4	83.6	0.011	0.048
7%	19.0	81.0	0.014	0.077
10%	24.1	75.9	0.016	0.135

Consider the dry mass of sand size particles and fine particles are M_s and M_f, respectively, the percent of sand particles in the untreated soil should be:

$$\%S_{untreated} = \frac{M_s}{M_s+M_f} \times 100\% \quad (5.1)$$

When mixing soil with cement, the total dry weight of the cement-treated soil, $M_{treated}$ included the dry mass of the soil, the mass of cement and the mass of hydration, and cementitious products, which were evaluated as follows:

$$M_{treated} = \left(M_s + M_f\right) \times [1 + (1 + \alpha)c_m] \quad (5.2)$$

in which α was the dry mass ratio between hydration and cementitious products and cement. The value of α was reported differently depending on the composition of the cement and types of soils. At 28 days of curing, Zhu et al. [126] reported that the value of α was about 0.16 for the mixture of cement with lake and marine sediments (high plasticity clay) and 0.21 for that with river sediment (high plasticity silt). For the hydration of Portland cement only, Chu et al. [127] found that the mass of water related to complete hydration was about 25.2% (i.e. α = 0.252), which was close to the value α = 0.23 reported by Concrete Society [128] at complete hydration.

The hydration and cementitious products increased particle size in cement-treated soil specimens. By assuming a uniform condition in the mixture, the mass of sand-sized particles in the treated sample was evaluated as follows:

$$M_{s\_treated} = M_s \times [1 + (1 + \alpha)c_m] + \beta M_f \times [1 + (1 + \alpha)c_m] \quad (5.3)$$

in which β is the coefficient that accounts for the effects of cement on integrating the fine particles with the sand-sized particles. Meanwhile, the first term is the new dry mass of sand-size particles mixed with cement with hydration and cementitious products. The percentage of sand-sized particles in the treated soil should be:

$$\%S_{treated} = \%S_{untreated} + \beta\%F_{untreated} \quad (5.4)$$

The percent of sand-size particles in the untreated soil as the first term in the above equation, illustrates that the cement and its hydration and cementitious products do not contribute to the increment in the value of $\%S_{treated}$, However, it might increase the particle size and form bonds between them. The increment in particle size due to cement treatment was also reported in granular soil mixed with 2% cement content [129]. It also concluded that the cement bonds were difficult to destroy by hand but might be destroyed under confining pressure and monotonic shearing.

The values of β for the cement-treated soil at 28 days were given in Table 5.6, in which it increased from 0.018 to 0.135 when increasing the cement content from 3% to 10%. In other words, up to 13.5% of the fine content in the soil was transferred to sand-size particles when treated with 10% of the cement contents. The increase in

particle size of the cement-treated soil was used to explain the significant improvement in the effective friction angle of the treated samples in the next section.

5.7. INTERFACE SHEAR STRENGTH BEHAVIOR OF CEMENT-TREATED SOIL UNDER CONSOLIDATED DRAINED CONDITIONS

5.7.1. Shear stress-strain behavior of cement stabilized soil under consolidated-drained conditions

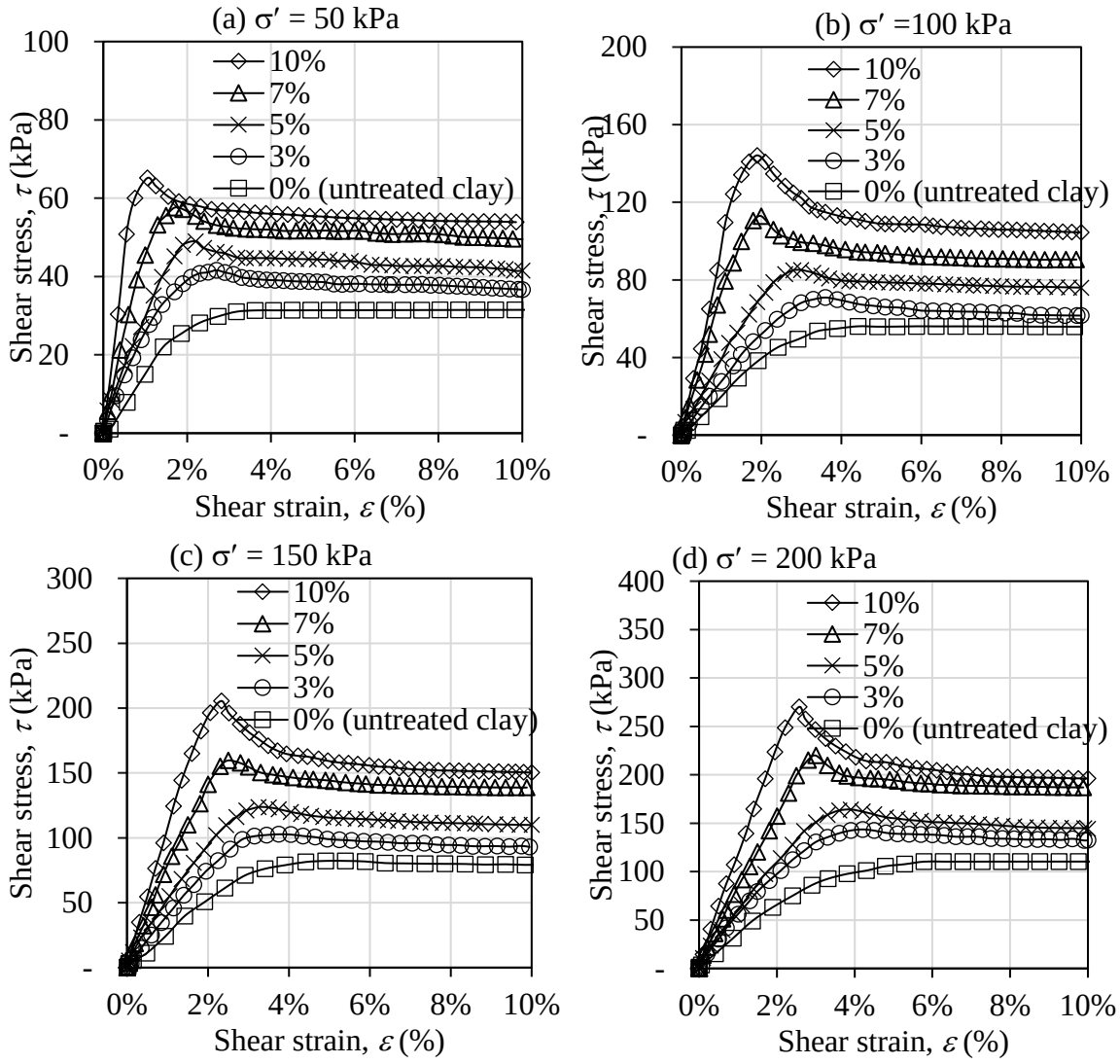

Figure 5.22: Shear stresses vs. shear strain of the untreated silty soil and the soil treated by different cement contents at 28 days of curing. The effective normal stress was set at (a) σ′=50 kPa; (b) σ′ = 100 kPa; (c) σ′ = 150 kPa; (d) σ′ = 200 kPa.

Figure 5.22 illustrates the stress-strain relationships of the soil and cement-stabilized soil after 28 days of curing under various effective normal stresses. At the

effective normal stress range of 50-200 kPa, the peak shear strength of cement-treated soil specimens was substantially higher than that of untreated soil. More cement content increases the shear strength of treated soil samples [65–69].

In addition, cement treatment shifted the stress-strain behavior of the untreated and treated soil specimens from ductile to brittle failure, respectively (Figure 5.22). The increase in cement content led to sample failures that were more brittle. These results are consistent with the brittle failure behavior of cement-treated soil observed in a variety of tests, such as unconfined compression tests [68, 72–74], direct shear tests [73, 74], and triaxial and plane strain tests [68]. As demonstrated in Figure 5.22, 10% of the shear strain was selected as the strain at failure of the untreated soil [95]. In contrast, the shear strain at the maximum shear stress of soil specimens treated with cement was much smaller and reduced as the cement content rose. Increased effective normal stress contributed to an increase in shear strain at failure.

5.7.2. Behavior of interface shear strength between cement-treated silty soil and steel under consolidated-drained conditions.

Figure 5.23 presents the interface between steel and silty soil after 28 days of curing. The interface shear strength of cement-treated soil with steel was greater but reached its maximum value at a smaller shear displacement than that of untreated soil and steel. Moreover, the increase in cement content led to an increase in peak interface shear strength and a reduction in peak shear displacement. Specifically, the interface shear stress of the untreated specimens peaked at a shear displacement of 1.2 mm to 3.2 mm, which corresponded to 2.0% to 5.3% of shear strain. These shear strains were considerably less than those at the highest shear strain of the soil (i.e., 10%), which were also observed in prior investigations [78].

Furthermore, the greater the effective normal stress, the greater the shear displacement at maximum interface shear stress. These findings are consistent with the shear behavior of the steel-soil contact as reported in previous research. Employing a modified interface direct shear test apparatus, Tsubakihara et al. [76] reported that the maximal interface shear strength of a normally cemented Kawasaki

clay and steel surface occurred at around 1-3 mm of shear displacement. In addition, the peak interface shear stress between the soil and stainless steel was less than the peak shear strength of the soil under an effective normal stress. This observation is consistent with the interface shear strength between the high-content clay and the smooth, polished surface [130].

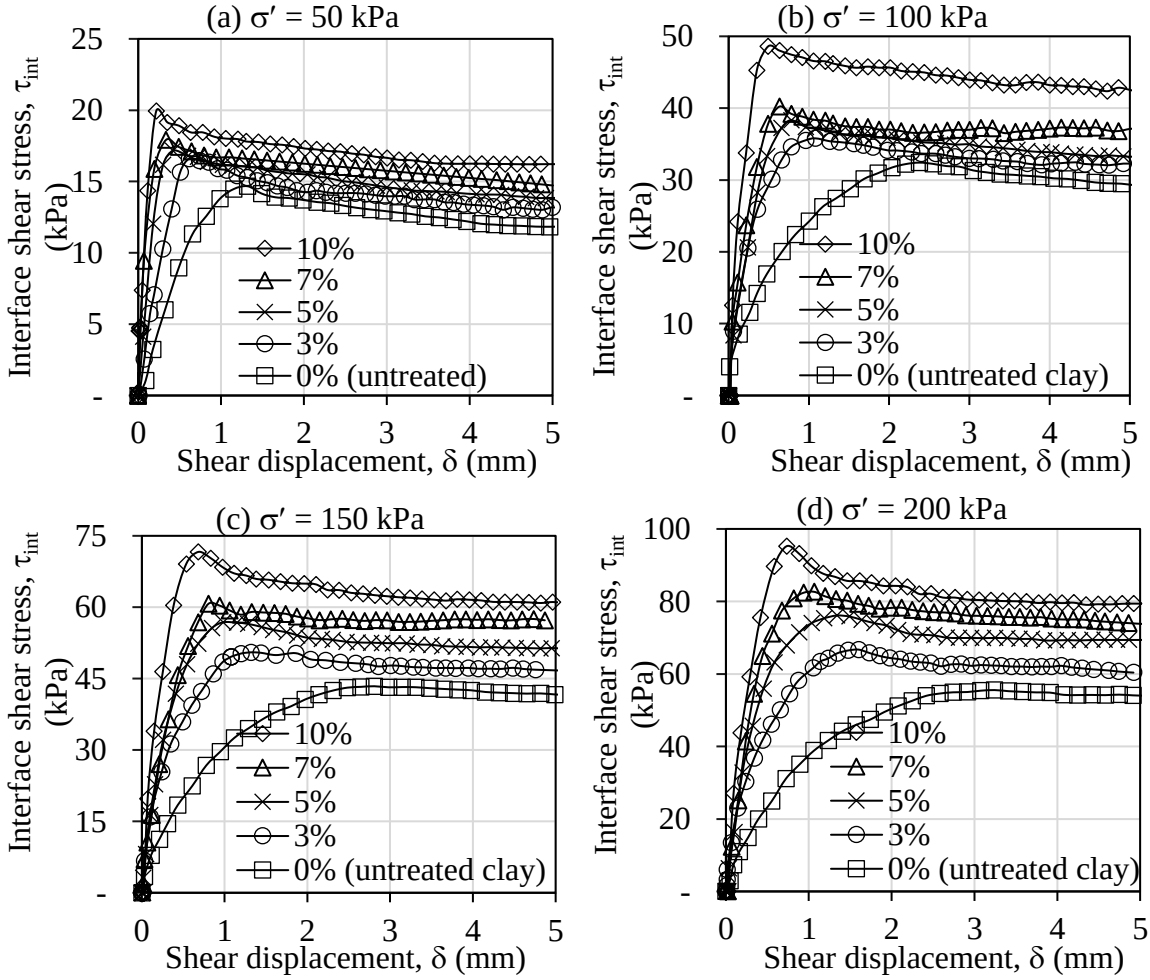

Figure 5.23: Interface shear stresses vs. shear displacement between corrosionless steel and silty soil treated by different cement contents, c_m under various effective normal stresses (a) σ′= 50 kPa; (b) σ′ = 100 kPa; (c) σ′ = 150 kPa; (d) σ′ = 200 kPa.

For soil treated with cement, the shear displacement at the highest interface shear strength ranged from 0.2 mm to 1.6 mm. Similar to the untreated soil, the cement-treated soil specimens required greater shear displacement under higher effective normal stress to reach their maximum interface shear strength. Compared to

untreated soil, the increased interface shear strength between steel and cement-treated soil would be mobilized at a smaller shear displacement. Su et al. [131] found a similar interface shear behavior on the red clay concrete interface in a large-scale direct shear test, where all the curves exhibit a stick-slip phenomenon after yielding. This failure mode was also observed in the interface shear test between dirt and smooth interfaces, such as polished stainless steel [76, 126].

5.7.3. Result of the effect of cement content on the shear strength and interface shear strength of cement-treated soil.

Using peak and residual strength values, the effects of cement content on enhancing the shear strength and interface shear strength of treated soil specimens were examined. As shown in Figure 5.22 and Figure **5.23**, after the shear and interface shear strengths of the treated specimens reached their maximum values, they would be reduced dramatically at the end of the tests. To account for the brittle shear-strain behavior of shear strength, 10% of the shear strain was used to calculate the residual shear strength. The interface shear stress at 5 mm of shear displacement was chosen as the residual value to investigate the stick-slip phenomenon of interface shear behavior of treated soil [76, 126].

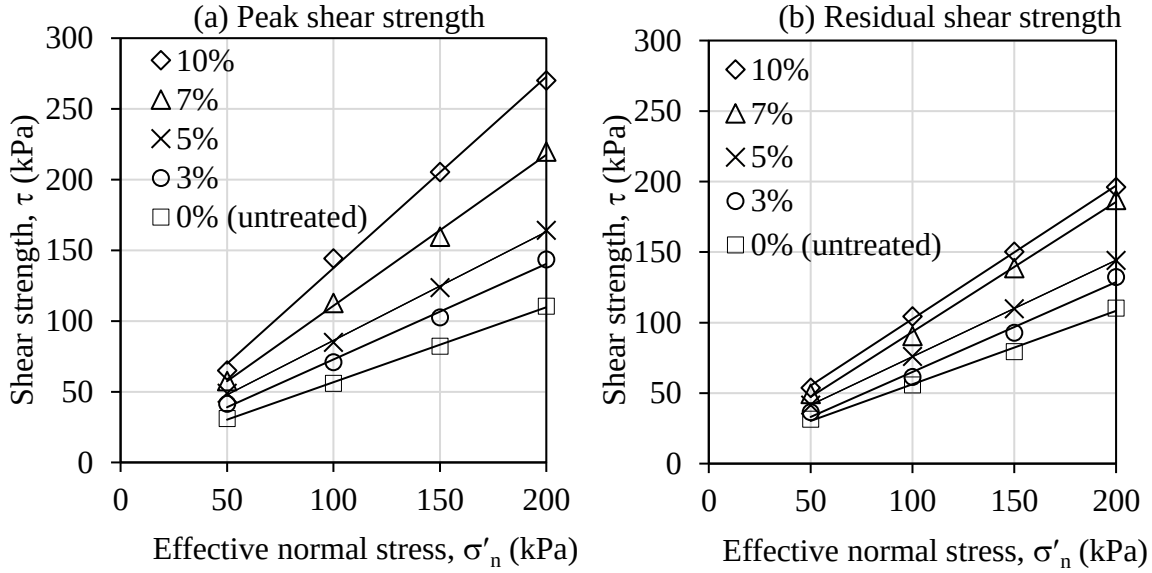

Figure 5.24: Peak and residual shear stress failure envelopes

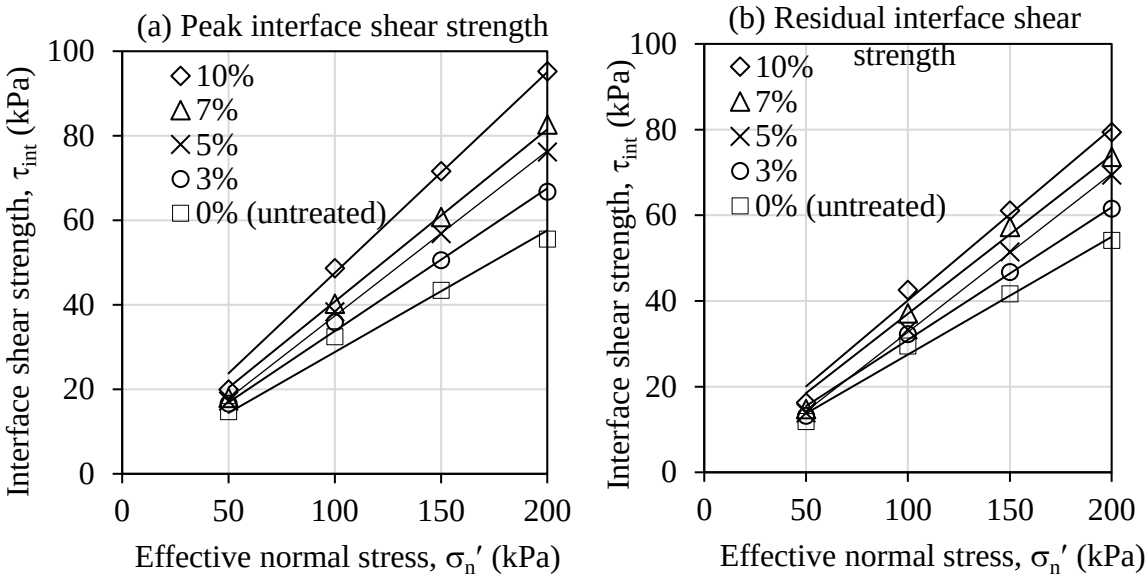

Figure 5.25: Peak and residual interface shear stress failure envelopes

Figure 5.24 and Figure **5.25** depict, respectively, the effective failure envelopes of the shear strength and interface shear strength of the cohesive soil treated with a change in cement content. The small effective cohesion of the untreated soil illustrated that the soil was in a normal consolidated condition. The shear strength of the cement-treated soil was manifested by relatively small increases in effective cohesions and significant increases in effective friction angle. In particular, the peak effective friction angle rose from 27.50 for the untreated soil to 53.50 for the soil specimens treated with 10% cement content (Figure 5.26).

Figure 5.26 also illustrates the effects of cement content on the enhancement of the interface shear strength of cement-treated soil. Similar to the shear strength, both the peak and residual effective interface friction angles, ϕ'_{int_max} and ϕ'_{int_res}, were higher when increasing the c_m value. The ϕ'_{int_max} values increased from 15.4^0 for the untreated soil specimens to 25.4^0 for the treated soil specimens with 10% cement content. At that cement content, the residual effective interface friction angle was smaller, about 21.9^0. That might be explained using Horpibulsuk et al. [54] investigation of the microstructure of cement-stabilized silty soil. For cement contents less than 10%, as cement content increased, more cementitious products were produced, which enhanced inter-cluster bonding and filled pore space. As a

result, it would result in the formation of larger particles (i.e., a higher fraction of sand size-particles and a higher mean particle size, D_{50}, as shown in Table 5.6 and bonding between them. The first factor would considerably increase the effective friction angle of treated soil. In contrast, the slight increase in effective cohesion under consolidated-drained shearing may expose weak particle bonding.

The increase in the percentage of sand-sized particles in cement-treated soil would increase its shear strength and interface shear strength. The effects of the sand size fraction on the shear strength of sand-clay mixtures could demonstrate this matter. Laboratory research reveals that shear strength is dependent on the relative concentrations of large particles and clay. For fine contents greater than 60 percent, the shear strength of the mixtures is equivalent to that of pure clay [131]. In these cases (i.e., fine content > 60%), the decrease in fine content (i.e., the increase in sand size particle fraction) results in an increase in the internal friction angle [131, 132]. Tsubakihara et al. [76] reported similar effects of particle size on the shear strength of the soil-steel interface. The results of this study indicated that the shear strength of the interface between a sand-clay mixture and steel increased significantly as the percentage of granular soil particles increased. Compared to the interface shear strength of the sand-clay mixture, the increase in the interface shear strength was more pronounced in soil specimens stabilized by a higher cement content. This can be attributed to cementitious materials, which increased particle size and decreased void space in the treated soil [54].

Nonetheless, these observations on the shear strength values of the cement-treated soil differed from those revealed in previous research. Issa and Reza [73] demonstrated, using a conventional direct shear apparatus, that cement treatment enhanced the shear strength of treated sand specimens, with the increase in cohesion being more dramatic than that in friction angle. In that investigation, specimens were made by compacting the soil-cement mixture to the optimum moisture content and then shearing it at a rate of 0.12 mm/min. Hence, the test findings demonstrated the total shear strength behavior of unsaturated specimens, which was significantly

different from those presented here (i.e., the effective strength behavior of saturated samples). For the shear behavior of the cement-treated soil under consolidated undrained triaxial compression, Azneb et al. [69] found that the effective cohesiveness increased significantly with the addition of cement. Nonetheless, it was discovered that the effective friction angle was essentially constant for all cement contents. The difference may be attributable to the increased cement content and water-to-cement ratio employed in the Azneb et al. [69] investigation. In particular, the treated specimens were created by combining soil with water content as high as 1.2 times the liquid limit of base soil with 10-20% cement. In addition, the cement was added as a slurry with a water-to-cement ratio of 0.6, resulting in an increase in the mixture's water content. For such a high cement concentration and water-to-cement ratio, it is believed that significant hydration products and cementitious products exist and produce strong intercluster bonding in treated soil samples. The test findings demonstrated a significant improvement in effective cohesiveness and effective friction angle [69].

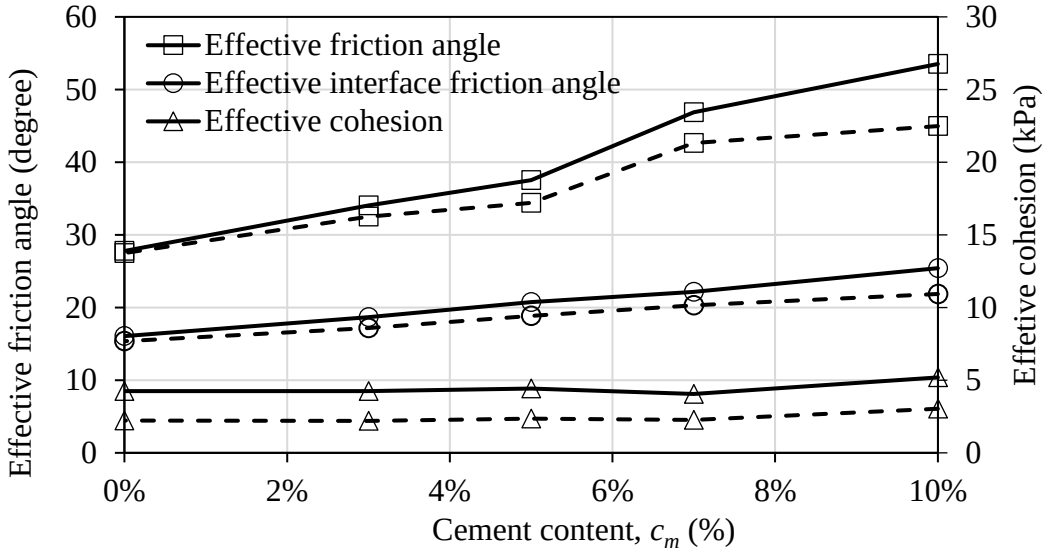

Figure 5.26: Shear strength and interface shear strength parameters of untreated and treated soil specimens. The continuous line and the dashed line exhibited the peak and residual values, respectively

In addition, there was a significant difference between the peak and residual shear strengths of cement-treated soil samples (Figure 5.26). Although there was a

little difference (about 2 kPa) between the peak and residual effective cohesiveness of the cement-treated soil, c'_{max} and c'_{res}, a significant difference between the peak and residual effective residual friction angles, ϕ'_{max} and ϕ'_{res}. The difference would be greater as the cement content increased. Specifically, ϕ'_{res} was 8.5 degrees less than ϕ'_{max} for specimens containing 10% cement content, equating to a 15% decrease in the highest effective friction angle. Similar results were observed for the peak and residual strength parameters of cement-stabilized soil during consolidated-undrained triaxial compression [72]. Between the peak undrained shear strength and the residual value of the treated soil samples, the results of the tests demonstrated a significant drop. The difference rose as effective consolidation and curing periods increased [72].

Last, the shear strength and interface shear strength improvements of the cement-treated soil were quantified using the shear strength ratio, R_s and interface efficiency ratio, *IEF*, respectively. The shear strength, R_s was defined for the shear strength of treated soil at each normal stress level, as follows:

$$R_s = \frac{\tau_{treated}}{\tau_{untreated}} \tag{5.5}$$

Similarly, the interface efficiency ratio, *IEF*, was defined as the ratio of the interface shear strength of the treated soil to that of the untreated soil, which was first presented by Hamid et al. [78].

$$IEF = \frac{\tau_{int}^{treated}}{\tau_{int}^{untreated}} \tag{5.6}$$

Figure 5.27 illustrates the average values of R_s and *IEF* obtained from cement-treated soil samples subjected to different effective normal stresses. It was observed that the relative standard deviation of the results was less than 5%. The peak shear strength ratio changed from 1.28 to 2.40 as the cement content increased from 3% to 10%. At 10% of the shear strain, however, the residual shear strength ratio was significantly lower, ranging from 1.16 to 1.80 in that cement content range.

Similarly, the peak values of the average interface efficiency factor, $IEF_{average}$, also increased from 1.15 to 1.55 when the cement content was raised from 3% to 10%.

Under this cement content range, the residual values of $IEF_{average}$ were smaller, ranging between 1.12 and 1.44.

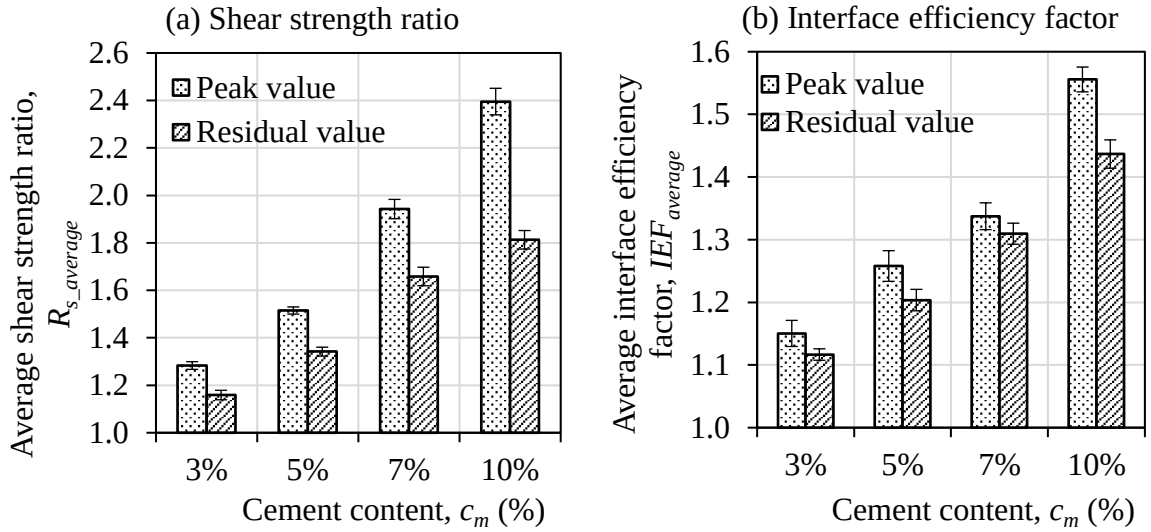

Figure 5.27: Average shear strength ratio and average interface efficiency factor of cement-treated soil with standard deviation.

A number of studies have reported that the soil-water/cement ratio is strongly correlated with unconfined compressive strength [69, 70, 139–142] and undrained shear strength [117]. For instance, a power function could present the unconfined compressive strength of cement-treated soil at 28 days of curing, q_u, as follows [138]:

$$q_u = \frac{A}{(w/c_m)^B} \tag{5.7}$$

in which A and B are empirical constants.

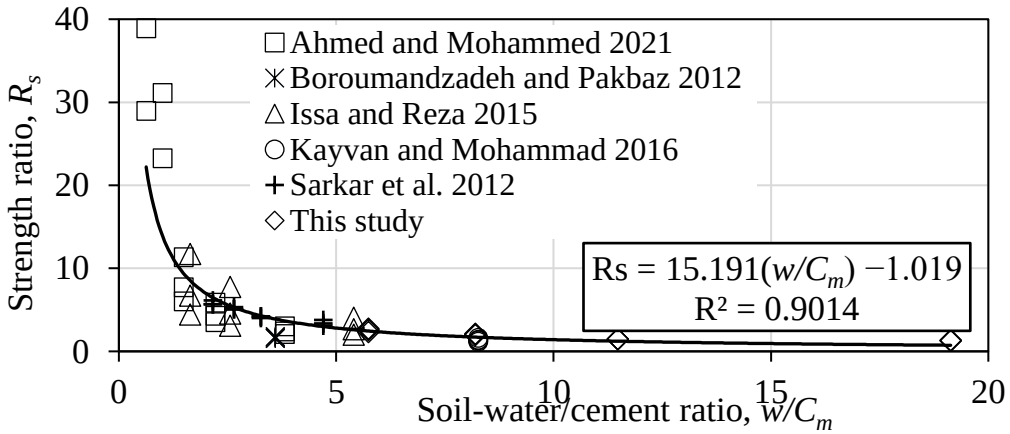

Figure 5.28: Shear strength ratio of cement-treated soil at 28 days of curing versus soil-water/cement ratio [79, 142, 144–146].

Based on the above correlation, the strength ratio of cement-treated soil could also be evaluated using w/C_m values. Figure 5.28 shows the values of the shear strength ratio plotted against soil-water/cement content. The relationship can be satisfactorily modeled by the following power function (R^2 = 0.92), which is in a similar form to Equation (5.7):

$$R_s = \frac{15.191}{(w/C_m)^{1.019}} \quad (5.8)$$

The points in Figure 5.28 represent the direct shear test results of different types of soil treated with varying amounts of ordinary Portland cement. As indicated in Table 5.7, test variations included normal stresses, cement contents, water contents, and drainage conditions. Notably, the correlation equation was devised without considering normal stress, which would result in a prediction error. Nevertheless, the error could be negligible because the strength ratio changed insignificantly with the variation of the normal stresses (i.e., the relative standard deviation was less than 5%). The proposed prediction for R_s values was also restricted to the shear strength at 28 days of soils with low organic or inorganic content treated with ordinary Portland cement, of which the value w/c_m is in the range of 0.6 to 19.1.

Table 5.7: Summary of direct shear test conditions on cement-treated soil in various studies at 28 curing days

Type of Soil	w, %	Drainage Condition	Normal Stress, kPa	C_m, %	w/C_m	References
Caspian Sea sand (SP)	12.3–14.4	Undrained	34–121	2.5–7.5	1.6–5.4	Issa and Reza [73]
Egypt's clean siliceous yellow sand (SP)	9.4–11.5	Undrained	50–105	3–15	0.6–3.8	Ahmed and Mohammed [137]
Bangladesh silty clayey soil (CL)	23.5–27	Undrained	35–105	5–12.5	2.2–4.7	Sarkar et al. [139]
50% Aeolian and 50% bentonite	24.8	Drained	55–416	3	8.3	Kayvan and Mohammad [140]
70% sand and 30% bentonite	18	Drained	24–347	5	3.6	Boroumandzadeh and Pakbaz [141]
Cai Lon riverbed soil (MH)	54.7	Drained	50–200	3–10	5.7–19.1	This study

5.7.4. Effect of the curing period on the shear strength and the interface shear strength of cement-treated soil.

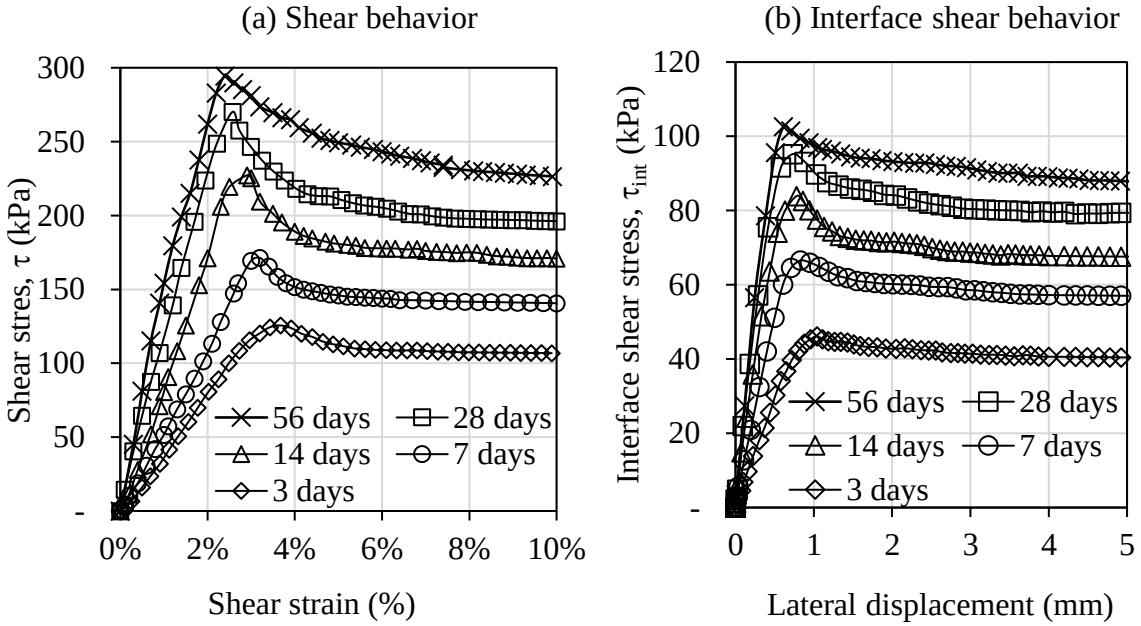

Figure 5.29: (a) Shear behavior and (b) Interface shear behavior of cement-treated soil specimens under 200 kPa of effective normal stress after different curing periods.

Figure 5.29: (a) Shear behavior and (b) Interface shear behavior of cement-treated soil specimens under 200 kPa of effective normal stress after different curing periods.Figure 5.29 shows the development of the shear and interface shear behavior of soil treated with 10% cement during the 56 days of the curing period. In addition, the lengthening of the curing period caused the shear and interface shear behavior of the treated soil to become more brittle.

Similar to previous research, the 28-day-old strength of cement-stabilized soil was used as a reference value to evaluate the rate of strength development [54, 64, 141]. As shown in Figure 5.30, a strong correlation ($R^2 = 0.981$) was found between the curing period and the strength development ratio of peak and residual strength derived from shear strength and interface shear strength of the treated soil samples:

$$R_{SD} = \frac{\tau_D^{max}}{\tau_{28}^{max}} = \frac{\tau_D^{res}}{\tau_{28}^{res}} = \frac{\tau_D^{int\_max}}{\tau_{28}^{int\_max}} = \frac{\tau_D^{int\_res}}{\tau_{28}^{int\_res}} = 0.2108\ ln(D) + 0.2833 \qquad (5.9)$$

in which

τ^{max}_{D}, τ^{res}_{D}, $\tau^{int\_max}_{D}$, and $\tau^{int\_res}_{D}$ are the peak shear stress, residual shear stress, peak interface shear stress, and residual interface shear stress after D days of the curing period, respectively.

τ^{max}_{28}, τ^{res}_{28}, $\tau^{int\_max}_{28}$, $\tau^{int\_res}_{28}$ are the peak shear stress, residual shear stress, peak interface shear stress, and residual interface shear stress after 28 days of curing, respectively.

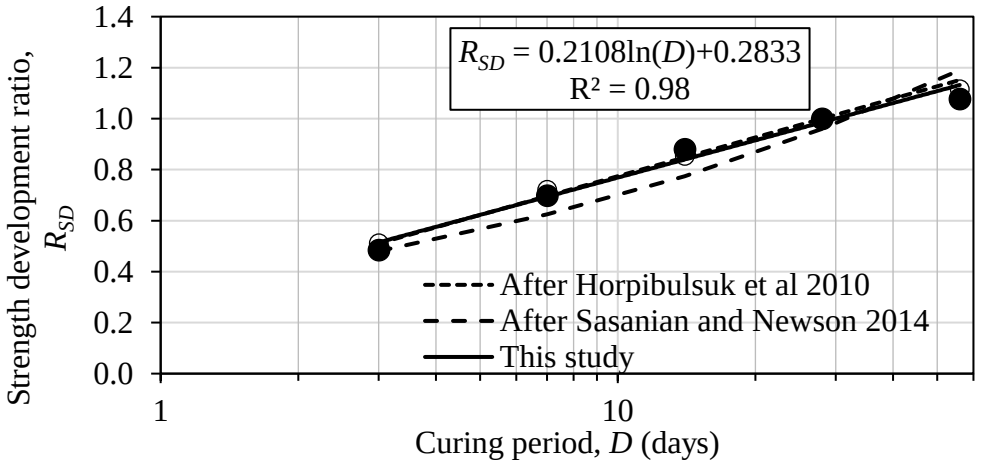

Figure 5.30: Shear strength and interface shear strength development with time in the silty soil treated with 10% cement content. The bold and empty nodes indicate the peak and residual strength values, respectively.

Although this relationship is related to the rate of shear strength and interface shear strength development of cement-treated soil in the curing period range between 3 and 56 days, as shown in Figure 5.30, the finding correlation is matched to the logarithmical relationship developed for the unconfined compressive strength with curing period of cement-stabilized low plasticity and coarse-grained soil [64]. In that study, the proposed relationship was valid for the longer range of curing periods (i.e. between 7 and 120 days) and accounted for the variations in soil types, water content, cement content, and compaction energy. In addition, the relationship in this study also agrees with the development of undrained shear strength of various clays cemented with Portland cement with curing time proposed by Sasanian et al., [117], which was developed using more than 440 data points for 12 different clays, with a wide range of liquidity indices (LI ~ 0.4-3.0) and cement content (c_m ~ 1-100%). To

conclude, it appears that the development rate of the effective shear strength of the cement-treated soil within 56 days of curing is comparable to that of the unconfined compressive strength and undrained shear strength of the cement-stabilized soil proposed by various previous studies.

5.8. CONCLUSION

A series of laboratory tests were conducted to examine the characteristics of cement-treated silty soil. Due to the cement's hydration and pozzolanic reaction, the swelling, the *CBR* value, the *UU* shear strength, the settlement, and the shear strength of the treated soil improved significantly. The remaining findings were as follows:

a) Behavior of silty soil with cement under swelling and the CBR test

The results illustrate the role of cement in improving the bearing capacity of reinforced expansive clay in the soaked condition. The other conclusions are:

1. The cement induced the swell faster by sucking water into the reinforced specimens. It also reduces the percent swell and soil density reduction after soaking by the hydration process, making the soil grains bind together. The higher the increment of cement in the reinforced specimens was, the lower the swell percentage was observed. The dry unit weight reduction due to soaking decreases from 4.2% (for unreinforced clay) to 1.75% (for 10% cement content).

2. The cement significantly improves the *CBR* behavior of expansive clay in the soaked condition. Compared to the *CBR* value of unreinforced clay, the highest strength ratio is 3.8 for the soaked specimens reinforced by a 10% cement ratio.

b) Behavior of silty soil with cement on UU shear strength under the triaxial test

Under both wetting and non-immersion conditions, the cement increased the soil's load-bearing capacity. Conclusions include:

1. The cement enhanced the shear resistance of the unsaturated soil. The cohesive force rose significantly while the angle of internal friction increased slightly. As lateral pressure increased, the R_{uf} index of strength increment decreased.

2. When adding cement, the samples had a brittle failure with a small strain, about 1%-2%. Besides, less excess pore water pressure was observed in the unreinforced samples at failure before dropping significantly.

c) Behavior of silty soil with cement under the consolidation test

Under compression pressure, soil cement settled quickly and stabilized after approximately 30 minutes. The secant modulus increased when the dried cement ratio and load pressure increased. The result showed that the modulus of soil cement increased lightly about 2 times when the cement ratio increased from 3% to 7%, and the modulus in the case of 10% cement was 6 times higher than that of 3% cement at 23.74 kPa. This figure decreased approximately 3 times when the compression pressure went up to 384.3 kPa.

Besides, the more cement added, the higher the soil cement specimens were. Cement content increased to 3%, and the void ratio increased from 1.1 to 1.33 times compared to unreinforced soil. This value is 1.14 to 1.77 times higher with a cement content of 10%.

d) Interface shear strength behavior of cement-treated soil under consolidated-drained conditions:

Due to the cement's hydration and pozzolanic reaction, the shear strength and interface shear strength of the treated soil specimens improved significantly. The remaining findings were as follows:

1. The cement caused the treated soil's particle size to increase. The greater the cement content, the greater the percentage of sand and the average particle size, D_{50}. Particularly, after 28 days of curing, the percentage of sand in soil treated with 10% cement decreased twofold. That increment was due to the integration of fines into sand-size particles (about 13.8% at 10% cement content), which was a result of cement treatment.

2. After yielding behavior, the treated soil's shear strength and interface shear strength exhibited the brittle shear-strain and stick-slip phenomena, respectively. The increase in effective friction angle mostly contributed to the improvement in the shear

strength of the cement-treated soil. In contrast, the treated soil exhibited an insignificant increase in effective cohesion.

3. The higher the cement content, the greater the shear strength ratio of the soil treated with cement. For specimens containing 3-10% cement, the peak and residual average shear strength ratios ranged from 1.28 to 2.40 and 1.16 to 1.80, respectively. The cement also enhanced the soil-steel interface's strength parameters. At its peak, the average interface efficiency factor was approximately 1.55 when 10% cement content was added.

4. The proposed equation may be used to predict the rate of shear strength and interface shear strength development of cement-treated silty soil with a strong correlation with the curing period. The proposed relationship also agrees with the unconfined compressive strength and undrained shear strength of cement-treated soil provided by previous studies.

Moreover, it should be noted that the data given in this study relates to cement-treated remolded soil under laboratory testing conditions. The objective of the conducted tests was to simulate the shear strength and interface shear strength behaviors of the cement-treated soil in the field, despite the fact that the mixing procedure, uniformity, and curing conditions of the treated soil specimens in the laboratory differ significantly from those in the field. In spite of these discrepancies, it is believed that the test results will give useful information regarding the effects of cement content and curing period on the effective shear strength and effective interface shear strength of the cement-treated silty soil.

CHAPTER 6: CONCLUSIONS AND RECOMMENDATIONS

6.1. COMPARISON:

After being saturated, silty soil swells and loses its strength, which is unsatisfactory for backfill material. Thus, the primary goal of this research was to evaluate the capacity of reinforcements, including geotextile, sand cushion, and cement, to improve the soil's properties. The laboratory tests, including the *CBR* test, the *UU* triaxial shear strength test, a one-dimensional consolidation test with a modified oedometer apparatus, and the modified direct shear test, were carried out to investigate the reinforcement capacity. The factors for a material backfill are swelling, strength, and the consolidation process, which are discussed as follows:

a) Percentage of swelling

These methods reduced the swelling of the soil, reducing density loss after soaking. For the soil reinforced by geotextiles and sand cushions, the permeable reinforcement accelerates swelling by increasing the drainage path within the reinforced specimens. In the soil cement samples, the hydration process occurred and bound the soil grains together, leading to a decrease in the swell. A lower percent expansion was observed as the number of geotextile layers, the sand cushion thickness, and the cement ratio increased. Figure 6.1 shows the highest, average, and lowest swelling of each reinforcement method in this study. The results illustrated that the swellings in the cement method got the lowest values, whereas the sand cushion got the highest numbers.

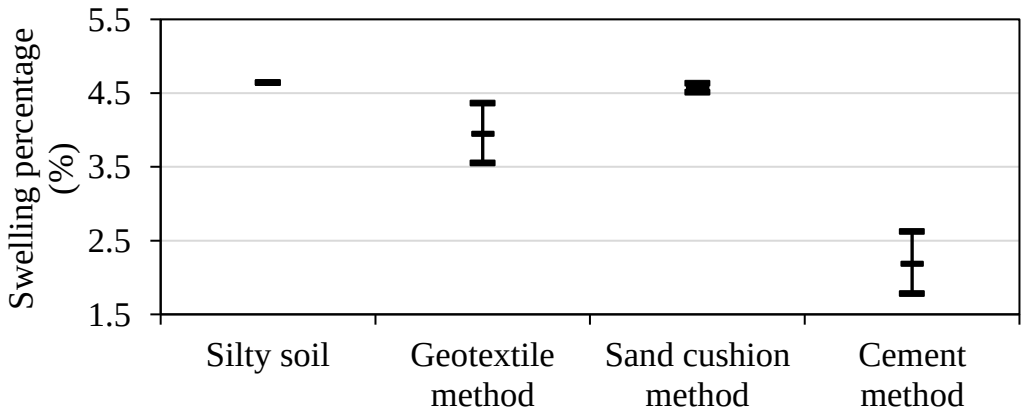

Figure 6.1: The swelling range of reinforcement methods in this study.

b) <u>CBR behavior</u>

After soaking, the *CBR* values of the soil decreased dramatically. By using geotextile, sand cushion, and cement, the *CBR* value was significantly improved. Interestingly, for the geotextile-soil mixture, the highest *CBR* value was obtained when the ratio between reinforcement spacing and the diameter of the load piston, achieved the optimum value of about 0.8 (2 geotextile layer samples). The observation can be explained by the mechanisms of reinforced soil under the load of a piston, including the confinement effect and the membrane effect. Under sand cushion reinforcement, again, the maximum improvement happened at the soil with 15 mm of sand cushion, of which the ratio of the height of the topsoil layer and the diameter of the penetrated piston got an optimum value equal to 1. The *CBR* increase in soil reinforced by geotextile and sand cushion in the case of soaking is greater than in the case of unsoaking. For the soil cement, after 28 days of soaking, the *CBR* value increased as the cement ratio increased due to the hydration process.

Comparing these methods, Figure 6.2 showed that the strength of silty soil was improved significantly. The cement method got the highest score. However, the value range of this method was larger than others. The geotextile *CBR* value was the smallest, indicating that increasing the number of geotextile layers did not significantly affect it

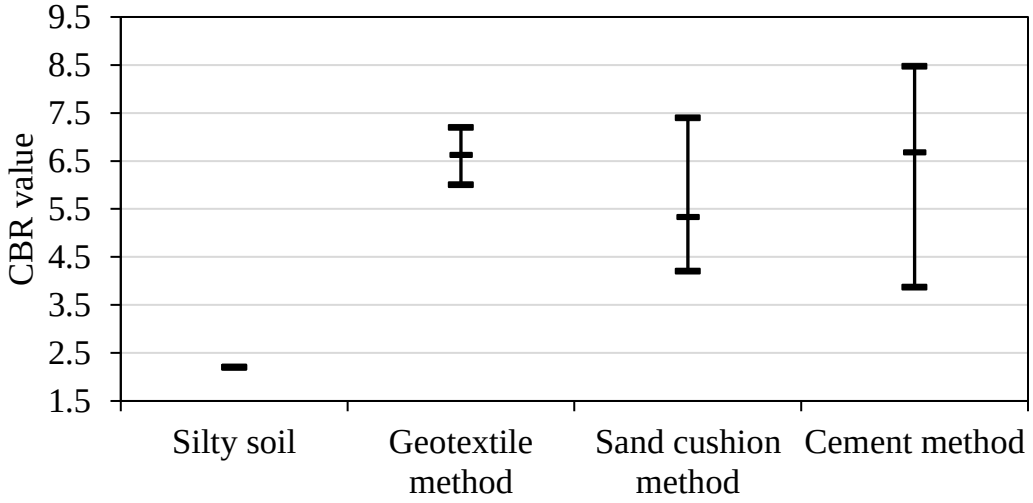

Figure 6.2: The CBR range of reinforcement methods for saturated samples

c) <u>UU shear strength</u>

After soaking, the shear strength of the soil decreased dramatically. Geotextile, sand cushion, and cement improved UU shear strength, especially in the case of saturated samples. The shear strength reduction decreased when the lateral pressure decreased, and the number of geotextile layers and sand cushion thickness increased.

For saturated samples, as the number of geotextile layers and the sand thickness increased, the UU shear strength and the excess pore water pressure increased with the small strain, as reinforcements can restrain the lateral deformation or the potential tensile strain of the soil. After that, the pore water pressure decreased. The soil-cement showed a brittle failure with minimal deformation. As the concentration of cement increased, its strength significantly increased. With the saturated samples, the results indicated that deviation stress increased when the axial strain and the cement content increased.

Figure 6.3 shows the UU shear strength S_u in the saturated condition for three methods. It revealed that the cement method gave the best reinforcement effect, whereas the geotextile and sand cushion methods had a lower reinforcement efficiency.

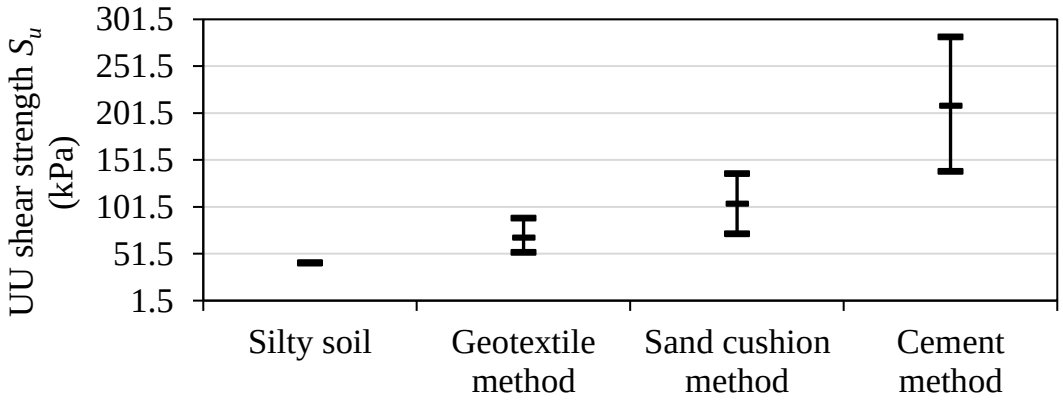

Figure 6.3: The UU shear strength S_u range of reinforcement methods for saturated samples.

d) <u>Consolidation</u>

When estimating the consolidation behavior of silty soils with a D/H_0 greater than 2.5, evaluating the side friction is essential.

In this study, a modified oedometer apparatus was created to determine the side friction between the soil and the consolidation ring. The total side friction pressure grew marginally as consolidation time rose, causing an important reduction in the average consolidation pressure at the end of primary consolidation (*EOP*). As D/H_0 increases, the friction pressure loss ratio at *EOP* decreases. Furthermore, it declined as the compression pressure was raised. Besides, the proposed analytical method can accurately predict the values of r_{EOP} and e_{EOP} for clay within the normal consolidation pressure range without requiring the height of test specimens. Furthermore, the void ratio at the conclusion of primary consolidation increases proportionally with depth due to side friction. Using *COV* values of the void ratio, the degree of soil sample uniformity at the *EOP* was determined. The *COV* values increase as the friction pressure loss ratio increases.

Regarding the effect of geotextile and sand cushion, the consolidation time significantly declined compared to that of soil, by 1-2 times for geotextile samples and 3.5- 5 times for sand cushion samples. Thus, the geotextile and sand cushion, as a drainage path, can improve the soil's capacity and the consolidation process.

In the soil-cement mixture, after roughly 30 minutes, the samples settled rapidly and stabilized. The secant modulus was displayed as one of the characteristics of a soil-cement mixture. When the cement ratio increased, the modulus of soil cement increased. Furthermore, the settlement of the mixture decreased significantly, leading to an increase in the void ratio.

Thus, when comparing the three methods, the cement method had the shortest time to reach consolidation and the smallest settlement.

e) The effects of cement content and curing time on the shear strength behavior of the cement-treated clay and steel interface

Due to the cement's hydration and pozzolanic reaction, the shear strength and interface shear strength of the treated soil specimens improved significantly. The remaining findings were as follows:

- The cement caused the treated soil's particle size to increase. Particularly, after 28 days of curing, the percentage of sand in soil treated with 10% cement increased twofold. That increment was due to the integration of fines into sand-size particles, which was a result of cement treatment.

- The treated soil's shear strength and interface shear strength exhibited the brittle shear-strain and stick-slip phenomena, respectively. The increase in effective friction angle mostly contributed to the improvement in the shear strength of the soil cement. In contrast, the treated soil exhibited an insignificant increase in effective cohesion.

- The higher the cement content, the greater the shear strength ratio of the soil treated with cement. For specimens containing 3-10% cement, the peak and residual average shear strength ratios ranged from 1.28 to 2.40 and 1.16 to 1.80, respectively. The cement also enhanced the soil-steel interface's strength parameters. At its peak, the average interface efficiency factor was approximately 1.55 when 10% cement content was added.

- The correlation calculation was proposed to estimate the increase in shear strengths based on the ratio of water content to cement weight. Additionally, another proposed equation may be used to predict the rate of shear strength and interface shear strength development in cement-treated silty soil with a curing period.

6.2. CONCLUSION

Based on the above comparison, in this research, the cement mixing method was the best method to improve the silty riverbed soil. Geotextile and sand cushions could enhance the physical and mechanical behaviors of soil, including swelling, strength, and consolidation.

According to the strength regulations of the pavement layer, the minimum *CBR* load capacity for rural roads with car-free traffic is 6 for the top 30 cm and 4 for the following 50 cm, based on TCVN 4054:2005 [3]. Thus, all the presented methods were applicable to improving the riverbed soil and applied to the foundation for rural roads in the Mekong Delta. Regarding rural roads with car traffic, TCVN 9436-2012 [4] requires the swelling of the backfill material to be lower than 3%. In this case,

together with the strength requirement, the cement method with 5% and above could be used as the backfill material.

6.3. LIMITATIONS AND RECOMMENDATIONS:

The results would illustrate the improvement of the soil. Because the water content increases, the silty soil loses its strength. Particularly, the case where the soil was saturated was considered the weakest and most dangerous. Thus, this study just demonstrates the effect of saturation on the strength behavior of reinforced soil. Therefore, this study did not focus on the mechanical behavior of the unsaturated samples when the strength changed. The mechanical behavior of unsaturated samples can be further researched.

Additionally, the outcome of this study would be a fundamental theory to enhance rural road design by using reinforced clay as backfill instead of costly sandy soil for rural road foundations. In the laboratory, the results showed that these methods satisfied the Vietnamese standard. The findings proved that these methods are efficient, quick, and cost-effective. However, the findings cannot be directly used in the design of the road's embankment. To apply these methods in reality, field conditions, construction methods, and field experiments need to be considered. The results of field experiments would be the most accurate basis for applying the methods widely. Thus, there needs to be more applied research about techniques, machines, materials, and field experiments. The result of field experiments would be that the methods could be widely used.

REFERENCES

[1] A. V. Da Fonseca, R. C. Cruz, and N. C. Consoli, "Strength properties of sandy soil-cement admixtures," *Geotechnical and Geological Engineering*, vol. 27, no. 6, pp. 681–686, 2009, doi: 10.1007/s10706-009-9267-y.

[2] "TCVN 10380:2014 Đường giao thông nông thôn– Yêu cầu thiết kế."

[3] "TCVN 4054:2005: Đường ô tô- Yêu cầu thiết kế."

[4] "TCVN 9436-2012: Nền đường ô tô - Thi công và nghiệm thu."

[5] W. Wang, H. Liu, Y. Li, and J. Su, "Development and management of land reclamation in China," *Ocean and Coastal Management*, vol. 102, no. PB, pp. 415–425, 2014, doi: 10.1016/j.ocecoaman.2014.03.009.

[6] A. W. Skempton and L. Bjerrum, "a Contribution To the Settlement Analysis of Foundations on Clay," *Selected Papers on Soil Mechanics*, pp. 74–84, 1984, doi: 10.1680/sposm.02050.0012.

[7] M. Zhang, X. Zhu, G. Yu, J. Yan, X. Wang, M. Chen, W. Wang , "Permeability of muddy clay and settlement simulation," *Ocean Engineering*, vol. 104, pp. 521–529, 2015, doi: 10.1016/j.oceaneng.2015.05.031.

[8] O. Plé and T. N. H. Lê, "Effect of polypropylene fiber-reinforcement on the mechanical behavior of silty clay," *Geotextiles and Geomembranes*, vol. 32, pp. 111–116, 2012, doi: 10.1016/j.geotexmem.2011.11.004.

[9] A. Marto and B. A. Othman, "The Potential Use of Bamboo as Green Material for Soft Clay Reinforcement System," *Proceedings of the International Conference on Environmental Science and Engineering*, vol. 8, pp. 129–133, 2011.

[10] C. Taechakumthorn and R. K. Rowe, "Performance of Reinforced Embankments on Rate-Sensitive Soils under Working Conditions Considering Effect of Reinforcement Viscosity," *International Journal of Geomechanics*, vol. 12, no. 4, pp. 381–390, 2012, doi: 10.1061/(asce)gm.1943-5622.0000094.

[11] K.-H. Yang, W. M. Yalew, and M. D. Nguyen, "Behavior of Geotextile-Reinforced Clay with a Coarse Material Sandwich Technique under Unconsolidated-Undrained Triaxial Compression," *International Journal of Geomechanics*, vol. 16, no. 3, pp. 1–15, 2015, doi: 10.1061/(asce)gm.1943-5622.0000611.

[12] A. Sridharan and H. B. Nagaraj, "Coefficient of consolidation and its correlation with index properties of remolded soils," *Geotechnical Testing Journal*, vol. 27, no. 5, pp. 469–474, 2004.

[13] ASTM D2435, "Standard Test Methods for One-Dimensional Consolidation Properties of Soils Using Incremental Loading," *West Conshohocken, PA: ASTM International*.

[14] D. W. Taylor, "Research on consolidation of clays," *Massachusetts Institute of Technology, Cambridge, MA*, 1942.

[15] H. Monden, "Characteristics of side friction in the one-dimensional consolidation test," *Soils and Foundations*, vol. 9, no. 1, pp. 11–41, 1969.

[16] O. Sivrikaya and E. Togrol, "Measurement of Side Friction between Specimen

and Consolidation Ring with Newly Designed Oedometer Cell," *Geotechnical Testing Journal*, vol. 29, no. 1, pp. 87–94, 2005.
[17] Y. Watabe, K. Udaka, M. Kobayashi, T. Tabata, and T. Emura, "Effects of friction and thickness on long-term consolidation behavior of osaka bay clays," *Soils and Foundations*, vol. 48, no. 4, pp. 547–561, 2008.
[18] Nakase and Akio, "Side friction in conventional consolidation tests," *Port and Harbour Technical Research Institute*, 1963.
[19] R. P. de Lima and T. Keller, "Impact of sample dimensions, soil-cylinder wall friction and elastic properties of soil on stress field and bulk density in uniaxial compression tests," *Soil and Tillage Research*, vol. 189, pp. 15–24, 2019.
[20] R. E. Olson, "State of the Art: Consolidation Testing." Consolidation of Soils: Testing and Evaluation, ASTM STP 892, ASTM International, West Conshohocken, PA, pp. 7–70, 1986.
[21] P. K. Kolay and G. Bhattacharya, "Remediation of the side friction in conventional oedometer tests by using large diameter consolidometer ring," *International Journal of Geotechnical Engineering*, vol. 2, no. 2, pp. 161–167, 2013.
[22] J. Lovisa and N. Sivakugan, "Tall Oedometer Testing: Method to Account for Wall Friction," *International Journal of Geomechanics*, vol. 15, no. 2, pp. 1–9, 2015.
[23] W. Yao, L Xi'an, W. Youjun, X. Quan, H. Zhitao, S. Jianfeng, Z. Chen, R. Yongbiao, "Effect of Height-to-Diameter Ratio on the Compression Test Results of Remodeled Loess and Its Mechanism," *Buildings*, vol. 13, no. 1, 2023.
[24] E. W. L. Atkinson, J. H.; Evans, J. S.; Ho, "Non-uniformity of triaxial samples due to consolidation with radial drainage," *Geotechnique*, vol. 35, no. 3, pp. 353–355, 1985.
[25] Y. A. Kolekar and S. M. Dasaka, "Variability in the soil properties of laboratory consolidated clay beds," *International Journal of Geotechnical Engineering*, vol. 8, no. 4, pp. 365–371, 2014.
[26] O. S. Mir, S. M. Dasaka, Y. A. Kolekar, and B. V. S. Viswanadham, "Evaluation of Uniformity of Soil Specimens Prepared in Large Tanks by Slurry Consolidation," *Geotechnical and Geological Engineering*, vol. 36, no. 3, pp. 1885–1895, 2018.
[27] A. Rawal, T. Shah, and S. Anand, "Geotextiles: Production, properties and performance," *Textile Progress*, vol. 42, no. 3, pp. 181–226, 2010, doi: 10.1080/00405160903509803.
[28] H. Wu, Y. Chongkai, L. Chenghan, M. Miao, Z, Yujian, L. Yuquan, L. Tong, "Review of application and innovation of geotextiles in geotechnical engineering," *Materials*, vol. 13, no. 7, pp. 1–21, 2020, doi: 10.3390/MA13071774.
[29] J. B. Park, H. S. Park, and D. Kim, "Geosynthetic reinforcement of sand-mat layer above soft ground," *Materials*, vol. 6, no. 11, pp. 5314–5334, 2013, doi:

10.3390/ma6115314.
[30] E. M. Palmeira, J. H. F. Pereira, and A. R. L. Da Silva, “Backanalyses of geosynthetic reinforced embankments on soft soils,” *Geotextiles and Geomembranes*, vol. 16, no. 5, pp. 273–292, 1998, doi: 10.1016/S0266-1144(98)00014-4.
[31] T. G. Sitharam and A. Hegde, “Design and construction of geocell foundation to support the embankment on settled red mud,” *Geotextiles and Geomembranes*, vol. 41, pp. 55–63, 2013, doi: 10.1016/j.geotexmem.2013.08.005.
[32] J. P. Malizia and A. Shakoor, “Effect of water content and density on strength and deformation behavior of clay soils,” *Engineering Geology*, vol. 244, pp. 125–131, 2018, doi: 10.1016/j.enggeo.2018.07.028.
[33] P. C. Wu, J. H. Yin, W. Q. Feng, and W. B. Chen, “Experimental study on geosynthetic-reinforced sand fill over marine clay with or without deep cement mixed soil columns under different loadings,” *Underground Space (China)*, vol. 4, no. 4. pp. 340–347, 2019. doi: 10.1016/j.undsp.2019.03.001.
[34] J. Guo, J. Han, X. Zhang, and Z. Li, “Evaluation of moisture reduction in aggregate base by wicking geotextile using soil column tests,” *Geotextiles and Geomembranes*, vol. 47, no. 3, pp. 306–314, 2019, doi: 10.1016/j.geotexmem.2019.01.014.
[35] A. K. Choudhary, J. N. Jha, and K. S. Gill, “A study on cbr behavior of waste plastic strip reinforced soil,” *Emirates Journal for Engineering Research*, vol. 15, no. 1, pp. 51–57, 2010, doi: 10.1007/978-3-030-02707-0_36.
[36] A. k. Choudhary, K. Gill, J. J.N., and S. Sk., “Improvement in CBR of the expansive soil subgrades with a single reinforcement layer,” *Proceedings of Indian Geotechnical Conference*, pp. 289–292, 2012.
[37] U. Rajesh, S. Sajja, and V. K. Chakravarthi, “Studies on Engineering Performance of Geogrid Reinforced Soft Subgrade,” *Transportation Research Procedia*, vol. 17, no. December 2014, pp. 164–173, 2016, doi: 10.1016/j.trpro.2016.11.072.
[38] D. M. Carlos, M. Pinho-Lopes, and M. L. Lopes, “Effect of Geosynthetic Reinforcement Inclusion on the Strength Parameters and Bearing Ratio of a Fine Soil,” *Procedia Engineering*, vol. 143, no. Ictg, pp. 34–41, 2016, doi: 10.1016/j.proeng.2016.06.005.
[39] C. A. Adams, Y. A. Tuffour, and S. Kwofie, “Effects of Soil Properties and Geogrid Placement on CBR Enhancement of Lateritic Soil for Road Pavement Layers "Effects of Soil Properties and Geogrid Placement on CBR Enhancement of Lateritic Soil for Road Pavement Layers,” *American Journal of Civil Engineering and Architecture*, vol. 4, no. 2, pp. 62–66, 2016, doi: 10.12691/ajcea-4-2-4.
[40] T. S. Ingold and K. S. Miller, “The performance of impermeable and permeable reinforcement in clay subject to undrained loading.,” *Quarterly Journal of Engineering Geology*, vol. 15, no. 3, pp. 201–208, 1982, doi:

10.1144/gsl.qjeg.1982.015.03.03.
[41] R. R. Al-Omari, H. H. Al-Dobaissi, Y. N. Nazhat, and B. A. Al-Wadood, "Shear strength of geomesh reinforced clay," *Geotextiles and Geomembranes*, vol. 8, no. 4, pp. 325–336, 1989, doi: 10.1016/0266-1144(89)90015-0.
[42] K. H. Yang, M. D. Nguyen, W. M. Yalew, C. N. Liu, and R. Gupta, "Behavior of geotextile-reinforced clay in consolidated-undrained tests: Reinterpretation of porewater pressure parameters," *Journal of GeoEngineering*, vol. 11, no. 2, pp. 45–57, 2016.
[43] H. Zhou and X. Wen, "Model studies on geogrid- or geocell-reinforced sand cushion on soft soil," *Geotextiles and Geomembranes*, vol. 26, no. 3, pp. 231–238, 2008, doi: 10.1016/j.geotexmem.2007.10.002.
[44] Y. Yu, B. Zhang, and J. M. Zhang, "Action mechanism of geotextile-reinforced cushion under breakwater on soft ground," *Ocean Engineering*, vol. 32, no. 14–15, pp. 1679–1708, 2005, doi: 10.1016/j.oceaneng.2005.02.007.
[45] S. K. Dash and M. C. Bora, "Improved performance of soft clay foundations using stone columns and geocell-sand mattress," *Geotextiles and Geomembranes*, vol. 41, pp. 26–35, 2013, doi: 10.1016/j.geotexmem.2013.09.001.
[46] M. R. Abdi, A. Sadrnejad, and M. A. Arjomand, "Strength enhancement of clay by encapsulating geogrids in thin layers of sand," *Geotextiles and Geomembranes*, vol. 27, no. 6, pp. 447–455, 2009, doi: 10.1016/j.geotexmem.2009.06.001.
[47] M. R. Abdi and M. A. Arjomand, "Pullout tests conducted on clay reinforced with geogrid encapsulated in thin layers of sand," *Geotextiles and Geomembranes*, vol. 29, no. 6, pp. 588–595, 2011, doi: 10.1016/j.geotexmem.2011.04.004.
[48] N. Unnikrishnan, K. Rajagopal, and N. R. Krishnaswamy, "Behaviour of reinforced clay under monotonic and cyclic loading," *Geotextiles and Geomembranes*, vol. 20, no. 2, pp. 117–133, 2002, doi: 10.1016/S0266-1144(02)00003-1.
[49] D. V. Raisinghani and B. V. S. Viswanadham, "Evaluation of permeability characteristics of a geosynthetic-reinforced soil through laboratory tests," *Geotextiles and Geomembranes*, vol. 28, no. 6, pp. 579–588, 2010, doi: 10.1016/j.geotexmem.2010.01.001.
[50] R. Hufenus, R. Rueegger, R. Banjac, P. Mayor, S. M. Springman, and R. Brönnimann, "Full-scale field tests on geosynthetic reinforced unpaved roads on soft subgrade," *Geotextiles and Geomembranes*, vol. 24, no. 1, pp. 21–37, 2006, doi: 10.1016/j.geotexmem.2005.06.002.
[51] T. Nogami and M. Li, "Consolidation of Clay with a System of Vertical and Horizontal Drains," *Journal of Geotechnical and Geoenvironmental Engineering*, vol. 129, no. 9, pp. 838–848, 2003, doi: 10.1061/(asce)1090-0241(2003)129:9(838).
[52] L. C. Soils, B. Herbert, D. L. F. Asce, S. Nair, and C. Markley, "Compressive

Strength of Soil Improved with Cement," pp. 558–565, 2009.
[53] C. A. Anagnostopoulos and M. Chatziangelou, "Compressive strength of cement stabilized soils. A new statistical model," *Electronic Journal of Geotechnical Engineering*, vol. 13 B, 2008.
[54] S. Horpibulsuk, R. Rachan, A. Chinkulkijniwat, Y. Raksachon, and A. Suddeepong, "Analysis of strength development in cement-stabilized silty clay from microstructural considerations," *Construction and Building Materials*, vol. 24, no. 10, pp. 2011–2021, 2010.
[55] A. Balkis and S. Macid, "Effect of Cement Amount on CBR Values of Different Soil," *Avrupa Bilim ve Teknoloji Dergisi*, pp. 809–815, 2019.
[56] V. O. Okonkwo and V. M. Nwokike, "Soil-Cement Stabilization For Road Pavement Using Soils Obtained From Agu- Awka In Anambra State," *Journal of Multidisciplinary Engineering Science and Technology (JMEST)*, vol. 2, no. 10, pp. 2668–2670, 2015.
[57] M. S. Al-Zoubi, "Undrained shear strength and swelling characteristics of cement treated soil," *Jordan Journal of Civil Engineering*, vol. 2, no. 1, pp. 53–62, 2008.
[58] B. V. Venkatarama Reddy and A. Gupta, "Characteristics of soil-cement blocks using highly sandy soils," *Materials and Structures/Materiaux et Constructions*, vol. 38, no. 280, pp. 651–658, 2005, doi: 10.1617/14265.
[59] J. Fan, D. Wang, and D. Qian, "Soil-cement mixture properties and design considerations for reinforced excavation," *Journal of Rock Mechanics and Geotechnical Engineering*, vol. 10, no. 4, pp. 791–797, 2018.
[60] D. T. Bergado, L. R. Anderson, N. Miura, and A. S. Balasubramaniam, *Soft ground improvement in lowland and other environments*. New York, USA, 1996.
[61] V. R. Schaefer, L. W. Abramson, J. C. Drumheller, and K. D. Sharp, "Ground Improvement, Ground Reinforcement and Ground Treatment : Developments 1987-1997," in *Sessions of Geo-Logan '97 Conference*, 1997, p. 616.
[62] S. H. Chew, A. H. M. Kamruzzaman, and F. H. Lee, "Physico-chemical and engineering behavior of cement treated Singapore marine clay," *Journal of Geotechnical and Geoenvironmental Engineering*, vol. 130(7), pp. 696–706, 2004.
[63] S. Horpibulsuk, N. Miura, and T. S. Nagaraj, "Assessment of strength development in cement-admixed high water content clays with Abrams' law as a basis," *Geotechnique*, vol. 53, no. 4, pp. 439–444, 2003.
[64] S. Horpibulsuk, W. Katkan, W. Sirilerdwattana, and R. Rachan, "Strength Development In Cement Stabilized Low Plasticity And Coarse Grained Soils: Laboratory And Field Study," *Soils and Foundations*, vol. 46, no. 3, pp. 351–366, 2006.
[65] K. Uddin, A. Balasubramaniam, and D. Bergado, "Engineering behaviour of cement-treated Bangkok soft clay," *Geotechnical Engineering*, vol. 28, pp. 89–119, 1997.

[66] G. A. Lorenzo and D. T. Bergado, “Fundamental Parameters of Cement-Admixed Clay — New Approach,” *Journal Of Geotechnical and Geoenvironmental Engineering*, vol. 130, no. 10, pp. 1042–1050, 2004.
[67] F.-H. Lee, Y. Lee, S.-H. Chew, and K.-Y. Yong, “Strength and Modulus of Marine Clay-Cement Mixes,” *Journal of Geotechnical and Geoenvironmental Engineering*, vol. 131, no. 2, pp. 178–186, 2005.
[68] F. Sariosseiri and B. Muhunthan, “Effect of cement treatment on geotechnical properties of some Washington State soils,” *Engineering Geology*, vol. 104, no. 1–2, pp. 119–125, 2009.
[69] A. S. Azneb, S. Banerjee, and R. G. Robinson, “Shear strength of cement-treated marine clay under triaxial and plane strain conditions,” *Proceedings of the Institution of Civil Engineers: Ground Improvement*, vol. 174, no. 3, pp. 143–156, 2021.
[70] T. A. Pham, J. Koseki, and D. Dias, “Optimum material ratio for improving the performance of cement-mixed soils,” *Transportation Geotechnics*, vol. 28, no. 3, pp. 1–10, 2021.
[71] K. Kasama, Z. Kouki, and K. Iwataki, “Undrained Shear Strength Of Cement-Treated Soils,” *Soils And Foundations*, vol. 2, no. 46, pp. 221–232, 2006.
[72] M. Suzuki, T. Fujimoto, and T. Taguchi, “Peak and residual strength characteristics of cement-treated soil cured under different consolidation conditions,” *Soils and Foundations*, vol. 54, no. 4, pp. 687–698, 2014.
[73] S. Issa and A. S. Reza, “Effect of cement stabilization on geotechnical properties of sandy soils,” *Geomechanics and Engineering*, vol. 8, no. 1, pp. 17–31, 2015.
[74] Z. Eliaslankaran, N. N. N. Daud, Z. M. Yusoff, and V. Rostami, “Evaluation of the effects of cement and lime with rice husk ash as an additive on strength behavior of coastal soil,” *Materials*, vol. 14, no. 5, pp. 1–15, 2021.
[75] A. Sukpunya and A. Jotisankasa, “Large simple shear testing of soft Bangkok clay stabilized with soil–cement-columns and its application,” *Soils and Foundations*, vol. 56, no. 4, pp. 640–651, 2016.
[76] Y. Tsubakihara, H. Kishida, and T. Nishiyama, “Friction between cohesive soils and steel,” *Soils and Foundations*, vol. 33, no. 2, pp. 145–156, 1993.
[77] L. Borana, J.-H. Yin, D. N. Singh, S. K. Shukla, and F. Tong, “Direct shear testing study of the interface behavior between steel plate and compacted completely decomposed granite under different vertical stresses and suctions,” *Journal of Engineering Mechanics*, vol. 144, no. 1, p. 04017148, 2018.
[78] T. B. Hamid and G. A. Miller, “Shear strength of unsaturated soil interfaces,” *Canadian Geotechnical Journal*, vol. 46, no. 5, pp. 595–606, 2009.
[79] L. B. Vinh, “Nghiên cứu giải pháp xử lý nền và tính toán ổn định của công trình đường cấp III trên nền có lớp đất yếu mỏng.” pp. 690–696, 2003.
[80] L. X. Roanh, “Công Nghệ Xử Lý Nền Và Thi Công Đê, Đập Phá Sóng Trên Nền Đất Yếu.” 2014.
[81] L. X. Khâm, “Nghiên cứu giải pháp gia cường ổn định cho mái dốc đứng,” *Yale*

Sustainability. 2013.
[82] N.M. Đức, L. A. Thắng, N. Q. Khải, "Nghiên cứu chỉ số CBR của đất bùn lòng sông đầm chặt gia cường hỗn hợp xi măng cắt," *Khoa Học và Công Nghệ Thuỷ Lợi*, no. 13. 2019.
[83] V. N. Bình, "Ảnh Hưởng Của Đặc Điểm Thành Phần Đến Chất Lượng Đất Loại Sét Yếu Vùng Đồng Bằng Sông Cửu Long Gia Cố Bằng Xi Măng," *Khoa Học và Công Nghệ Thuỷ Lợi*, no. 38. 2017.
[84] T. A. Nguyen, D. T. Nguyen, and A. D. Nguyen, "A novel approach to use soil-cement piles for steel sheet pile walls in deep excavations," *Civil Engineering and Architecture*, vol. 9, no. 2, pp. 301–316, 2021.
[85] T. N. Quang, B. T. Anh, T. V. Cong, and T. M. Cao, "Combination of Cement Deep Mixing (CDM) and Steel Sheet Piles for the Cofferdam Used in Construction of Deep Foundation Pit in Soft Ground in the Mekong Delta Coast," in *Proceeding of the 6th International Conference on Geotechnics, Civil Engineering and Structure*, 2022, pp. 97–106.
[86] F. . Chen, *Foundation on Expansive Soils*. New York, USA: Elsevier Scientific Publishing Co, 1983.
[87] H. . Seed, R. J. Woodward, and R. Lundgren, "Prediction of swelling potential for compacted clays," *Journal of Soil Mechanics and Foundation Division*, vol. 88 (SM3), pp. 53–87, 1962.
[88] V. Daksanamurthy and V. Raman, "A simple method of identiying an expansive soil," *Soil and Foundations*, vol. 13, no. 1, pp. 97–104, 1973.
[89] IS 2720-40, "Methods of test for soils, Part 40: Determination of free swell index of soils," *Bureau of Indian Standards*.
[90] M. J. J. Hoogsteen, E. A. Lantinga, E. J. Bakker, and P. A. Tittonell, "An Evaluation of the Loss-on-Ignition Method for Determining the Soil Organic Matter Content of Calcareous Soils," *Communications in Soil Science and Plant Analysis*, vol. 49, no. 13, pp. 1541–1552, 2018.
[91] Đ. Nguyễn Minh and L. Lê Đức, "Nghiên cứu cải tạo đất bùn nạo vét lòng sông thay thế cát trong công tác san lấp mặt bằng tỉnh An Giang," *Tạp chí Xây dựng*, vol. 11, pp. 59–63, 2018.
[92] ASTM C188, "Standard Test Method for Density of Hydraulic Cement," *West Conshohocken, PA: ASTM International*.
[93] ASTM C595, "Standard Specification for Blended Hydraulic Cements," *West Conshohocken, PA: ASTM International*.
[94] ASTM C191, "Time of Setting of Hydraulic Cement by Vicat Needle," *West Conshohocken, PA: ASTM International*.
[95] BS EN 197-1:2011, "Cement Composition, specifications and conformity criteria for common cements."
[96] 22 TCN 332-06, "Quy trình thí nghiệm Xá định chỉ số CBR của đất, đá dăm trong phòng thí nghiệm."
[97] ASTM D1883-07, "Standard Test Method for CBR (California Bearing Ratio) of Laboratory-Compacted Soils," *West Conshohocken, PA: ASTM*

International, [Online]. Available: http://www.astm.org/Standards/D4429.htm
[98] ASTM D2850-03, "Standard Test Method for Unconsolidated-Undrained Triaxial Compression Test on Cohesive Soils," *West Conshohocken, PA: ASTM International*, [Online]. Available: http://compass.astm.org/download/D2850.10761.pdf
[99] ASTM D3080, "Standard Test Method for Direct Shear Test of Soils Under Consolidated Drained Conditions," *West Conshohocken, PA: ASTM International*.
[100] I. B. Gratchev and K. Sassa, "Shear Strength of Clay at Different Shear Rates," *Journal of Geotechnical and Geoenvironmental Engineering*, vol. 141, no. 5, pp. 2–4, 2015, doi: 10.1061/(asce)gt.1943-5606.0001297.
[101] TCVN 4199-1995, "Phương pháp xác định sức chống cắt trong phòng thí nghiệm ở máy cắt phẳng."
[102] Y. Tsubakihara and H. Kishida, "Frictional Behaviour between Normally Consolidated Clay and Steel by Two Direct Shear Type Apparatuses," *Soils and Foundations*, vol. 33, no. 2, pp. 1–13, 1993.
[103] J.-F. Chen and S.-B. Yu, "Centrifugal and Numerical Modeling of a Reinforced Lime-Stabilized Soil Embankment on Soft Clay with Wick Drains," *International Journal of Geomechanics*, vol. 11, no. 3, pp. 167–173, 2011.
[104] J. K. Zornberg, J.G., & Mitchell, "Downloaded by [York University] on [26/09/16]. Copyright © ICE Publishing, all rights reserved.," 1994.
[105] A. M. Abduljauwad, S. N., Bayomy, F., Al-Shaikh and O. S. B. Al-Amoudi, "Influence of Geotextiles on Performance of Saline Sebkha Soils," *J. Geotech. Eng*, vol. 120, no. 11, pp. 1939–1960, 1994.
[106] R. M. Koerner and D. Narejo, "Bearing capacity of hydrated geosynthetic clay liners," *Journal of Geotechnical Engineering*, vol. 121, no. 1, pp. 82–85, 1995, doi: 10.1061/(ASCE)0733-9410(1995)121:1(82).
[107] M. A. Kamel, S. Chandra, and P. Kumar, "Behaviour of subgrade soil reinforced with geogrid," *International Journal of Pavement Engineering*, vol. 5, no. 4, pp. 201–209, 2004, doi: 10.1080/1029843042000327122.
[108] N. Keerthi, "Study on Improvement of Sub Grade Soil using Soil-Reinforcement Technique," *International Journal of Applied Engineering Research*, vol. 13, no. 7, pp. 126–134, 2018, [Online]. Available: http://www.ripublication.com
[109] M. Singh, A. Trivedi, and S. K. Shukla, "Strength enhancement of the subgrade soil of unpaved road with geosynthetic reinforcement layers," *Transportation Geotechnics*, vol. 19, no. November 2018, pp. 54–60, 2019, doi: 10.1016/j.trgeo.2019.01.007.
[110] M.-D. Nguyen and M.-P. Ho, "The influence of saturation on the interface shear strength of clay and nonwoven geotextile," *Journal of Science and Technology in Civil Engineering (STCE) - NUCE*, vol. 15, no. 1, pp. 41–54, 2020, doi: 10.31814/stce.nuce2021-15(1)-04.
[111] T. Nguyễn Thanh, N. M. Đức, T. V. Tiếng, and L. P. Bình, "Ứng xử cố kết của

đất sét lòng sông khi gia cường đệm cát và vải địa kỹ thuật dưới điều kiện nén 3 trục.pdf," *Tạp chí Vật liệu và Xây dựng*, vol. 4, pp. 75–82, 2021.
[112] P. Raju, N. Pandian, and T. Nagaraj, "Analysis and Estimation of the Coefficient of Consolidation," *Geotechnical Testing Journal*, vol. 18 (2), pp. 252–258, 1995.
[113]G. R. Retnamony, "Effect of Clay Mineralogy on Coefficient of Consolidation," *Clays and Clay Minerals*, vol. 46, no. 5, pp. 596–600, 1998.
[114] G. A. Leonards and P. Girault, "A study of the one-dimensional consolidation test," *Proceeding 9th ICSMFE, Paris 1*, pp. 116–130, 1961.
[115] R. Nini, "Effect of soaking period of clay on its california bearing ratio valuec," *World Congress on Civil, Structural, and Environmental Engineering*, pp. 1–7, 2019, doi: 10.11159/icgre19.162.
[116] I. Bushra and R. G. Robinson, "Shear strength behavior of cement treated marine clay," *International Journal of Geotechnical Engineering*, vol. 6, no. 4, pp. 455–465, 2012.
[117] S. Sasanian and T. A. Newson, "Basic parameters governing the behaviour of cement-treated clays," *Soils and Foundations*, vol. 54, no. 2, pp. 209–224, 2014.
[118] ASTM D4440, "Standard Test Method for Plastics: Dynamic Mechanical Properties Melt Rheology," *West Conshohocken, PA: ASTM International*.
[119] ASTM D5321, "Standard Test Method for Determining the Coefficient of Soil and Geosynthetic or Geosynthetic and Geosynthetic Friction by the Direct Shear Method," *West Conshohocken, PA: ASTM International*.
[120] S. K. Shukla, N. Sivakugan, and B. M. Das, "Methods for determination of the coefficient of consolidation and field observations of time rate of settlement - An overview," *International Journal of Geotechnical Engineering*, vol. 3, no. 1, pp. 89–108, 2013.
[121] R. F. Scott, "New method of consolidation–coefficient evaluation," *Journal of the Soil mechanics and Foundations Division*, vol. 87, no. 1, pp. 29–39, 1961.
[122] A. Sridharan, N. S. Murthy, and K. Prakash, "Rectangular hyperbola method of consolidation analysis," *Geotechnique*, vol. 37, pp. 355–368, 1987.
[123] G. Mesri and P. M. Godlewski, "Time and Stress-Compressibility Interrelationship," *Geotechnics*, pp. 417–430, 1977.
[124] H. Xing, X. Yang, C. Xu, and G. Ye, "Strength characteristics and mechanisms of salt-rich soil-cement," *Engineering Geology*, vol. 103, no. 1–2, pp. 33–38, 2009, doi: 10.1016/j.enggeo.2008.07.011.
[125] ASTM C136, "ASTM C 136-06: Standard Test Method for Sieve Analysis of Fine and Coarse Aggregates," *West Conshohocken, PA: ASTM International*.
[126] W. Zhu, C. Zhang, and A. C. F. Chiu, "Soil–Water Transfer Mechanism for Solidified Dredged Materials," *Journal of Geotechnical and Geoenvironmental Engineering*, vol. 133, no. 5, 2007.
[127] D. C. Chu, J. Kleib, M. Amar, M. Benzerzour, and N. E. Abriak, "Determination of the degree of hydration of Portland cement using three different approaches: Scanning electron microscopy (SEM-BSE) and

Thermogravimetric analysis (TGA)," *Case Studies in Construction Materials*, vol. 15, p. e00754, 2021.
[128] "Report of joint working party of the Concrete Society and Society of the Chemical Industry," in *Analysis of Hardened Concrete*, vol. 32, no. 117, Concrete Society Technical Report, 1989.
[129] M. Rezaeian, P. M. V. Ferreira, and A. Ekinci, "Mechanical behaviour of a compacted well-graded granular material with and without cement," *Soils and Foundations*, vol. 59, no. 3, pp. 687–698, 2019.
[130] L. J. Lemos and P. R. Vaughan, "Clay - interface shear resistance," *Géotechnique*, vol. 8, no. 1, pp. 55–64, 2000.
[131] L. J. Su, W. H. Zhou, W. Bin Chen, and X. Jie, "Effects of relative roughness and mean particle size on the shear strength of sand-steel interface," *Measurement: Journal of the International Measurement Confederation*, vol. 122, no. 7, pp. 339–346, 2018.
[132] E. Balaban, A. Šmejda, and M. I. Onur, "An experimental study on shear strength behavior of soils under low confining pressure," in *Poceedings of the 4th World Congress on Civil, Structural, andEnvironmental Engineering (CSEE'19)*, pp. 1–8.
[133] M. Shahin, M. Mehedi Hasan Khan, and M. Niamul Bari, "A Disaster Resilient Road: Effects of Fines on Density and Shear Strength of Sands," *International Journal of Transportation Engineering and Technology*, vol. 6, no. 2, p. 38, 2020.
[134] S. Horpibulsuk, N. Miura, and T. S. Nagaraj, "Clay–Water/Cement Ratio Identity for Cement Admixed Soft Clays," *Journal of Geotechnical and Geoenvironmental Engineering*, vol. 131, no. 2, pp. 187–192, 2005.
[135] N. Miura, S. Horpibulsuk, and T. S. Nagaraj, "Engineering behavior of cement stabilized clay at high water content," *Soils and Foundations*, vol. 41, no. 5, pp. 33–35, 2001.
[136] E. Yamashita, A. Aristo Cikmit, T. Tsuchida, and R. Hashimoto, "Strength estimation of cement-treated marine clay with wide ranges of sand and initial water contents," *Soils and Foundations*, vol. 60, no. 5, pp. 1065–1083, 2020.
[137] E.-H. Ahmed M and A. Mohammed H, "Effect of using cemented sand as a replacement layer beneath a strip footing," *HBRC Journal*, vol. 17, no. 1, pp. 1–17, 2021.
[138] S. Horpibulsk, R. Rachan, A. Suddeepong, and A. Chinkulkijniwat, "Strength development in cement admixed bangkok clay: Laboratory and field investigations," *Soils and Foundations*, vol. 51, no. 2, pp. 239–251, 2011.
[139] G. Sarkar, M. D. Rafiqul Islam, M. Alamgir, and M. D. Rokonuzzaman, "Study on the geotechnical properties of cement based composite fine-grained soil," *International Journal of Advanced Structures and Geotechnical Engineering*, vol. 01, no. 02, pp. 42–49, 2012.
[140] A. Kayvan Karimi and P. Mohammad Sirous, "Drained Shear Strength of Over-Consolidated Compacted Soil-Cement," *Journal of Materials in Civil*

Engineering, vol. 28, no. 5, pp. 1–7, 2016.
[141] B. Boroumandzadeh and M. S. Pakbaz, “Evaluation of effect of cementation on drained shear strength of overconsolidated clay soils,” *World Applied Sciences Journal*, vol. 16, no. 10, pp. 1375–1379, 2012.
[142] K. Yin, A.-L. Fauchille, E. Di Filippo, P. Kotronis, and G. Sciarra, “A Review of Sand–Clay Mixture and Soil–Structure Interface Direct Shear Test,” *Geotechnics*, vol. 1, no. 2, pp. 260–306, 2021.

LIST OF PUBLICATIONS

The publications related to this dissertation are:

International Journal

1. T. Nguyen Thanh, D. Nguyen Minh, T. Nguyen, and C. Phan Thanh, "Interface Shear Strength Behavior of Cement-Treated Soil under Consolidated Drained Conditions," *Buildings*, vol. 13, no. 7, 2023, doi: https://doi.org/10.3390/buildings13071626.

International Conference

2. T. Nguyen Thanh, D. Nguyen Minh, and T. Le Huu, "The Effects of Soaking Process on the Bearing Capacity of Soft Clay Reinforced by Nonwoven Geotextile," *Lecture Notes in Civil Engineering*, vol. 62, pp. 669–676, 2020, doi: 10.1007/978-981-15-2184-3_87.
3. T. Nguyen Thanh and D. Nguyen Minh, "Effects of Soaking Process on CBR Behavior of Geotextile Reinforced Clay with Sand Cushion," *Proceedings of 2020 5th International Conference on Green Technology and Sustainable Development, GTSD 2020*, pp. 162–167, 2020, doi: 10.1109/GTSD50082.2020.9303053

National Journal

4. T. Nguyễn Thanh, Đ. Nguyễn Minh, T. Trần Văn, and B. Lê Phương, "Ứng xử cố kết của đất sét lòng sông khi gia cường đệm cát và vải địa kỹ thuật dưới điều kiện nén 3 trục," *Tạp chí Vật liệu và Xây dựng*, vol. 4, pp. 90–97, 2021. Available: http://ojs.jomc.vn/index.php/vn/article/view/159
5. T. Nguyễn Thanh, Đ. Nguyễn Minh, N. Mai Trần, T. Trần Văn, and P. Lê, "Ảnh hưởng của bão hoà đến sức kháng cắt không thoát nước của đất bùn sét lòng sông gia cường vải địa kỹ thuật trong điều kiện nén 3 trục," *Tạp chí Xây dựng*, vol. 5. pp. 68–71, 2022. Available: https://tapchixaydung.vn/anh-huong-cua-bao-hoa-den-suc-khang-cat-khong-thoat-nuoc-cua-dat-bun-set-long-song-gia-cuong-vai-dia-ky-thuat-trong-dieu-kien-nen-3-truc-20201224000011282.html.